

# **Advanced Spectroscopic Techniques for the Analysis of Illicit Drugs and Explosives**

**Adriano De Grazia**

A thesis submitted for the

Degree of Doctor of Philosophy (Science)

University of Technology, Sydney

**2016**

## **Certificate of authorship and originality**

I certify that the work in this thesis has not previously been submitted for a degree nor has it been submitted as part of the requirements for a degree except as fully acknowledged within the text.

I also certify that the thesis has been written by me. Any help that I have received in my research work and the preparation of the thesis itself has been acknowledged. In addition, I certify that all the information sources and literature used are indicated in the thesis.

Adriano De Grazia

19/10/2016

## **Acknowledgements**

A number of people have contributed to the success of this project. This thesis is the result of a seven-year project that started in 2009 following a discussion with two very talented scientists, my supervisors. I owe thanks to Dr Brian Reedy and Dr Mark Tahtouh, who started me on this journey and assisted me with the transition from a full-time to part-time student in 2011. This has been a long road and I cannot thank you both enough for your encouragement and support throughout the entire project. Your tireless efforts (mostly out of regular business hours) have definitely not gone un-noticed and I am grateful for all you have taught me as an undergraduate student and during the transition into a professional in the field of forensic science.

Dr Ronald Shimmon, thanks for guidance, the synthetic chemistry support, but mostly the laughs. You are a true gentleman and a good friend. I cannot thank you enough for your guidance along the way. Thanks to Dr Helen Rutledge and Dr Fiona Burger for your guidance with Matlab and PARAFAC. Dr Linda Xiao, you truly realised the pressures of performing a PhD part-time and I thank you for allowing me to take over instruments, sometimes for days on end.

The past and present management and staff of the Forensics (Specialist Operations) portfolio of the Australian Federal Police, this thesis would not have been possible without the support that I received from the AFP and I will be forever thankful. I am honoured to be part of the organisation. To the past and present team members of the Australian Illicit Drug Data Centre (AIDDC) and Forensic Drug Intelligence (FDI), no doubt this PhD has had some impact on you all, I thank you all for your continued encouragement and support. To one AIDDC/FDI member in particular, Karly, not only for all the laughs, but also for your encouragement, kind words and guidance through some of the toughest times of this project, they will never be forgotten. Paul G for introducing me to AutoIT, this software package was a godsend.

Nat, Nikki and Sam, true friends, sources of inspiration and forever encouraging voices. Thank you all for checking in on those late nights and weekends, for the long chats on the runs and for acknowledging those times when I just didn't want to talk about it. Your support has helped me get through some of the longest and darkest days.

To my fellow students and members of office 4.39, thanks for celebrating the good times, and helping me through the bad. Dr David Bishop, a true friend. The games of brain ball, the pizza and poker nights and beers at Eve's place were some of the best times of my university life. You definitely lightened the pressure of PhD life. To (the almost Dr) Joyce Chan, we have been riding this wave together since 2009. Thank you for all the encouragement and words of wisdom, having another part-time student feeling the same pains has definitely helped me get through.

To my closest friends and family, thank you for your continued love and support. To my closest friends, Andrew, Chris, Joe and Nathan for always being there when I needed to escape PhD life and for understanding the many times that it had to take over. My siblings, Robert and Romina, thank you for support over the past several years, you have picked up some of the slack left behind by my study, you have both been a source of inspiration, for that I thank you. To mum and dad, I love you, thank you for all you have given me and continue to give to your family, for always letting me chase my dreams and truly believing that I could achieve them, no matter the obstacles. You have paved a great path for us all and I will forever be in awe of what you have both achieved.

Finally, my wife Nicole, thank you for all the sacrifices you have made to make this happen. This thesis is as much a testament of your hard work and dedication as it is mine. I could not have done this without you by my side, thank you for all the love and support you continue to give, you are amazing – I love you... Yes, now we can holiday!

# Table of contents

<b>CHAPTER 1: INTRODUCTION.....</b>	<b>2</b>
1.1.1 <i>Infrared (IR) hyperspectral imaging .....</i>	<i>3</i>
1.1.2 <i>Raman Spectroscopy and Mapping.....</i>	<i>11</i>
1.1.3 <i>Fluorescence Landscapes.....</i>	<i>15</i>
1.1.3.1 Fluorescence.....	15
1.1.3.2 Fluorescence landscapes .....	16
1.2 UNSUPERVISED COMPOSITIONAL ANALYSIS OF DATA .....	18
1.2.1 <i>Pre-processing methods .....</i>	<i>19</i>
1.2.1.1 Linear Baseline Correction .....	20
1.2.1.2 Normalisation .....	20
1.2.1.3 Principal Components Analysis (PCA) noise reduction .....	20
1.2.1.4 (Extended) Multiplicative Scatter Correction ((E)MSC).....	21
1.2.2 <i>“Analysis” techniques.....</i>	<i>21</i>
1.2.2.1 Endmember techniques.....	21
1.2.2.2 Principal components analysis (PCA) .....	22
1.2.2.3 Multivariate curve resolution (MCR) .....	23
1.2.2.4 Simple to use interactive self-modelling mixture analysis (SIMPLISMA) .....	25
1.3 PARALLEL FACTOR ANALYSIS (PARAFAC).....	26
1.3.1 <i>The PARAFAC model.....</i>	<i>28</i>
1.4 PROJECT AIMS .....	29
<b>CHAPTER 2: ADVANCED VIBRATIONAL SPECTROSCOPIC TECHNIQUES FOR THE ANALYSIS OF ILLICIT DRUGS 31</b>	
2.1 INTRODUCTION .....	31
2.1.1 <i>Illicit Drugs.....</i>	<i>31</i>
2.1.2 <i>ATR-FTIR hyperspectral imaging .....</i>	<i>32</i>
2.1.3 <i>Raman mapping.....</i>	<i>33</i>

---

2.1.4	<i>MCR and SIMPLISMA</i> .....	34
2.1.5	<i>Aims</i> .....	34
2.2	EXPERIMENTAL AND DATA ANALYSIS METHODS .....	36
2.2.1	<i>Sample preparation</i> .....	36
2.2.2	<i>Instrumentation and data collection</i> .....	37
2.2.2.1	FTIR .....	37
2.2.2.2	Raman .....	38
2.2.3	<i>Data Pre-processing</i> .....	39
2.2.3.1	ATR-FTIR.....	39
2.2.3.2	Raman.....	39
2.2.4	<i>Data analysis</i> .....	40
2.2.4.1	Multivariate Curve Resolution (MCR) .....	40
2.2.4.2	SIMPLISMA.....	40
2.3	RESULTS AND DISCUSSION .....	41
2.3.1	<i>Choice of compounds</i> .....	41
2.3.2	<i>Data collection considerations</i> .....	42
2.3.2.1	Collection of ATR-FTIR hyperspectral images .....	42
2.3.2.2	Selection of Raman laser.....	43
2.3.2.3	Particle vs pixel size .....	44
2.3.3	<i>End member classification</i> .....	48
2.3.4	<i>Classification approaches</i> .....	49
2.3.4.1	ATR-FTIR.....	50
2.3.4.2	Raman mapping .....	64
2.3.4.3	Currently used FTIR technique.....	73
2.3.5	<i>Application to case samples</i> .....	75
2.4	CONCLUSIONS.....	76

---

<b>CHAPTER 3: FLUORESCENCE LANDSCAPES AND PARAFAC FOR THE ANALYSIS OF EXPLOSIVES (FEASIBILITY STUDY)</b> .....	<b>79</b>
3.1 INTRODUCTION .....	79
3.1.1 Nitro Explosives .....	79
3.1.2 Current detection.....	80
3.1.3 Fluorescence landscapes .....	84
3.1.4 Reduction to amine groups .....	85
3.1.5 Derivatisation of amino groups.....	87
3.1.6 Parallel Factor Analysis (PARAFAC) .....	89
3.1.7 Aims.....	91
3.2 EXPERIMENTAL.....	92
3.2.1 Sample preparation.....	92
3.2.1.1 Compounds.....	92
3.2.1.2 Reduction.....	94
3.2.1.3 Derivatisation.....	95
3.2.2 Collection of landscapes .....	95
3.2.3 Data analysis - PARAFAC .....	96
3.3 RESULTS AND DISCUSSION .....	96
3.3.1 Reduction of nitro aromatics.....	97
3.3.2 Derivatisation .....	102
3.3.3 Collection of landscapes .....	110
3.3.4 PARAFAC.....	111
3.4 CONCLUSIONS.....	128
<b>CHAPTER 4: CONCLUSIONS AND FURTHER WORK .....</b>	<b>132</b>

---

## List of figures

Figure 1-1 Schematic of a typical Michelson interferometer. <sup>9</sup> (NB: The mirrors do not need to be perpendicular to one another) .....	6
Figure 1-2 Schematic of the optical arrangement using an inverted ATR prism. Image adapted from Kazarian et al. <sup>11</sup> .....	9
Figure 1-3 Imaging Golden Gate diamond ATR accessory (left) and schematic of internal features (right). (Images adapted from <a href="http://www.specac.com">http://www.specac.com</a> ).....	10
Figure 1-4 Basic Jablonksi diagram outlining energy transitions between electronic states and different types of Raman scattering. ....	12
Figure 1-5 Graphical comparison of Raman mapping and imaging capabilities. Adopted from Stewart et. al. <sup>61</sup> .....	13
Figure 1-6 Basic Jablonksi diagram outlining energy transitions between electronic states. Adopted from Lakowicz. <sup>77</sup> .....	16
Figure 1-7 Example of a fluorescence landscape, before removal of scattering (Ex: 250-500 nm).....	17
Figure 1-8 Sketch of the scattering that often occurs in fluorescence EEM data. Adopted from Bahram et al. <sup>83</sup> .....	18
Figure 1-9 Equation for multivariate curve resolution model .....	23
Figure 1-10 Equation for PARAFAC model .....	28
Figure 2-1 Basic outline of process and expected results.....	35
Figure 2-2 Chemical structure of phenylethylamine and some common illicit drugs encountered by Australian LEAs. ....	41
Figure 2-3 Examples of hyperspectral images resulting from good and poor contact between sample and ATR crystal.....	43



---

Figure 2-4 Graphical representation of the hypothesis regarding variation of particle size in FTIR-ATR hyperstpectral imaging.....	45
Figure 2-5 Effect of particle size on the apparent composition of Caffeine (CAF) and microcrystalline cellulose (MCC) mixtures using multivariate curve resolution (MCR). .....	47
Figure 2-6 MCR results for two images (a, b) of two tablets (set 1 and 2) made from the same powder mixture. i.e multiple bars for a mixture indicate replicate analyses. ....	51
Figure 2-7 Schematic representation of purity the calculations applied to an infrared image.	52
Figure 2-8 Example of MCR-calculated spectrum vs pure FTIR spectra of caffeine and glucose. ....	54
Figure 2-9 MCR results for two tablets made from the same three component powder mixture.....	56
Figure 2-10 SIMPLISMA results for two images (a, b) of two tablets (set 1 and 2) made from the same powder mixture.....	58
Figure 2-11 Pure ATR-FTIR spectra of caffeine, glucose and paracetamol.....	62
Figure 2-12 Infrared spectra of methamphetamine hydrochloride and dimethylsulfone. ....	63
Figure 2-13 Raman MCR results. Results are displayed for two maps of each powder sample. ....	65
Figure 2-14 Raman MCR results for three part mixture. Results are displayed for two maps of each powder sample.....	67
Figure 2-15 Pure Raman spectra of caffeine (CAF), paracetamol (PAR) and phenylethylamine (PEA).....	68
Figure 2-16 Raman SIMPLISMA results for two-part mixtures. (two maps of each powder sample).....	70
Figure 2-17 Raman SIMPLISMA results for three-part mixtures. (two maps of each powder sample).....	71

---

Figure 3-1 Chemical names and structures for some common nitro-containing explosives TNT, PETN and RDX. ....	80
Figure 3-2 Schematic outlining reduction pathway from TNT to TAT, adopted from Bandstra. <sup>219</sup> .....	85
Figure 3-3 Structures of derivatising agents OPA, NDA and DPMA.....	88
Figure 3-4 Work flow diagram for the analysis of explosives. ....	91
Figure 3-5 Samples of commercial explosive samples as supplied by the AFP. ....	93
Figure 3-6 <sup>1</sup> H-NMR spectra of pure 2,4-DNT (green), pure 2,4-DAT (red) and 2,4-DAT from a reduced sample of 2,4-DNT, demonstrating a full conversion to the amine. ....	99
Figure 3-7 Schematic of TLC reaction monitoring, showing the reduction of 2,4-DNT to 2,4-DAT. 1 = DNT, at start of reaction. 2= intermediate and DNT present within minutes of reaction starting. 3 = disappearance of DNT and appearance of DAT (sometimes DAT/DNT co-exist) 4 = full conversion to DAT with no intermediate or DNT present. ....	100
Figure 3-8 Fluorescence landscape of blank OPA buffer solution showing minimal fluorescence.....	103
Figure 3-9 Fluorescence landscape of aniline solution. Note change in scale relative to that in Figure 3-8 and Figure 3-10.....	104
Figure 3-10 Fluorescence landscape of Aniline derivatised with OPA.....	105
Figure 3-11 Proposed mechanism for OPA derivatisation of primary amine.....	107
Figure 3-12 Isoindole adducts identified by LCMS. These are the expected products for the diaminotoluene and triaminotoluene derivatisation with o-phthalaldehyde.....	108
Figure 3-13 Mass spectrum of pure 2,4-DAT derivatised with OPA. The red outline of the signal shows the expected library splitting pattern for the formula provided.....	108

---

Figure 3-14 Mass spectrum of crude 2,4-DAT (reduced from 2,4-DNT without purification) derivatised with OPA. The red outline of the signal shows the expected library splitting pattern for the formula provided. ....	109
Figure 3-15 Mass spectrum of crude TAT derivatised with OPA. The red outline of the signal show the expected library splitting pattern for the formula provided. ....	109
Figure 3-16 Sample fluorescence landscapes before (left) and after removal of scattering using EEMCut (right). ....	112
Figure 3-17 Chemical structures of Aniline and 4-aminobenzoic acid.....	113
Figure 3-18 Fluorescence landscape for a 1:1 mixture of aniline and 4-aminobenzoic acid derivatised with OPA (EEMCut performed).....	113
Figure 3-19 Fluorescence landscape of OPA buffer solution prior to addition of amine (EEMCut performed).....	114
Figure 3-20 Loading and leverage plots for two (top) and three (bottom) component PARAFAC models as predicted by the OutlierTest for the derivatised mixture of aniline and 4-aminobenzoic acid. ....	115
Figure 3-21 Fluorescence landscapes for components 1 (top) and 2 (bottom) as predicted by PARAFAC for aniline and 4-aminobenzoic acid.....	117
Figure 3-22 PARAFAC solution for mixture of aniline and 4-aminobenzoic acid derivatised with OPA. ....	118
Figure 3-23 Fluorescence landscape of 2,4-DAT, 2,6-DAT and TAT derivatised with OPA (EEMCut performed).....	119
Figure 3-24 Emission Spectra of 2,4-DAT, 2,6-DAT, TAT and a mixture of the three derivatised with OPA (EEMCut performed).....	120
Figure 3-25 Excitation spectra of 2,4-DAT, 2,6-DAT, TAT and a mixture of the three derivatised with OPA (EEMCut performed).....	121

Figure 3-26 Fluorescence landscapes of 2,4-DAT and TAT derivatised with OPA (EEMCut performed)..... 122

Figure 3-27 Emission spectra of OPA adducts and components as predicted by PARAFAC... 125

Figure 3-28 Excitation spectra of OPA adducts and components predicted by PARAFAC. .... 126

Figure 4-1 Example graph to demonstrate how result are to be interpreted..... 138

---

## List of tables

Table 2-1 Compositions of the powder mixtures. XYZ may not relate to the same substance in all examples; combinations of these were developed for each analysis.....	37
Table 2-2 Average %relative error for MCR Vs SIMPLISMA for examples presented in Figure 2-6 and Figure 2-10. * not counted towards average .....	61
Table 2-3 Example of average %relative error for Raman analysis. Relative error calculated for date presented in Figure 2-13 and Figure 2-16. ....	72
Table 2-4 Comparison of results for the analysis of binary mixtures with currently used FTIR technique and method proposed by this research. ✖ - No correct library matches, ± - one correct component identified, ✓ - both components correctly identified. ....	74
Table 3-1 Some analytical methods for the analysis of organic explosives adopted from Royds et al. <sup>187</sup> .....	82
Table 3-2 Explosive samples supplied by the AFP - Sample numbers relate to number in Figure 3-5. ....	94
Table 3-3 Outline of desired products and average reaction time for the reduction of target compounds. *picric acid was not tried in mixtures with other explosive compounds due to the known instability of this compound. †reaction times from 5 minutes to 48 hours were trialed with limited success. **see comments below regarding reduction products of RDX and PETN. ....	98
Table 3-4 Intermediates and products obtained from the reduction of nitroaromatic explosives TNT, 2,4-DNT and 2,6-DNT. ....	101
Table 3-5 End products obtained from the reduction of explosives PETN and RDX. ....	102
Table 3-6 Core consistency diagnostic (CORCONDIA) values for PARAFAC models of aniline and 4-aminobenzoic acid mixtures derivatised with OPA. ....	116
Table 3-7 Ratios of 2,4-DAT, 2,6-DAT and TAT in mixtures and derivatised with OPA and analysed vis PARAFAC. *these samples were at half concentration. ....	123

Table 3-8 Core consistency diagnostic (CORCONDIA) values for PARAFAC models of 2,4-DAT, 2,6-DAT and TAT derivatised with OPA..... 124

---

## Abbreviations

ABF	Australian Border Force
ADA	anthracene-2,3-dicarboxaldehyde
AFP	Australian Federal Police
ALS	alternating least squares
ATR	attenuated total reflection
CORCONDIA	core consistency diagnostic
2,4-DAT	2,4-diaminotoluene
2,6-DAT	2,6-diaminotoluene
DMS	dimethylsulfone
2,4-DNT	2,4-dinitrotoluene
2,6-DNT	2,6-dinitrotoluene
DOM	dissolved organic matter
DPMA	diphenylmaleic anhydride
EEM	excitation emission matrix
EMSC	extended multiplicative scatter correction
FPA	focal plane array
FTIR	Fourier transform infrared
GC-ECD	gas chromatography electron capture detector
GC-MS	gas chromatography mass spectrometry
GC-TEA	gas chromatography thermal energy analyser
GUI	graphical user interface
HPLC-DA	high pressure liquid chromatography diode array
HPLC-UV	high pressure liquid chromatography ultra violet
IDDR	Illicit drug data report
IED	improvised explosive device
IMS	ion mobility spectrometry
IR	infrared

---

LC-MS	liquid chromatography mass spectrometry
LEA	law enforcement agency
MCC	microcrystalline cellulose
MCR	multivariate curve resolution
MS	mass spectrometry
MSC	multiplicative scatter correction
NDA	naphthalene-2,3-dicarboxaldehyde
NIR	near infrared
NMR	nuclear magnetic resonance
NPS	new psychoactive substances
OPA	<i>o</i> -phthalaldehyde
PARAFAC	parallel factor analysis
PCA	principal components analysis
PEA	phenylethylamine hydrochloride
PETN	pentaerythritol tetranitrate
PIDI	preliminary illicit drug identification
RDX	cyclotrimethylenetrinitramine (research development explosive)
SAM	spectral angle mapper
SERS	surface enhanced raman spectroscopy
SFF	spectral feature fitting
SIMPLISMA	simple-to-use interactive self-modelling mixture analysis
TAT	2,4,6-triaminotoluene
TLC	thin layer chromatography
TNT	2,4,6-trinitrotoluene
TOF-MS	time of flight mass spectrometry



## **Abstract**

Law enforcement agencies are on a path to intelligence-led-policing, with an aim of gaining as much information as possible and interpreting that into actionable intelligence as quickly as possible. The focus on this information is not necessarily how accurate it is, but in what intelligence it can provide. In the illicit drugs environment, information about mixtures and purity could take months to obtain under current procedures. In the field of explosives analysis there is always a need for field- deployable methodologies that do not require the acquisition of expensive equipment.

Currently available spectroscopic techniques used for the preliminary identification of illicit drugs are limited to "single point" spectroscopic methods. Samples that can prove particularly problematic for these methods include drug mixtures, especially those of low purity (e.g. tablets or powders with a range of diluents, adulterants and cutting agents) or new psychoactive substances (NPS) that have not previously been encountered. Furthermore, the information that these methods provide offers little value in the realm of intelligence to policing organisations. In a move to intelligence-led-policing and the desire for more data, ATR-FTIR hyperspectral imaging and Raman mapping are two techniques that have the potential to rapidly provide law enforcement with actionable intelligence on potential illicit drug samples. Both of these methods have been shown to have superior information content in comparison to their single point equivalents. This research compares the performance of the unsupervised chemometric techniques multivariate curve resolution (MCR) and simple-to-use interactive self-modelling mixture analysis (SIMPLISMA) in identifying components of mixtures (from hyperspectral image data) and estimating their purity, without the need for calibration. While all of the hyperspectral methods provided more information than current techniques, Raman mapping coupled with analysis by MCR was found to provide the most precise and accurate results.

A feasibility study on the analysis of nitroaromatic explosives via fluorescence landscapes and PARAFAC was conducted. Although the initial aim of the project was to determine a field-deployable, 'one-size-fits-all' approach to nitro-containing explosives detection via reduction to amines, the reduction method was only found to be suitable for nitroaromatic explosives. Following the reduction to amines, derivatisation with *o*-phthalaldehyde (OPA) was performed to form fluorescent isoindoles. This two-step derivatisation process was demonstrated to take less than 60 minutes and was assessed to be field-deployable. However, fluorescence landscapes of the derivatised amines were found to be too similar for PARAFAC to separate and quantify.

***Chapter 1:***  
***Introduction***

## Chapter 1: Introduction

Forensic science has traditionally been a tool to aid in the resolution of crime in the courts. Increasingly, the information provided by forensic analyses is evolving from its sole use in criminal investigation and prosecution support to operating as an aid in tactical, operational and strategic decision-making. Importantly, forensic intelligence should not be considered a new discipline in forensic science, but rather a new and previously unexplored unknown avenue of data exploitation. It represents a consensus by forensic scientists and analysts to effectively utilise the forensic data collected to proactively inform investigations, policing and policy. <sup>1,2</sup>

Law enforcement agencies are on a path to intelligence-led-policing, with an aim of gaining as much information as possible and interpreting that into actionable intelligence as quickly as possible. The focus on this information is not necessarily how accurate it is, but in what intelligence it can provide. In the illicit drugs environment, information about mixtures and purity could take months to obtain under current procedures, at which time the intelligence value is significantly reduced. In the field of explosives analysis, there is always a need for field-deployable methodologies using inexpensive equipment to aid in the rapid identification of explosives present, as this can give indications of perpetrators or syndicates involved.

Overall, this project aims to develop methods using advanced spectroscopic techniques that will give frontline forensic practitioners more information than currently available techniques when an unknown substance is presented to them. This will aid forensic practitioners in identifying unknowns, and aid policing by providing actionable forensic intelligence almost immediately.

## 1.1 Advanced Spectroscopic Techniques

Due to a growing need for multidimensional analytical information, enhancements to traditional spectroscopic techniques have been developed in recent years. This research broadly classes these enhancements as *advanced spectroscopic techniques* and will focus in particular on chemical (or hyperspectral) mapping or imaging, and the application of fluorescence landscapes as multi-way data to explore and analyse chemical inhomogeneity in targeted samples.

The vibrational spectroscopic analysis of spatial regions within a sample can be accomplished in two ways, mapping or imaging. Mapping, either in the x direction (line mapping) or in both x and y directions, involves the sequential collection of spectra by moving the sample, point-by-point under a focussed beam of light. Imaging, on the other hand requires an image of the sample to be focussed on an array detector. A spectrum is collected at each pixel of the image.<sup>3</sup> The end result of both mapping and imaging experiments is an array of spectra (or a hyperspectral cube) from which identifying characteristics of heterogeneous samples can be obtained.<sup>3</sup>

Traditionally, fluorescence data is presented as either emission or excitation spectra. The collection of a fluorescence landscape, or an excitation-emission matrix (a two-dimensional array of data), shows the fluorescence intensity at different combinations of excitation and emission wavelengths.

### 1.1.1 Infrared (IR) hyperspectral imaging

Traditionally, structural elucidation of complex organic molecules was performed solely by infrared (IR) spectroscopy. Today IR is used as a complementary technique to nuclear magnetic resonance (NMR), x-ray diffraction and mass spectrometry. None-the-less, Fourier transform infrared (FTIR) spectroscopy still plays an important

role in chemical analysis. In addition to its use as a qualitative tool, the selectivity of IR spectroscopy and the linearity of absorbance with concentration make it possible to quantify the components of mixtures with little to no prior separation. This is possible as each organic molecule (except enantiomers) gives a unique or *fingerprint* spectrum, as described below.<sup>4,6</sup>

The complexity of an infrared spectrum arises from the coupling of vibrations over a large part or over the complete molecule and even simple molecules will have many different vibrations.<sup>7</sup> This is advantageous for structural elucidation, and for library searching against spectra of known compounds, and thus for the purposes of this research.

Any covalent bond that has a dipole moment that changes as a function of time in its vibrational (stretching or bending) or rotational modes, whether as a part of an organic or inorganic compound, will absorb infrared radiation.<sup>5,6</sup> A change in dipole moment in these modes is essential for the transfer of energy, coupling to the changing electromagnetic field of the incoming radiation to yield a characteristic absorption. Thus, symmetric bonds, such as those within H<sub>2</sub> and Cl<sub>2</sub>, will not absorb in the infrared, but most molecules will yield unique absorption patterns.<sup>5</sup>

The infrared region of the electromagnetic spectrum lies at wavelengths longer than those associated with visible light, but shorter than microwaves.<sup>5</sup> Infrared spectroscopic measurements are generally made in three separate sections of the infrared region, the mid (4000 – 400 cm<sup>-1</sup>), near (13000 – 4000 cm<sup>-1</sup>) and far (400 – 10 cm<sup>-1</sup>) IR regions.<sup>7,8</sup> This study will only deal with the mid-IR region and thus “IR” (or “FTIR”) spectroscopy will refer to the mid-IR region for the remainder of this thesis.

Mid-infrared spectroscopy is arguably the most commonly used for the qualitative and quantitative determination of organic matter (solids, liquids and gases) because the spectral range corresponds to the stretching and bending vibration energies in most covalent molecules.<sup>5</sup>

The higher energy (shorter wavelength) near-IR spectrum is used to study vibrational overtone and combination bands. These bands usually appear broader and less intense than the corresponding features in the mid-IR spectrum and the spectra are usually harder to interpret. Due to this, many multivariate analysis techniques have been developed for use with NIR spectroscopy.<sup>4</sup> Far-IR spectroscopy, at the lower energy end of the IR spectrum, is rarely used for structural elucidation, but can be used to gain information on the vibration of heavy (metal) atoms and weak bonds such as hydrogen bonds.<sup>4,5</sup>

Today, due to the increased reliability, speed, signal-to-noise and sensitivity that they offer, FTIR spectrometers are almost exclusively used rather than dispersive instruments. The design of FTIR spectrometers is based on the Michelson interferometer (Figure 1-1), originally designed in 1891. The interferometer consists of a beamsplitter, situated between a fixed mirror and a moving mirror, which are generally perpendicular to one another. These mirrors act to recombine the split radiation, producing a wave-like pattern called an interferogram, which contains all the frequencies that make up an infrared spectrum.<sup>4,5,9</sup>

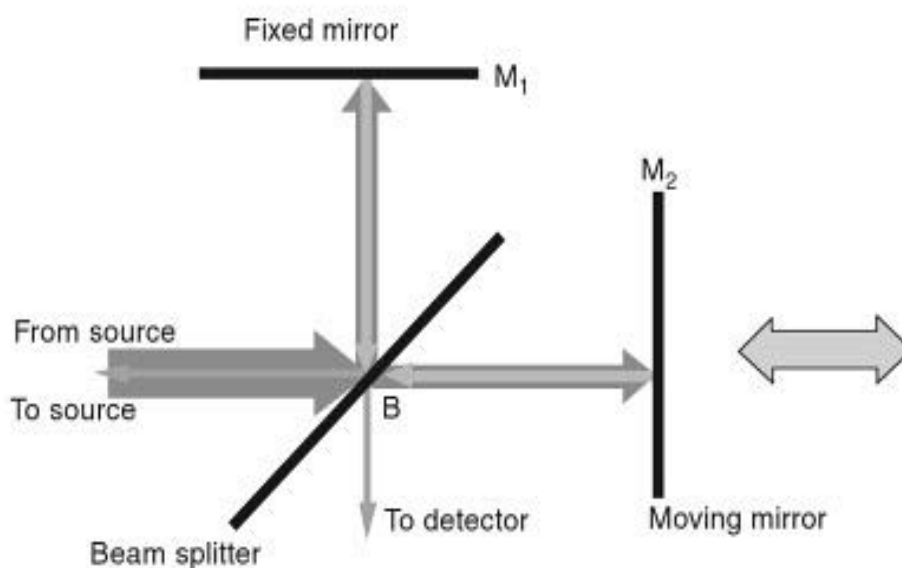


**Figure 1-1 Schematic of a typical Michelson interferometer.<sup>9</sup> (NB: The mirrors do not need to be perpendicular to one another)**

To obtain an infrared spectrum from an interferogram, the software employs a mathematical operation known as a Fourier transform to convert a time-domain signal (interferogram) into a frequency-domain spectrum, where each absorption frequency is separated. In chemistry, the infrared frequency is usually expressed as wavenumbers with units of inverse centimetres ( $\text{cm}^{-1}$ ) due to the proportional relationship between wavenumbers and energy, rather than actual wavelength values (used by physicists, and older literature) which are inversely proportional to energy and generally presented in nanometres (nm) or micrometres ( $\mu\text{m}$ ).<sup>5</sup>

Before the use of focal plane array (FPA) detectors in IR instruments, users were restricted to using IR mapping techniques if both spatial and spectral information about a sample were required. Mapping experiments are performed by mounting a sample on a computer-controlled x-y stage and taking point-by-point spectra in a grid. This can be performed either in one direction (line mapping) or in both, and is a very time consuming process. The data obtained can be treated as a hyperspectral image once compiled, containing both spatial and spectral information. A hybrid



between mapping and imaging uses a linear array of detectors to acquire data which is then "stitched" together to form an image, but this process is still more time-consuming than acquiring an image with an FPA detector, where one 'snapshot' contains thousands of spectra.<sup>3,4,6,9</sup>

Infrared hyperspectral imaging, also referred to as chemical, spectral or spectroscopic imaging, has been made possible by replacing the single element infrared detector used in conventional infrared spectroscopy with multichannel or FPA detectors that were originally developed for military applications.<sup>9,10</sup> FPA detectors consist of a large number of small detectors (pixels) laid out in a grid pattern. Each single pixel detector is capable of the simultaneous collection of an infrared spectrum from a specific area on the sample, giving rise to spatial and spectral information about a sample.<sup>11</sup> The use of FPA detectors for mid-infrared imaging was first reported in scientific literature in 1995.<sup>12-14</sup> Previous research in this field has highlighted the advantage of the technique for the non-invasive characterisation of heterogeneous materials, including the ability to precisely characterise the chemical composition and physical make-up of a variety of substances.<sup>14</sup>

In the early imaging configurations, step-scan interferometers were favoured as the acquisition of data by early FPA detectors was too slow for the more efficient, continuous-scan instruments.<sup>9</sup> As the name suggests, step-scan interferometers acquire interferograms point-by-point, recording the detector signal at discrete mirror positions.<sup>10</sup> Continuous (or rapid-scan) interferometers record it with continuous mirror movement, significantly decreasing the time taken to collect an infrared image, although this is still slightly greater than a single-point FTIR spectrum.<sup>10</sup>

Since its inception, the use of FTIR hyperspectral imaging has spread widely. Applications have been developed for a range of industries, including, materials<sup>15</sup> and polymer<sup>16</sup> analysis, the visualisation of cells and tissues for the biomedical industry<sup>17-19</sup> and the analysis of heterogeneous powder samples.<sup>20</sup>

Forensic applications of FTIR hyperspectral imaging have been developed for a range of areas including, but not limited to, fingerprints<sup>21-23</sup> and the identification of illicit substances in fingerprints,<sup>24</sup> and the analysis of multilayered paint chips.<sup>25</sup> The use of FTIR mapping has been demonstrated in the analysis of drugs in hair<sup>26</sup> and IR synchrotron imaging has been used in the analysis of automotive paint chips<sup>27</sup> and contaminated fingerprints.<sup>28</sup>

While FTIR remains the most widely-used form of vibrational spectroscopy, it does have some drawbacks for routine use in the forensic field. Mid-IR light does not penetrate far into many common materials, thus reducing the flexibility of sampling and the ability to remotely analyse material. Furthermore, conventional FTIR analyses can also require time-consuming and often destructive sample preparation such as KBr disks or nujol mulls.<sup>29,30</sup> The attenuated total reflection FTIR (ATR-FTIR) technique is used to negate the need for sample preparation. ATR is a non-destructive method with the sample able to be recovered from the sampling stage.

#### *1.1.1.1 Attenuated Total Reflection FTIR (ATR-FTIR) hyperspectral imaging*

Attenuated total reflection (ATR) FTIR spectroscopy (macro-ATR) and ATR-FTIR micro-spectroscopy (micro-ATR) are well-established techniques for measuring the absorbance spectra of the surface of highly absorbing samples with minimal sample preparation.<sup>29</sup> Hyperspectral imaging using micro and macro-ATR-FTIR is a technique of growing interest. ATR is based on the phenomenon of internal reflection, where total reflection of a light beam occurs at the interface between two media of different refractive indices (ATR crystal and sample). At that interface, an evanescent wave penetrates a few micrometres into the sample (Figure 1-2), resulting in the absorption of radiation by the sample to give a spectrum that closely resembles the transmission spectrum.<sup>6,16,31</sup> In conventional FTIR hyperspectral imaging, multiple images can be

'stitched' together to cover a bigger surface area of a sample. In ATR-FTIR, the area is restricted to the field of view of the ATR accessory.

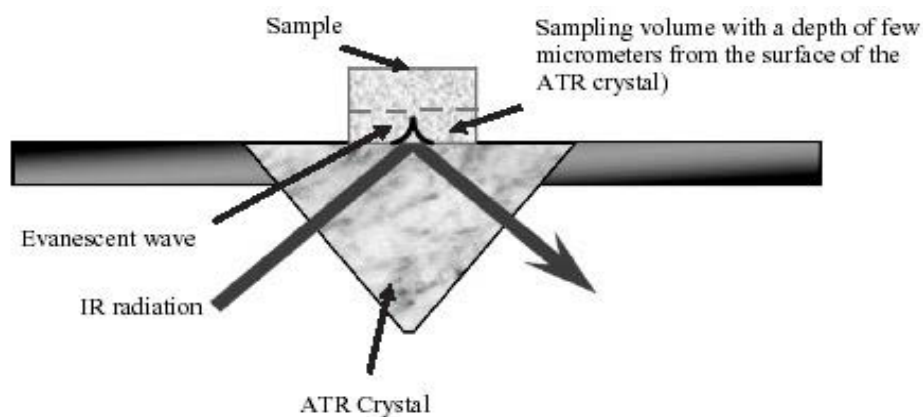


**Figure 1-2 Schematic of the optical arrangement using an inverted ATR prism. Image adapted from Kazarian *et al.*<sup>11</sup>**

As previously discussed, before the use of FPA detectors in IR spectroscopy, users requiring spatial information about a sample were restricted to using a mapping approach. This is problematic in ATR experiments as carry-over effects and damage to soft samples can occur due to the application of pressure in multiple areas.<sup>32</sup> In an attempt to resolve these issues, Esaki *et al.*<sup>33</sup> developed a purpose-built hexagonal shaped crystal on which the map was only limited to the size of the crystal used. Lewis *et al.*<sup>34</sup> reported the use of a hemispherical germanium (Ge) crystal and its translation together with the sample to reduce smearing. This work has been extended to use with linear array detectors by Patterson *et al.*<sup>35,36</sup> who claimed that the speed of analysis could rival FPA analysis; they also noted some advantages of the linear array over an FPA, such as larger spectral range and more flexible imaging size.<sup>32,36</sup> Experiments using the FPA detector have the advantage of being able to simultaneously record thousands of spectra, which is especially important in dynamic systems such as tablet dissolution.<sup>37</sup> ATR-FTIR often suffers from improper sample-to-crystal contact. For imaging applications, uneven contact between the sample and the

crystal across the imaged area creates an image which would appear to have come from a heterogeneous distribution in the sample, when in fact the heterogeneity in the image is due to the poor contact and hence variation in absorbance at those positions.

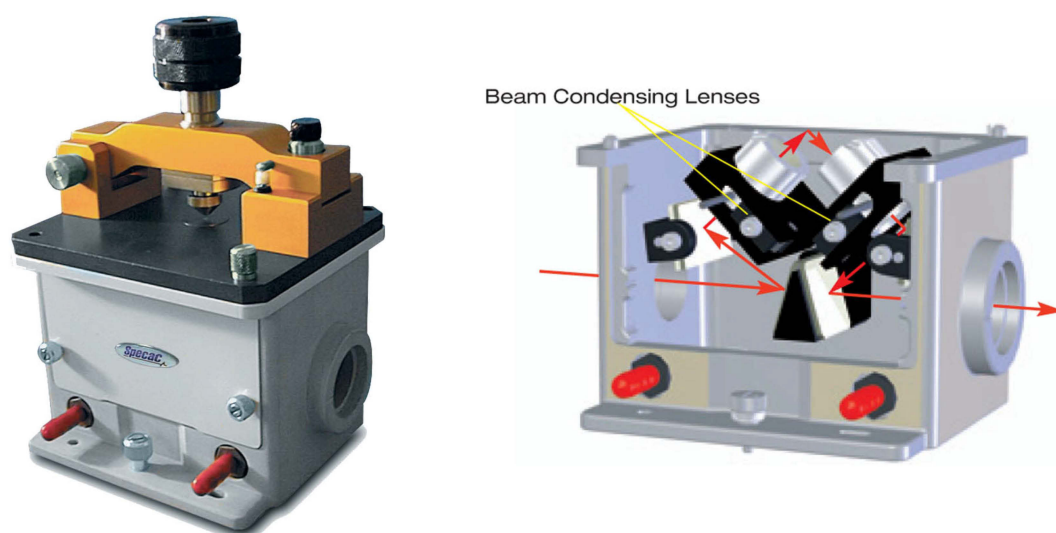


**Figure 1-3 Imaging Golden Gate diamond ATR accessory (left) and schematic of internal features (right). (Images adapted from <http://www.specac.com>)**

The Specac imaging Golden Gate diamond ATR accessory was designed specifically for imaging purposes (see Figure 1-3).<sup>32,38,39</sup> The accessory reduces the image aberration and distortion encountered with ATR accessories designed for single point infrared spectroscopy but used in imaging applications.<sup>40,41</sup> As shown above, the accessory is a single reflection device that uses a number of lenses and mirrors that specifically act to achieve the distortion-free data. The sampling area is made up of a monolithic diamond, which for powder and tablet samples, allows the application of high pressure to improve the sample to crystal contact without the risk of damaging the surface, which can affect the quality of the spectra obtained.<sup>39</sup>

Kazarian and co-workers at Imperial College, London are well known for their pioneering work in micro and macro ATR-FTIR hyperspectral imaging. They have achieved spatial resolution beyond the diffraction limit in air with micro ATR-FTIR

imaging using a Ge crystal, allowing for the imaging of small features that were not previously resolvable.<sup>32,41-43</sup> Their work in macro-ATR imaging led to the development of the new Golden Gate diamond ATR accessory described above.<sup>32,38</sup>

While predominately focussing on applications for ATR-FTIR in the pharmaceutical industry, Kazarian's research in the field of macro ATR-FTIR hyperspectral imaging is applied across a number of industries including biomedical and pharmaceutical,<sup>44-48</sup> pharmaceutical counterfeiting<sup>49</sup> and polymer science.<sup>32,50</sup> Kazarian's research group also demonstrate examples in forensic science,<sup>51,52</sup> including the visualisation of fingerprints either deposited directly on the crystal or from tape-lifts<sup>53,54</sup> as well as fingermarks contaminated with small-particles.<sup>51,52,55</sup>

Forensic applications of ATR-FTIR hyperspectral imaging by other research groups include the areas of counterfeit pharmaceuticals,<sup>56</sup> document and handwriting analysis,<sup>57</sup> and the analysis of explosives<sup>58</sup> and gunshot residue.<sup>59</sup>

### **1.1.2 Raman Spectroscopy and Mapping**

Raman spectroscopy is another vibrational spectroscopic technique that differs from IR spectroscopy by using the scattering, rather than the absorption, of light by a sample.<sup>60</sup> Owing to its high specificity, low sensitivity to water and minimal requirement for sample preparation, Raman spectroscopy as an analytical tool is of significant interest.<sup>61</sup> The Raman signal results from the same type of vibrational energies described above for infrared. Raman is the converse of infrared, in that symmetrical vibrations of molecules yield strong Raman signals, making Raman spectra complementary to the information provided by FTIR.<sup>30,60</sup> Raman scattering is approximately  $10^{-10}$  times as likely as the corresponding mid-IR absorption, hence the collection of a Raman spectrum requires an intense light source (laser) to improve sensitivity.<sup>30</sup>

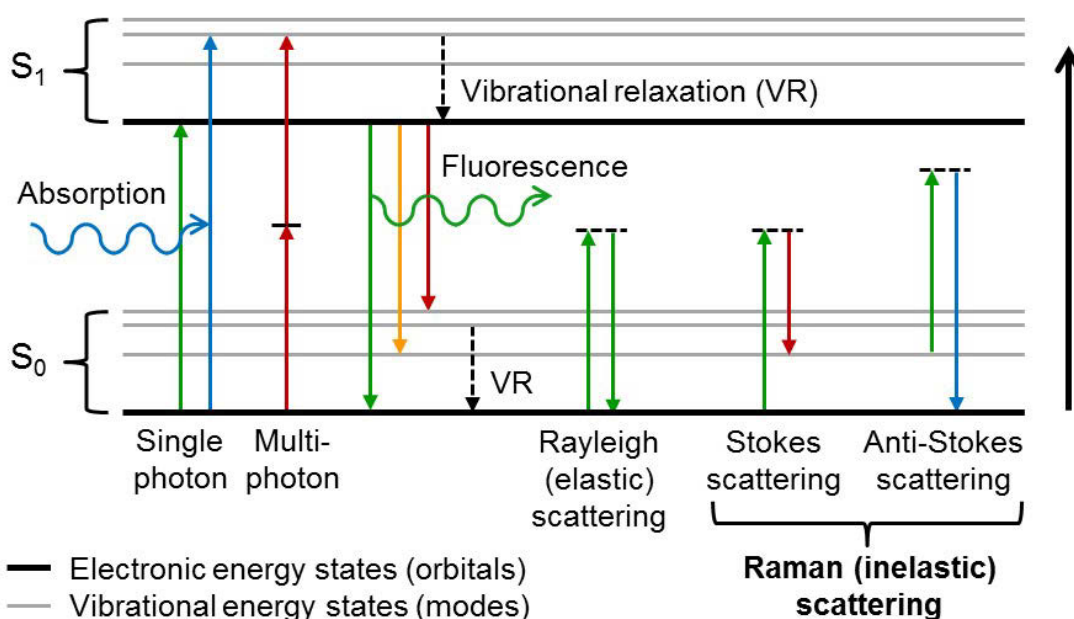


**Figure 1-4 Basic Jablonski diagram outlining energy transitions between electronic states and different types of Raman scattering.**

Monochromatic light, when irradiated onto a sample, will induce a change in dipole moment across a molecular bond. A photon is released (scattered) in order for the molecule to return to its ground state. Most photons are scattered at the same wavelength and this process is known as Rayleigh scattering.<sup>7,61</sup> Raman scattering occurs when these photons are scattered at a different wavelength (longer or shorter) than the incident light (See Figure 1-4).<sup>61,62</sup> The difference in energy between the incident photon and the Raman scattered photon corresponds to the vibrational energy of the molecular bond, and hence allows a spectrum to be plotted.<sup>62</sup> The main disadvantage of Raman spectroscopy is fluorescence. Many samples, even those that would not be considered fluorescent in normal circumstances, yield problematic levels of fluorescence in comparison to the low absolute level of Raman scattering observed.<sup>63</sup>

The two most common methods to minimise fluorescence are the use of surface-enhanced Raman spectroscopy (SERS) and changing the wavelength of the laser source.<sup>7,63</sup> The SERS technique involves the adsorption of a target analyte onto the surface of certain metals, followed by analysis using a Raman spectrometer. The most commonly used substrates are silver and gold.<sup>64</sup> Alternatively, fluorescence can be minimised by using higher wavelength near-infrared sources.<sup>7</sup>

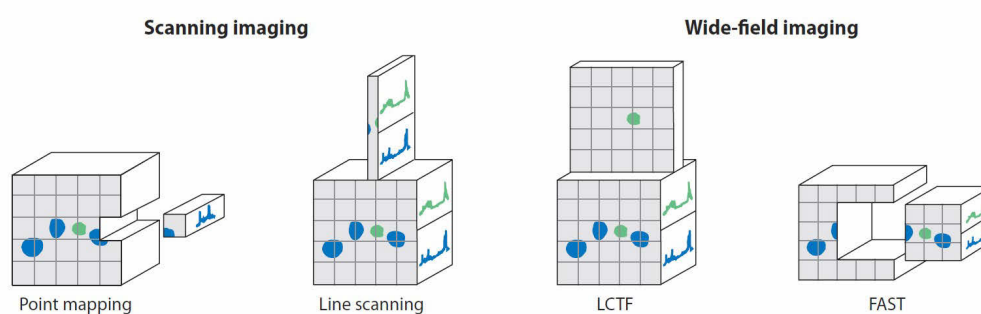


**Figure 1-5 Graphical comparison of Raman mapping and imaging capabilities. Adopted from Stewart et. al.<sup>61</sup>**

As for infrared spectroscopy, the collection of Raman hyperspectral data can also be performed. Generally, the methods used are mapping-based. Point-by-point and line mapping are the two main approaches used for the collection of Raman hyperspectral data (See Figure 1-5). Point-by-point Raman mapping is the simplest and most common.<sup>65</sup> A spectrum is acquired at each spatial location before the sample is moved to the next point using a mapping stage. The spatial resolution is limited by the spot size of the laser and the step size chosen by the operator or offered by the moving stage.<sup>3,61,65</sup> Line mapping offers more rapid image generation at the expense of spatial resolution. A cylindrical or Powell lens is used to focus the laser beam in one direction across the sample, and a spectrum is captured for each row on the detector, corresponding to a spatial location on the sample.<sup>61,66</sup> Global (wide-field or “true”) Raman imaging instruments are also available; here the entire sample is illuminated

and imaged onto the detector and a spectrum is collected for a discrete number of wavelengths.<sup>61,65</sup>

The use of Raman mapping and imaging is widespread, with examples including applications in the pharmaceutical field,<sup>48,67,68</sup> in materials analysis<sup>69,70</sup> and in the analysis of writing inks.<sup>71</sup> In a forensic context, Raman mapping has also been utilised for a number of applications; including the imaging of fingerprints treated with diacetylene copolymers,<sup>72</sup> the detection of trace materials on fingerprints,<sup>73,74</sup> and the detection of explosives on banknotes<sup>75</sup> and gunshot residue on adhesive tape.<sup>76</sup>

In contrast to ATR-FTIR hyperspectral imaging, the size of a Raman map or image is, theoretically at least, infinite. While the ATR technique is restricted by the size of the crystal, a Raman map can be made to cover an area defined by the user. In practice, this is restricted by the size or movement in the motorised stage. Other factors, such as time to acquire the data, and processing power/memory of the computer, would also play a factor in deciding the size of the map. For use in industry, the time taken to collect a map would be a major factor to determine whether a given technique would be viable for routine use. For example, a pharmaceutical company is unlikely to use Raman mapping to confirm excipient content in tablets if the map will take 24-48 hours to collect; however, in histological samples, it might be important that an entire tissue be imaged so that tumour cells can be identified. Thus, it is important that an ideal map size be determined for the purpose of the analysis, and to ensure that a reasonable cross section of the entire sample is captured. In the case of powders suspected to contain illicit substances, forensic testing regimes will more than likely include a homogenisation step; this ensures consistency across the sample. For tablets, the very nature of the tableting process is likely to play a role in homogenising the sample, but again, the majority of forensic testing processes include a crushing/homogenisation step for tablet samples.



Another contrasting feature between the collection of ATR-FTIR and Raman images is spatial resolution. The maximum resolution obtainable by ATR-FTIR is a function of the size of the crystal and the size of the FPA detector, and can only be altered by 'binning' or combining pixels (effectively averaging the spectra collected by adjacent pixels). In Raman mapping, the spatial resolution is governed by the spot size of the laser, and the chosen step-size between data acquisition points.

### **1.1.3 Fluorescence Landscapes**

#### *1.1.3.1 Fluorescence*

Luminescence is the emission of light from any substance and occurs from electronically excited states. Fluorescence is distinguished from other types of luminescence by its short life-time, of the order of nanoseconds. It typically occurs in aromatic and other compounds with delocalised  $\pi$  (pi) electrons, such as highly conjugated hydrocarbon chains.<sup>77-79</sup> Phosphorescence is another example of luminescence, and is characterised by life times of the order of milliseconds to seconds due to forbidden transitions (for example glow-in-the-dark items). This phenomenon is often illustrated by a Jablonski diagram. A basic Jablonski diagram is shown in Figure 1-6 below, outlining an electron's passage from a ground to an excited state and back again, releasing energy that can be measured.<sup>77,80</sup>

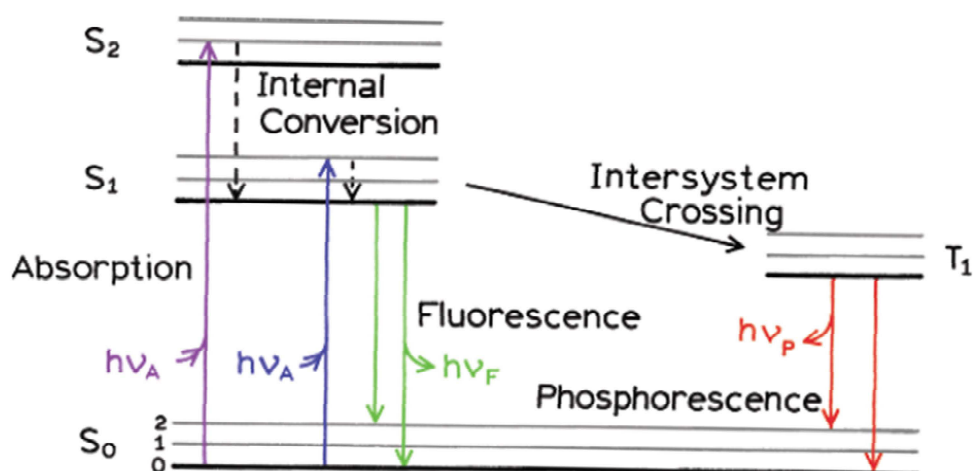


**Figure 1-6 Basic Jablonski diagram outlining energy transitions between electronic states. Adopted from Lakowicz.<sup>77</sup>**

A fluorescence (emission) spectrum is the plot of the fluorescence intensity as a function of wavelength, either on a nanometre (nm) or wavenumber ( $\text{cm}^{-1}$ ) scale.<sup>80</sup> Generally, a compound will have the same shape emission spectrum irrespective of the excitation wavelength used (Kasha's rule) and will only differ in intensity; exceptions to this include molecules with two ionisation states.<sup>77,80</sup>

### 1.1.3.2 Fluorescence landscapes

Fluorescence spectral data is generally presented as an emission spectrum for each single excitation wavelength.<sup>77</sup> Alternatively, fluorescence landscapes are obtained by the collection of a range of emission spectra at multiple excitations, yielding a landscape (see Figure 1-7) or excitation-emission matrix (EEM), as they are commonly known. The collection of EEMs is a powerful method for the analysis of complex mixtures.<sup>81,82</sup> The number of data points in a single landscape is equivalent to the multiplication of the number of excitation and emission wavelengths. It is common for a landscape to have thousands of data points. Chemometric analysis of the data is often required. While Figure 1-7 shows the graphical representation of a landscape or EEM, the data that is processed in this work is essentially a rectangular

matrix with rows and columns of excitation and emission spectra respectively. This data is extracted directly from the instrument used to collect the landscape.

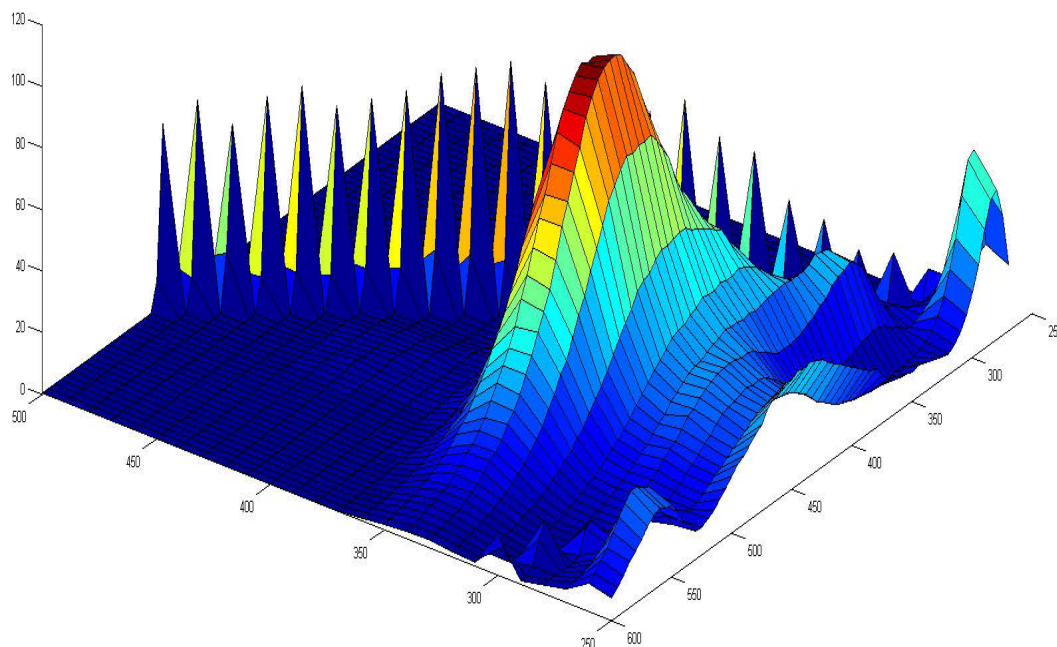


**Figure 1-7 Example of a fluorescence landscape, before removal of scattering (Ex: 250-500 nm).**

In fluorescence landscapes, Rayleigh and Raman scattering occurs in regions where the excitation and emission values are similar (see Figure 1-8). This scatter, seen as a diagonal line of very narrow peaks, can be more intense than the fluorescence of interest and is removed prior to the analysis of landscapes.

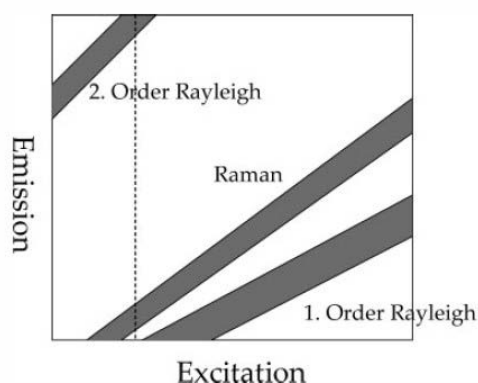


**Figure 1-8 Sketch of the scattering that often occurs in fluorescence EEM data. Adopted from Bahram et al.<sup>83</sup>**

Fluorescence landscape spectroscopy is a sensitive, fast and inexpensive analytical method; it has thus been applied in many areas of science, including pharmaceutical,<sup>84</sup> food<sup>85,86</sup> and hormone<sup>87</sup> analysis and the analysis of cervical swabs from pap smear examinations.<sup>88</sup> Its main application has been in environmental areas, looking at dissolved organic matter (DOM) in waterways.<sup>89-91</sup>

## 1.2 Unsupervised compositional analysis of data

Hyperspectral instruments generate large data sets, or data cubes, that cannot be taken full advantage of without the application of multivariate chemometric tools. These tools are therefore crucial in order to take advantage of the full data set and to extract any interpretable knowledge into a useful form. For the classification of spectral data in a qualitative and quantitative manner, there are two multivariate chemometric approaches, supervised (with *a priori* information) and unsupervised (without *a priori* information).<sup>92,93</sup>

A number of multivariate chemometric techniques continue to be applied to the analysis of hyperspectral images\* by different authors,<sup>94-98</sup> but there are few examples of using a one-hyperspectral-image-per-observation approach.<sup>20</sup> The vast majority of applications focus on the production of training data sets which are then used to predict information about an unknown, analogous to the use of library searching with single point vibrational spectroscopic libraries.

Two such unsupervised techniques are multivariate curve resolution (MCR) and simple-to-use interactive self-modelling mixture analysis (SIMPLISMA). These techniques are explored to determine if they can independently yield the sought after information from a single hyperspectral image, without any prior knowledge or training data sets.

### 1.2.1 Pre-processing methods

By their very nature, hyperspectral images contain a wealth of information; a consequence of this is that the raw data is often affected by noise or instrumental variations that can hamper the extraction of chemical information.<sup>93</sup> These signals can arise from a number of interactions including light scattering, cosmic ray spikes, particle-size effects and morphological differences such as surface roughness (tablets) and detector artefacts. Pre-processing is thus an important step that is applied prior to hyperspectral image analysis. It is employed to ensure the quality of the desired signal and avoid misleading conclusions by removing or reducing the influence of undesirable signals in the dataset.<sup>93,99</sup> There are many algorithms available for the pre-processing of spectral data; the choice of method will depend on the type of data (NIR, FTIR, Raman etc.) and the goal of the analysis.<sup>93,100,101</sup> For example, scattering may be disruptive for compound identification or quantification, but it can provide

---

\* While discussion in this section mentions hyperspectral “images” the same approach is applied to any form of hyperspectral data, including the data obtained in this research from Raman mapping and fluorescence landscapes (excitation-emission matrices).

useful information in studies on the physical properties of certain materials and thus should not be removed in these analyses.<sup>102</sup>

Careful consideration must be taken when choosing the pre-processing method and order of operation when combinations are used so as not to modify the shape of the data and thus introduce more data perturbations. Commonly-used spectral pre-processing tools for multivariate analyses are baseline correction, smoothing, normalisation and scatter correction.<sup>102,103</sup>

### *1.2.1.1 Linear Baseline Correction*

Baseline correction aims to adjust for spectral offsets in the data. It can be based on linear models or more complex mathematical functions.<sup>93</sup> Linear baseline correction involves choosing two variables (wavelengths) to define a new baseline; the correction sets the response of these wavelengths to 0 and the remaining wavelengths are transformed accordingly.

### *1.2.1.2 Normalisation*

Sample normalisation is considered a critical step in hyperspectral image analysis.<sup>99</sup> Many types of normalisation are available, depending on the needs of the application. Normalisation aims to remove intensity differences between spectra in an image; in some circumstances these can affect subsequent data analysis and must thus be treated with care.<sup>104</sup>

### *1.2.1.3 Principal Components Analysis (PCA) noise reduction*

A brief description of Principal Components Analysis (PCA) as a classification technique is given in Section 1.2.2.2. Basically, PCA is a pattern recognition tool, which allows for the simplified visualisation of a dataset. This can be used for a

number of applications, including dimensional reduction of data, and the removal of noise, without a significant loss of information.<sup>105</sup> This is performed by choosing the most significant components (according to the variability they contain) and recalculating the spectra based on these. The process of choosing the significant components can be highly subjective and thus careful consideration must be given when components are discarded, as removal of too many components can result in the loss of data or the introduction of spectral artefacts.<sup>105,106</sup> PCA noise reduction has been used on hyperspectral images prior to analysis by supervised chemometric techniques.<sup>107,108</sup>

#### 1.2.1.4 *(Extended) Multiplicative Scatter Correction ((E)MSC)*

Multiplicative scatter correction (MSC) is used to compensate for offset (additive) and/or amplification (multiplicative) effects in spectral data.<sup>109</sup> MSC is a two-step process that first estimates the correction coefficient required before correcting the recorded spectra.<sup>103</sup> In addition, extended MSC (EMSC) also corrects for wavelength-dependent spectral effects such as physical light scattering or chemical light absorbance effects in spectra.<sup>110</sup> The correction is performed by making a linear regression of each spectrum against a reference spectrum.<sup>109,111</sup> When no *a priori* information is provided, the average spectrum is used as the reference.<sup>99</sup>

### 1.2.2 “Analysis” techniques

#### 1.2.2.1 *Endmember techniques*

The end member approach involves two steps: (i) determination of end members (spectra), which can be either supplied from a reference library or extracted from the image; and (ii) classification of pixels in the image, based on the supplied/chosen endmembers. Two methods employed by ENVI, a widely used software package in

remote sensing and hyperspectral image analysis, are the Spectral Angle Mapper (SAM) and Spectral Feature Fitting (SFF).<sup>112</sup>

SAM is an algorithm that evaluates similarity between image and endmember spectra by treating them as vectors in an n-dimensional space. The angle between these vectors is measured; smaller angles represent closer matches to the reference spectrum. Spectra (pixels) are then classified based on a pre-determined threshold.<sup>113,114</sup> SAM has been used for the detection of opium poppy fields using hyperspectral data.<sup>115</sup>

The SFF algorithm compares the physical shape fit of the spectra from the image against reference spectra using a least-squares technique. The comparison can be visualised through the creation of a 'fitting' image for each pixel per endmember, and indicates how each image pixel (spectrum) resembles the endmember spectrum. SFF has been used in combination with SAM and remote sensing to study sandstone rock formations.<sup>116</sup>

### *1.2.2.2 Principal components analysis (PCA)*

Principal components analysis (PCA) is the most well-known of all chemometric methods and forms the basis of many classification, regression and multi-way methods.<sup>110,117,118</sup> The PCA method reduces the original data matrix into so called 'principal components'. The principal components model the statistically significant variation in the data as well as measurement error and each principal component is calculated to express the maximum variance in the data, in decreasing order.<sup>93,104,119</sup> However, principal components are abstract mathematical entities and thus themselves have no physical (or chemical) meaning.<sup>117</sup> It is often used as a data visualisation tool to find patterns, identify outliers and explore the data cube prior to the application of more complex chemometric methods.<sup>105</sup>



The use of PCA on hyperspectral image data is well documented. It has been used for data reduction,<sup>119,120</sup> band selection and classification in the field of remote sensing<sup>121</sup> and in the analysis of heterogeneous solids.<sup>20</sup>

### 1.2.2.3 Multivariate curve resolution (MCR)

Multivariate curve resolution (MCR) is an unsupervised chemometric method that aims to identify the pure components that make up a multicomponent system.<sup>122</sup> The assumption made by MCR is that the experimental data follows a linear model, or Beer-Lamberts law for spectroscopic data.<sup>123</sup>

$$D = CS_T + E$$

**Figure 1-9 Equation for multivariate curve resolution model**

Figure 1-9 shows how MCR decomposes the original two-way data matrix, **D**, into the product of two smaller matrices, **C** and **S<sub>T</sub>**, which, applied to spectroscopic data, are usually referred to as the relative concentrations and spectral profiles of the pure components, respectively. **E** is the error matrix.<sup>122,124</sup> Iterative and non-iterative resolution methods can be implemented to resolve the components. Iterative resolution methods are considered to be the most popular due to their flexibility to evolve during the process and yield profiles (spectra) that are chemically meaningful.<sup>125</sup> The alternating least squares (ALS) algorithm was among one of the first algorithms used for MCR and is the one employed in this research. For the remainder of this work MCR will refer to the MCR-ALS approach unless otherwise stated. MCR uses initial estimate spectra as an input to find optimised pure spectra for each compound.<sup>126</sup>

While MCR delivers impressive results from raw experimental measurements, there are two classes of ambiguities, rotational and intensity related, that may be associated with the recovered profiles. Tauler outlines that the intensity ambiguity is

always present in factor analysis and curve resolution and results in an unknown scaling of resolved spectra and concentrations.<sup>123,127</sup> Intensity ambiguities do not affect the qualitative results of MCR but are a problem for the resultant quantification of the pure components. Rotational ambiguities are more important and result from two or more components that are linearly independent, such that the estimated profiles will be an unknown linear combination of the true profiles. The extent of ambiguity can be managed by the use of constraints such as non-negativity, unimodality and closure.<sup>123-125</sup>

The ability of MCR to yield both qualitative and quantitative information with no prior information presents advantages with respect to classical multivariate calibration approaches such as Partial Least Squares (PLS), that require training sets of reference spectra in order to identify the pure components.<sup>125</sup>

The recent use of MCR to model data from separation methods is well documented.<sup>128-133</sup> Recent applications of MCR in vibrational spectroscopy are wide spread. It is predominantly used to model hyperspectral data and has been used in biological science,<sup>134,135</sup> including plant histology,<sup>136</sup> as well as in polymer,<sup>137</sup> pharmaceutical,<sup>138-140</sup> and remote sensing applications.<sup>141</sup> In the area of Forensics, MCR has been combined with vibrational spectroscopy in the detection of explosives on banknotes,<sup>75</sup> document<sup>142</sup> and ink<sup>143</sup> analysis and the identification of counterfeit pharmaceuticals.<sup>144</sup>

As described by the MCR model above, the output is the spectral profiles and relative concentrations of each pure component in the mixture. This has practical advantages for the current research as FTIR or Raman spectra of pure components can be searched through a library or (for expert users) examined and interpreted when a library reference spectrum is not available. An estimation of the relative purities relating to each of those components can also be calculated.

#### 1.2.2.4 *Simple to use interactive self-modelling mixture analysis (SIMPLISMA)*

Another un-supervised analysis technique is SIMPLISMA. This technique can also be considered a curve resolution technique<sup>124,145</sup> i.e. it aims to extract component spectra and concentrations with no prior knowledge. As suggested by its name, SIMPLISMA is an interactive modelling tool, which requires user intervention and decision making to arrive at the final solution. This has positive and negative implications for the current work which will be discussed in the relevant section.

As described by Windig and Guilment,<sup>146</sup> the SIMPLISMA approach of mixture analysis is a pure variable based method. Here, a pure variable is described as a wavelength in the collected spectra whose intensity is due to only one component in that mixture.

Thus, an assumption that SIMPLISMA makes is that each component has at least one pure variable.<sup>146</sup> For cases with highly overlapping variables, poor baselines or where no pure variables are present, the resolution can result in pure component spectra and concentrations that are exaggerated. The rationale behind this is that the "pure component" spectrum will contain contributions from other components in the mixture. The use of second or higher derivative spectra in the SIMPLISMA algorithm has been shown to be able to resolve the mixture data in these circumstances.<sup>147,148</sup> Generally, inverted second derivative spectra are used as they are recognisable to spectroscopists and contain positive peaks where the original spectra do. This is an intermediate step and the resolved results are expressed in terms of the conventional data.<sup>148,149</sup>

The pure variables in SIMPLISMA are found one-by-one. The 'purity' of a variable is represented graphically by a so called *purity spectrum*, for which the maximum value in each purity spectrum, represents the pure variable (wavelength) for the component being calculated.<sup>150</sup> An important aspect of a satisfactory SIMPLISMA model is the

correct determination of the number of components. An underdetermined model will result in incorrect spectra and an overdetermined model will start to model the error or noise in the data. As SIMPLISMA is an interactive method, the determination of the correct number of components is performed by analysing the diagnostics of the current algorithm step.<sup>150</sup>

As for MCR above, the output of SIMPLISMA is the spectra of the pure components, along with their relative concentrations. SIMPLISMA has been applied to aid in the identification of essential oils by GC-MS,<sup>151,152</sup> the analysis of mono-aromatic hydrocarbon environmental contaminants by Raman spectroscopy,<sup>153</sup> and reaction kinetics.<sup>154,155</sup> SIMPLISMA has also been used to obtain initial guesses for an MCR-ALS analysis of Raman spectra.<sup>156</sup>

The interactive nature of SIMPLISMA can be disadvantageous in some applications as knowledge of IR spectroscopy and the basic chemistry of the compounds in the mixture may be required.<sup>157</sup> In the current research, some of the intended end-users (front of line police and customs officers) do not necessarily possess these skills and thus additional training would be required. The automation of SIMPLISMA has been demonstrated and may alleviate the need for the hands-on application of the algorithm.<sup>153</sup>

### **1.3 Parallel factor analysis (PARAFAC)**

Parallel factor analysis (PARAFAC) is a method commonly used to model fluorescence excitation-emission data, or matrices (EEMs). Compared with principal components analysis (PCA), PARAFAC can be thought of as a simpler, but more constrained version. Furthermore, it is capable of modelling data in higher dimensional arrays than PCA, and uses fewer degrees of freedom to generate a model. Consequently, PCA will usually result in a better fit of the data than PARAFAC, generally because the extra degrees of freedom allow for the modelling of noise. Additionally, the

constrained nature of PARAFAC results in a more robust and interpretable model than PCA.<sup>85,158,159</sup>

Bro<sup>160</sup> has effectively reviewed the application of PARAFAC to model EEMs, with approximately 50 applications, ranging from the analysis of pesticides at parts per trillion (ppt) concentrations to the analysis of drugs in plasma.

Important assumptions for a successful PARAFAC model include variability between the landscapes of components within a mixture and that the data obeys Beers Law, i.e. the fluorescence increases approximately linearly with concentration and the total signal is an approximate linear superposition of a number of components.<sup>161</sup>

While for the most part, the data contained within EEMs complies with the tri-linearity requirement for PARAFAC, light scattering effects known as Rayleigh and Raman scattering do not. First and second order Rayleigh scattering is the most common. First order Rayleigh scattering is the most intense and occurs where emission equals excitation. Second order Rayleigh scatter occurs where the emission equals twice the excitation.<sup>161</sup> Raman scattering is less common, and depends on the solvent used with the sample. It occurs at certain energy differences from the first order Rayleigh scatter line.<sup>162</sup> This scattering must be removed prior to the application of PARAFAC. Methods have been developed in software packages (e.g. the N-WAY<sup>163</sup> and DOMFLUOR<sup>89</sup> toolboxes for MATLAB) that remove Rayleigh and Raman scattering and noise from selected regions of the landscape. This pre-processing is an important aspect: it renders the data more suited to PARAFAC modelling and makes the resulting models easier for the end user to interpret.

### 1.3.1 The PARAFAC model

A PARAFAC model of a three-way array is described by three loading matrices, A, B and C, and the model can be written as:

$$x_{ijk} = \sum_{f=1}^F a_{if} b_{jf} c_{kf} + e_{ijk}$$

**Figure 1-10 Equation for PARAFAC model**

where  $x_{ijk}$  is the intensity of the  $i$ th sample at the  $j$ th variable (emission) and at the  $k$ th variable (excitation), and  $a$ ,  $b$  and  $c$  are the  $f$ th columns of the loading matrices for  $F$  number of components. The residuals,  $e$ , contains the variation not captured by the model.<sup>86,160,164</sup>

PARAFAC is a decomposition model that results in the minimum number of components, each consisting of:

- one score vector (**A**), yielding the relative ratio, or concentrations of the component;
- Two loading vectors (**B** and **C**) which represent the excitation and emission spectra of the pure component.

An important advantage of PARAFAC over conventional statistical modelling techniques is the uniqueness of the solution, and the resulting true spectra (in the form of landscapes) of a complex sample.<sup>85,165</sup> The true landscape of each component is visualised by the multiplication of A, B and C above.

## 1.4 Project Aims

This project is divided into two parts i) the use of ATR-FTIR hyperspectral imaging and Raman mapping for the preliminary analysis of illicit drugs and ii) to study the potential of fluorescence landscapes for the analysis of explosives. Overall the project aims to develop methods which will give front line forensic practitioners more information than currently available techniques when an unknown substance is presented to them.

ATR-FTIR spectroscopy is commonly used for the preliminary identification of illicit drugs but has some limitations, particularly when an adulterated sample or mixtures are encountered. This project seeks to advance current methods to aid in the identification of compounds that may have otherwise been classified as 'unknown' under currently-used methods. Additionally, the method will aim to provide further information about other components present in a mixture and the relative amount (purity) of each component. This rapid collection of information can be immediately used in intelligence-led policing to combat the ever-growing illicit drug trade.

The analysis of mixtures of explosives is commonly performed by chromatographic means. The current project explores the potential of PARAFAC, applied to fluorescence landscapes to detect and quantify mixtures of organic explosives at trace level concentrations. The focus of this feasibility study was to identify methods that could realistically be performed in-field, such that the presence of an explosive could be identified, regardless of whether in trace amounts in post-blast scenarios or if encountered in bulk.

***Chapter 2: Advanced vibrational  
spectroscopic techniques for the  
analysis of illicit drugs***



# Chapter 2: Advanced vibrational spectroscopic techniques for the analysis of illicit drugs

## 2.1 Introduction

### 2.1.1 Illicit Drugs

Australian drug seizure data reports a growing number of drug seizures at the international border and on Australian streets. The most recent Australian Illicit Drug Data Report (IDDR) reveals that a record 27.3 tonnes of illicit drugs were seized across Australia during the 2013-14 reporting period.<sup>166</sup> The high seizure amounts have been observed not only for the four main drug types - cocaine, heroin, 3,4-methylenedioxymethamphetamine (MDMA, or 'ecstasy') and methamphetamine - but also in a relatively new group of drugs termed *new psychoactive substances* (NPS).

Many preliminary illicit drug identification (PIDI) techniques are available for use by law enforcement agencies (LEAs). These techniques range from colour (or spot) tests, to commercial handheld or benchtop spectroscopic techniques such as Fourier Transform Infrared (FTIR) or Raman. These techniques are primarily aimed at identifying, to a reasonable standard, the presence of a banned substance so that grounds for arrest can be established and/or the suspected banned substance can be seized. These PIDI techniques can be problematic in the identification of NPS due to the number of different compounds available to drug suppliers and the delay in LEAs' ability to keep up to date with analytical standards for new compounds. Furthermore, the presence of multiple compounds in a mixture can be difficult for current PIDI techniques to identify; this is especially true for low purity mixtures, where the cutting agents dominate the collected signal. Current PIDI methods do not provide any information on the purity of the samples being tested.

At the Australian border, potential illicit substances are usually first encountered by Australian Border Force (ABF). Based on the results of the PIDI tests, ABF will undertake their own investigation or refer the consignment onto the Australian Federal Police (AFP) for investigation. The AFP will conduct further PIDI on the samples before the seized material is sent on for further confirmatory analysis by an accredited laboratory. The process is slightly different for State and Territory LEAs, but all jurisdictions utilise PIDI techniques in some capacity. In some jurisdictions, the confirmatory analysis of the compounds present and determination of purity can take months to obtain. In others, the purity is not required for prosecution and is never determined.

In a movement towards intelligence-led policing<sup>167</sup> many policing agencies would benefit from more intelligence (such as purity and other components in the mixture) about the suspected illicit substance as it is encountered rather than awaiting results from the confirmatory analysis. Currently, the majority of PIDI techniques rely on known reactions or libraries of spectra to be able to identify a banned substance. With highly cut (diluted) samples, or samples of drugs that have not yet been encountered/entered into the spectral library, there is little information available to the agency and little that a user can do to definitively identify the components of a sample. Some handheld devices do not allow the collected spectra to be viewed, meaning that any attempt at spectral interpretation is not possible.

### **2.1.2 ATR-FTIR hyperspectral imaging**

One potential application of ATR-FTIR hyperspectral imaging is the classification and purity estimation of illicit drugs and cutting agents from a single observation (a single hyperspectral image). ATR-FTIR hyperspectral imaging was chosen for this work for a number of reasons. Primarily, conventional single-point ATR-FTIR is a familiar technique for front-line forensic practitioners. Additionally, it provides a non-destructive method to collect a large number of highly characteristic spectra from a

sample in a relatively short time frame, noting that a spectrum is collected at each pixel of the FPA detector in a simultaneous measurement. An FPA detector typically has thousands of pixels, so a very large amount of data is collected in each image.

Prior to the development of hyperspectral imaging, a multicomponent sample could only be represented by one spectrum that averaged contributions from the substances it contained. Hyperspectral images, however, can contain a variety of pure and mixed constituent spectra whose relative abundances are characteristic of the sample. Ultimately, this results in a larger number of spectra available to improve the identification and quantification of the sample.

As outlined in Section 1.1.1.1, a wide variety of applications for ATR-FTIR hyperspectral imaging have been published, including the analysis of heterogeneous solid samples.<sup>20,41,168-170</sup> These examples demonstrate that this technique has the potential to deliver on the aims outlined for this research.

The miniaturisation of ATR-FTIR instruments is now wide-spread, with a number of portable and hand-held varieties on the market at different levels of sophistication. Examples include the Smiths Detection HazMatID and the Agilent Technologies 4500 Portable FTIR. As these devices rely on single point spectroscopy, they attempt to resolve the components of a mixture based on one spectrum, and depend on the spectra saved in the on-board spectral libraries for a match. It is hypothesised that with advances in technology, hyperspectral variations of these instruments could be developed.

### **2.1.3 Raman mapping**

Much like ATR-FTIR hyperspectral imaging, Raman mapping has the potential to address some of the short comings of conventional PIDI techniques, as it also offers a non-destructive method to collect a large number of spectra. However, the collection of a Raman map can take considerably longer than a single spectrum or a

hyperspectral image, as the spectra are not collected simultaneously as in FTIR imaging. Much like FTIR, Raman spectroscopy is also a familiar technique for front-line forensic practitioners, with many LEAs incorporating the use of handheld Raman devices such as the Thermo Scientific FirstDefender™ or TruNarc™ in PIDI analysis. Depending on their level of sophistication, some hand-held devices (such as the TruNarc™) do not allow the user to view the spectrum and thus no options for interpretation are available for materials that do not get a 'hit' against the on-board library. Furthermore, information about purity or adulterants and diluents is not provided by current handheld instruments, unless the spectrum of a mixture of similar composition has been loaded into the library.

#### **2.1.4 MCR and SIMPLISMA**

No previous studies have utilised ATR-FTIR hyperspectral imaging or Raman mapping combined with MCR or SIMPLISMA for the analysis of illicit drugs (see sections 1.2.2.3 and 1.2.2.4 for a description of these techniques). Forensic applications of MCR applied to hyperspectral images are limited to document forgery<sup>126</sup> and the detection of explosive residues on the surface of banknotes.<sup>75</sup>

The application of SIMPLISMA to the field of forensic science has been limited to aiding the interpretation of the results obtained from ion mobility spectrometry (IMS) in the screening of explosive and drug residues at airports and crime scenes,<sup>171,172</sup> in the visualisation of latent blood stains on fabric<sup>173</sup> and in the analysis of automotive paints.<sup>172,174</sup>

#### **2.1.5 Aims**

In this project, the aim was to investigate the potential of advanced spectroscopic techniques to improve the information obtained from current PIDI techniques and thus better inform LEAs. Two techniques were trialled, ATR-FTIR hyperspectral imaging and Raman mapping. These were coupled with the unsupervised

chemometric techniques SIMPLISMA and MCR to identify the compounds present in the mixtures.

To improve on current PIDI methods, these techniques must not only provide an identification of the main component (drug) in the mixture but also other minor components, such as other drugs or cutting agents. Additionally they should provide rough estimates of the purity of each component for policing intelligence purposes. The effectiveness of these techniques in comparison to a currently used handheld device will also be examined.

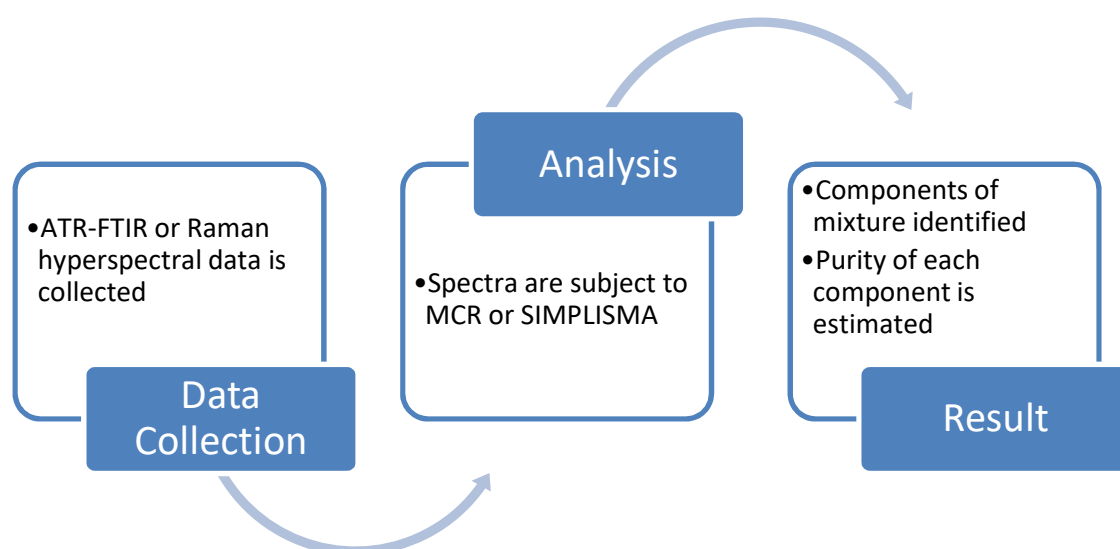


**Figure 2-1 Basic outline of process and expected results.**

The above figure outlines the relatively simple process that is proposed in this research, with the targeted output as described above. Importantly this process yields an advantage over current techniques by identifying multiple components in a mixture and estimating their corresponding purities. If a calculated component cannot be matched to an appropriate spectrum in the library, the spectrum of that component is made available for spectral interpretation by an expert.

## **2.2 Experimental and data analysis methods**

### **2.2.1 Sample preparation**

Powder mixtures consisting of up to three components were prepared, with each component present at a fixed level between 15 and 85% w/w of the mixture as per Table 2-1 below. Unless otherwise stated, caffeine (CAF), paracetamol (PAR), glucose (GLU), microcrystalline cellulose (MCC), dimethylsulfone (DMS), magnesium stearate and phenylethylamine hydrochloride (PEA) were purchased from Sigma-Aldrich and used as supplied, without further grinding or refinement. For particle size experiments each component was individually ground with a mortar and pestle, and then sieved, with the desired particle size fraction retained for use.

Each mixture was made by accurately weighing out the desired amount of each component and then mixing on a roller mixer for approximately 1 hour. The mixture was either analysed as a powder, or pressed into two 'tablets' by use of a KBr press. Multiple infrared images and/or Raman maps were collected from each sample.

Mixture	X (%)	Y (%)	Z (%)
XY1	15	85	0
XY2	30	70	0
XY3	45	55	0
XY4	50	50	0
XY5	60	40	0
XY6	70	30	0
XY7	85	15	0
XYZ1	15	25	60
XYZ2	15	52	33
XYZ3	15	25	60
XYZ4	15	60	25
XYZ5	25	15	60
XYZ6	33	15	52
XYZ7	34	33	33
XYZ8	40	45	15
XYZ9	45	40	15
XYZ10	52	33	15

**Table 2-1 Compositions of the powder mixtures. XYZ may not relate to the same substance in all examples; combinations of these were developed for each analysis.**

A case sample of illicit material was provided by the AFP under strict reporting, storage and usage guidelines.

## 2.2.2 Instrumentation and data collection

### 2.2.2.1 FTIR

ATR-FTIR hyperspectral images were collected using a Digilab<sup>†</sup> Stingray system, comprised of a FTS 7000 FTIR spectrometer coupled with a UMA 600 IR microscope and a Lancer 64 × 64 focal plane array (FPA) detector. The large sample compartment was equipped with a specially designed diamond ATR accessory for hyperspectral imaging, the Imaging Golden Gate<sup>™</sup> (Specac/Varian). Images and

<sup>†</sup> Digilab Inc, next known as Bio-Rad, then Digilab LLC and followed by Varian Inc., has now been acquired by Agilent Technologies. The company name is given as it appears on the instrument/software used.

spectra were collected and processed with Varian Resolutions Pro™ software. Spectra were collected between 4000 and 900  $\text{cm}^{-1}$  at a resolution of 4  $\text{cm}^{-1}$ , and each hyperspectral image consisted of 4096 spectra. The sampling area was approximately 1.1 x 1.1  $\text{mm}^2$ , which translated to a spatial resolution (pixel size) of approximately 17 x 17  $\mu\text{m}$ . This was the area over which each spectrum is 'averaged'.

Tablets or powder samples were placed on the sampling area of the Golden Gate ATR accessory. With the aid of a torque wrench, the maximum pressure of 160 lbs was applied to the anvil to achieve even contact across the surface. Some tablets, particularly those low in glucose or microcrystalline cellulose content, broke into pieces while being sampled.

ATR-FTIR 'in-field' analysis was performed on a Smiths Detection HazMATID 360 as currently used by Australian Federal Police crime scene teams. Single point ATR spectra were collected on the diamond crystal interface with the user-saved PIDI method. Spectra were collected and library searching performed with HazMatID software v3.1 the on-board software. Spectra were collected with 64 co-added scans between 4000 and 650  $\text{cm}^{-1}$  at a resolution of 4  $\text{cm}^{-1}$ . Following the initial match, a search of the residual was performed to determine whether a second component could be identified.

#### 2.2.2.2 *Raman*

Raman experiments were performed on a Renishaw inVia Raman Microscope. The software used to edit and process the spectra in the first instance was WIRE 3.1 (Renishaw, Gloucestershire, United Kingdom) instrument control software. Spectra were collected using a 785 nm laser with a 50x objective, laser strength of 10% and an exposure time of 10 seconds using an extended SynchroScan of 2000-120  $\text{cm}^{-1}$ .

For Raman experiments, powders or tablets were placed on the microscope stage and then focussed under white light prior to collection of a visible light image montage.



Raman mapping was performed on a pre-determined area of the image with steps of 125  $\mu\text{m}$ . FocusTrack™ was used to limit deviations in focus across the surface of the powder/tablet.

A trial using FT-Raman was performed on a Nicolet iS50 Raman Module (Thermo Fisher Scientific, Madison WI). Spectra were collected using a 1064 nm laser at 0.2 W with 256 scans and a resolution of 8  $\text{cm}^{-1}$ .

## 2.2.3 Data Pre-processing

### 2.2.3.1 ATR-FTIR

For data to be analysed using the MCR technique, pre-processing was performed in The Unscrambler (CAMO Software, Oslo, Norway) software package. The ATR-FTIR spectra were truncated to 900-1750  $\text{cm}^{-1}$  in order to remove variables which were unlikely to have a high discriminating power. Following the spectral truncation, linear baseline correction and Savitsky-Golay seven-point smoothing were performed prior to analysis.

For data to be analysed using SIMPLISMA, spectral truncation was performed on the data using MATLAB (MathWorks®). The spectra were truncated as per above. Normalisation and Savitsky-Golay five-point smoothing were performed using the Cytospec™ GUI (64-bit) for MATLAB.

### 2.2.3.2 Raman

For Raman data analysed by MCR, pre-processing was performed in The Unscrambler X (CAMO Software, Oslo, Norway) software package. The most accurate and reproducible results were obtained by truncating the spectra to 2000-251  $\text{cm}^{-1}$ , and performing linear baseline correction and Savitsky-Golay five-point smoothing.

For Raman data to be analysed with SIMPLISMA, the regions that did not provide discriminating power were marked inactive, effectively truncating the spectra to 2000-251  $\text{cm}^{-1}$ . Savitsky-Golay five-point smoothing was performed prior to analysis.

## 2.2.4 Data analysis

As described below, MCR and SIMPLISMA algorithms were run in separate software packages, but importantly the output from each package allowed for the results to be treated in a similar manner. This also meant that the performance of each method could be accurately compared to the other.

### 2.2.4.1 *Multivariate Curve Resolution (MCR)*

MCR was performed using The Unscrambler X (CAMO Software, Oslo, Norway). The maximum ALS iterations allowed was set to 5000 and sensitivity to pure components was set between the minimum value of ten (10) and fifteen (15). Non-negativity constraints were placed on spectra and resulting concentrations. The additional option of supplying the MCR with *initial estimates* of pure spectra was trialled. Spectra for this work were collected as per the procedures outlined above.

MCR is an automated process that outputs the individual spectra of the pure components with the corresponding contributions of each component at each pixel. All further calculations were performed via automated scripts written with the AutoIt software package and Visual Basic macros written for Microsoft Excel.

### 2.2.4.2 *SIMPLISMA*

SIMPLISMA was performed using the ACD/UV-IR processor module of ACD/SpecManager (Advanced Chemistry Development, Inc. Toronto, Canada). Unlike MCR, the SIMPLISMA algorithm requires user intervention to decide the ideal pure variable at each stage of the analysis and importantly, to stop modelling at the

correct number of components. A range of in-built statistical tools are made available to the operator and are designed to assist in determining the correct number of components.

As for MCR, the output from SIMPLISMA is the spectra of the pure components with their corresponding contributions to each pixel. All further calculations were performed via automated scripts written with the AutoIt software package and Visual Basic macros written for Microsoft Excel.

## 2.3 Results and Discussion

### 2.3.1 Choice of compounds

The compounds used in the analysed mixtures were chosen based on compounds commonly encountered as cutting agents in illicit drugs. The compound phenylethylamine is a legal alternative that is closely related in structure to a number of illicit drugs and was chosen as a substitute for illicit samples.<sup>175</sup>

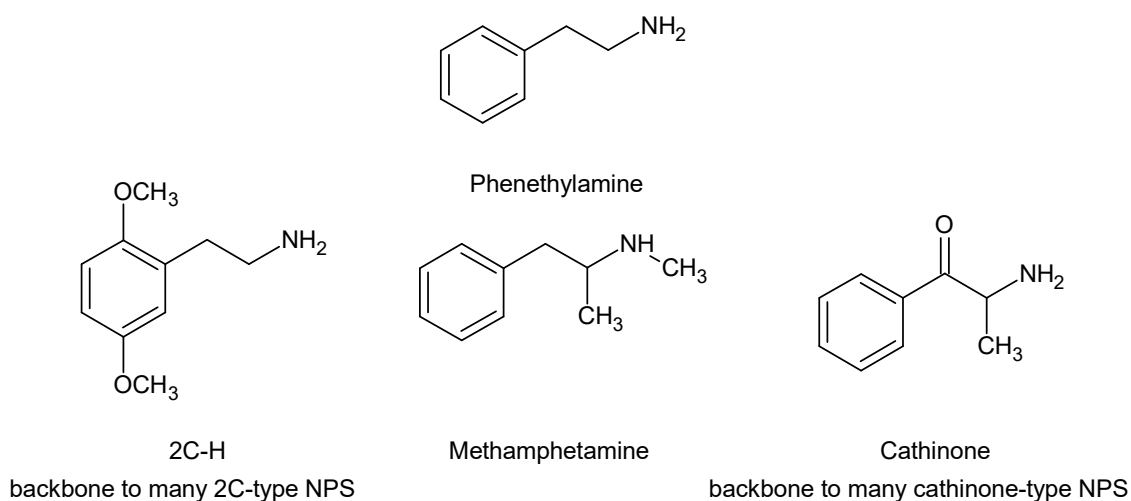


**Figure 2-2 Chemical structure of phenylethylamine and some common illicit drugs encountered by Australian LEAs.**

Previous research has referred to the effect that variations in particle size can have on the estimation of the composition of heterogeneous solids using hyperspectral imaging.<sup>176</sup> However, in the current work, to mimic the samples that may be presented to LEAs, compounds were used as received without any further refinement, grinding or sieving, unless otherwise stated.

Case samples were chosen based on those made available to the project, as supplied by the AFP.

## **2.3.2 Data collection considerations**

### *2.3.2.1 Collection of ATR-FTIR hyperspectral images*

Initial experiments with a ZnSe ATR crystal were unsuccessful as, when firmly pressed, many powders and tablets caused damage to the surface of the crystal; this not only damaged the accessory but also affected the quality of the collected spectra. The Specac Imaging Golden Gate diamond ATR imaging accessory was therefore used for the remainder of this research. Given the relatively large sample area ( $\sim 1.1 \times 1.1 \text{ mm}^2$ ) compared with single point ATR-FTIR measurements, it was observed that consistent contact across the area of the diamond was a major factor in the end result. Figure 2-3 outlines the effect that pressure variation across the sampling area has on the intensity of the spectra collected.

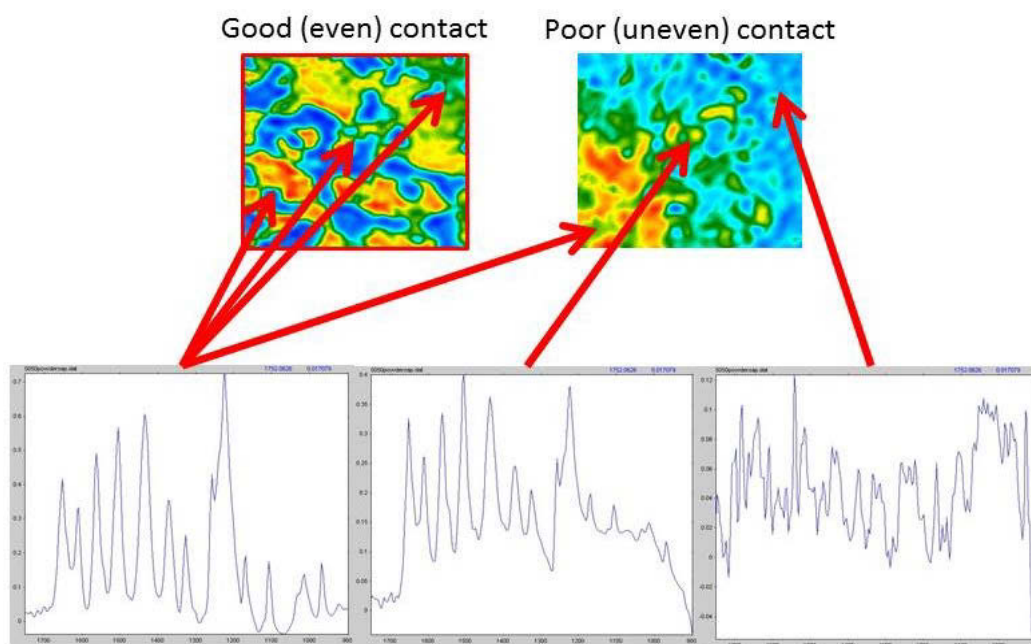


**Figure 2-3 Examples of hyperspectral images resulting from good and poor contact between sample and ATR crystal.**

This has previously been documented by Chan and Kazarian,<sup>43</sup> who showed that poor contact between the sample and ATR crystal could lead to an image that shows an apparent heterogeneous distribution of a substance when in fact it is an image with poor contact quality.

The load capability of the Specac Diamond ATR accessory was increased from the standard 80 lbs to 160 lbs with the use of a torque wrench. This was found to solve the poor contact issue for all powder and tablet samples, but caused some tablets to be crushed under the anvil, particularly those with low levels of glucose or MCC.

### 2.3.2.2 Selection of Raman laser

The instrument used in this research was equipped with 635 nm (red) and 785 nm (near-IR) lasers.

Initial experiments were performed with a 635 nm laser as the 785 nm was not available for use throughout the entire research project. Due to high fluorescence of the samples under this laser, a very low Raman signal-to-noise ratio was obtained,

which could not be appropriately corrected for with pre-processing methods. The use of the 785 nm laser resolved fluorescence issues for the test samples and significantly increased the signal-to-noise ratio. Thus all Raman data reported in this project were collected with the 785 nm laser as per the outlined procedure above.

The MDMA tablet supplied by the AFP exhibited strong fluorescence under both the 635 nm and 785 nm lasers, and so the FT-Raman instrument equipped with a 1064 nm laser was trialled for the analysis of this sample, and the fluorescence issue was resolved.

### 2.3.2.3 *Particle vs pixel size*

Overall, the goal of this research was to determine if hyperspectral imaging could be used to identify components in a mixture and provide an estimation of their purity. Over the course of this work, a greater understanding of the relationship between the particle size of the solid analysed and the pixel size of the detector was achieved. Previous research had shown that the particle size of powders could affect classification results in hyperspectral imaging experiments.<sup>176</sup>

Based on the size of the FPA detector on the FTIR instrument and the sampling area on the ATR crystal, the effective pixel size (i.e. the area that each spectrum is collected from) was approximated to be  $17 \times 17 \mu\text{m}^2$ . Potentially, the particle size of the powder analysed in relation to the effective pixel size of the detector could greatly affect the results obtained in two ways.

First, it was hypothesised that if the particle size of the powder was much smaller than the size of the pixel, then the response from each pixel would simply be an average of the components in the mixture, thus negating the advantages of hyperspectral imaging. If the particles are much larger than the pixels, hyperspectral images may be dominated by one component and thus not give a true representation of the mixture composition (see Figure 2-4 below). Secondly, it has been observed in

our laboratory that if one component is in the form of extremely fine particles, these finer particles can coat the coarser ones, resulting in an image that is dominated by spectra of the finer material.

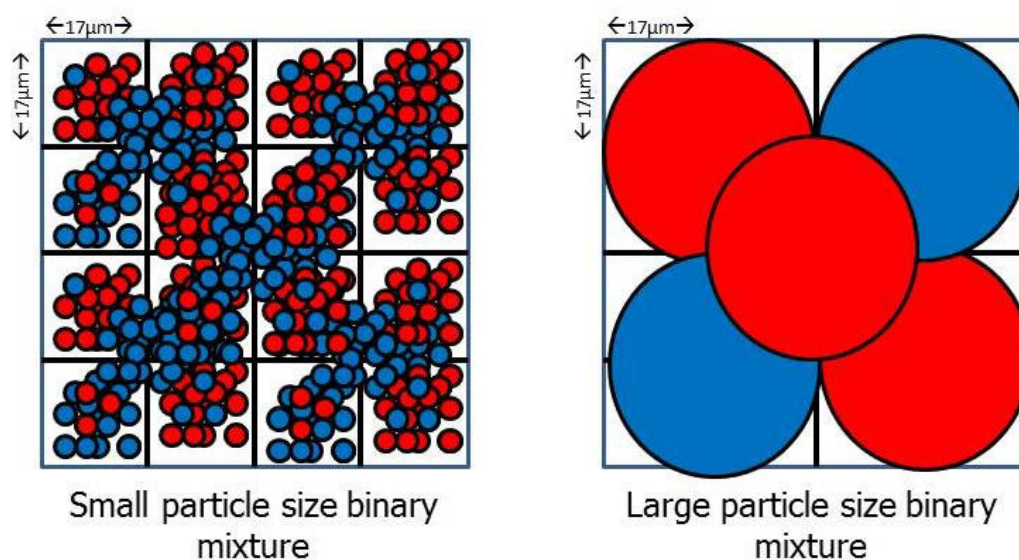


**Figure 2-4 Graphical representation of the hypothesis regarding variation of particle size in FTIR-ATR hyperspectral imaging.**

The option to 'bin' or aggregate pixels would not reduce the above two issues as the sampling area of the ATR is fixed. Aggregating pixels would only average out the collected spectra even further rather than provide any further discriminating features. Furthermore, using fewer spectra than collected by programmatically excluding them from the analysis did not provide any advantage. This effectively results in a greater separation between collected data points and is analogous to using larger step-sizes as discussed below for the collection of Raman spectra.

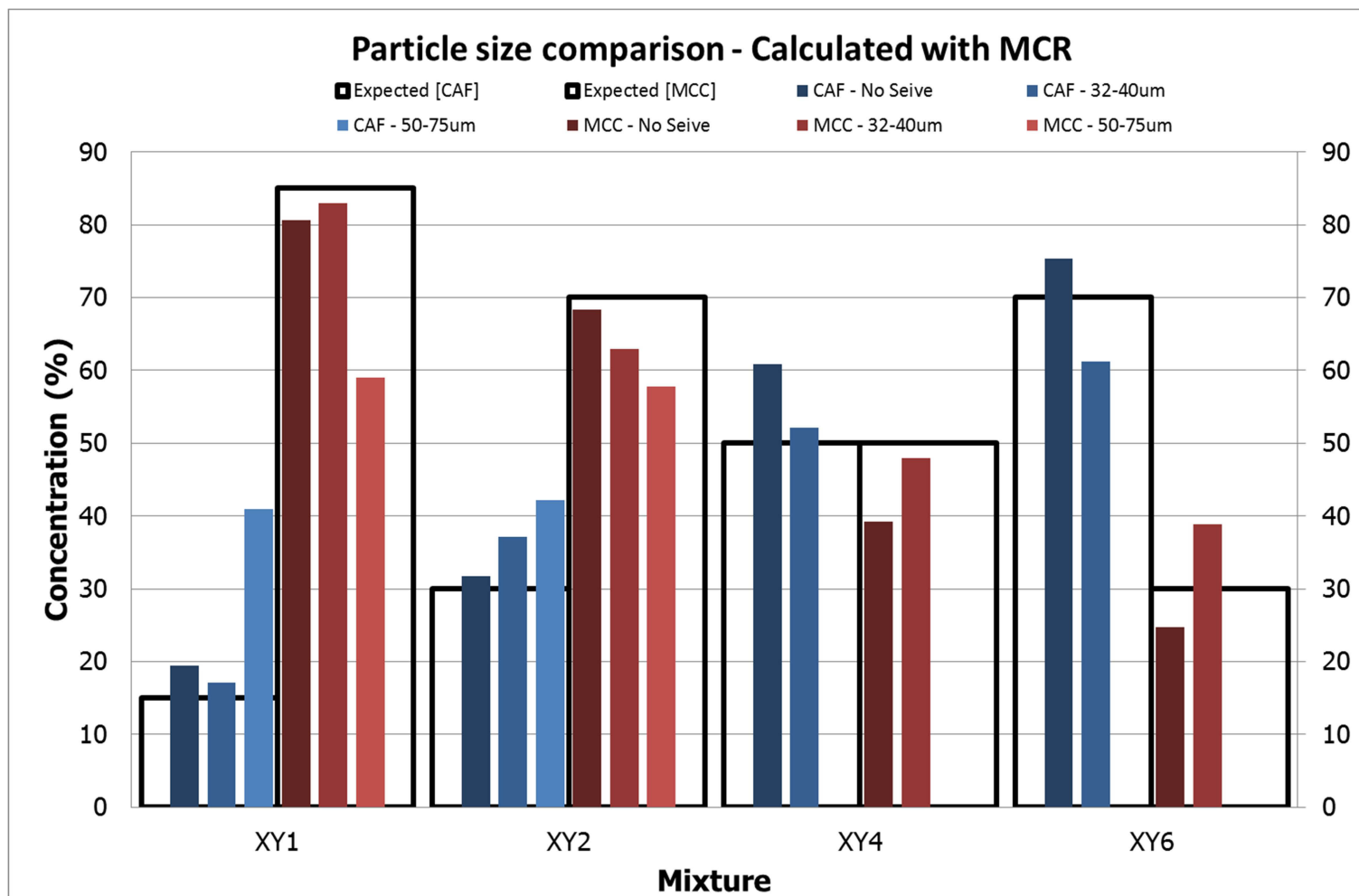
It was acknowledged that, unlike pharmaceutical companies, the operators of clandestine laboratories are unlikely to ensure that their product has a narrow range of, or even consistent particle sizes. Thus, it was clear that, in the real world, the particle size of the samples could not be controlled. The effect of particle size on the overall result must thus be determined.

Figure 2-5<sup>‡</sup> below outlines the effect of varying particle size in a binary mixture of caffeine (CAF) and microcrystalline cellulose (MCC). As demonstrated in Figure 2-5, sieving had little effect on the ability of this technique to identify components in binary mixtures and their relative abundances. However, MCR yielded the most similar results on mixtures not sieved and those sieved to 32-40  $\mu\text{m}$ . MCR was not able to resolve correct profiles for the 50:50 and 65:35 mixtures of the binary mixtures that had been sieved to 50-75  $\mu\text{m}$ . One hypothesis to explain this is that the 50-75  $\mu\text{m}$  sieved samples are the most different to the pixel size of the ATR ( $17 \times 17 \mu\text{m}^2$ ) i.e. the scenario set out above for large particles in Figure 2-4 above is occurring.

---

<sup>‡</sup> A guide to interpreting the graphs used in this thesis can be found in Appendix 1.





**Figure 2-5 Effect of particle size on the apparent composition of Caffeine (CAF) and microcrystalline cellulose (MCC) mixtures using multivariate curve resolution (MCR).**

Given the similarity in results between unsieved and 32-40  $\mu\text{m}$ , it was decided to analyse all powders as they were received, with no further grinding or sieving. Furthermore, attempts to process and sieve real world samples, which are unlikely to have a uniform particle size, may change the final ratio of components as they separate into different particle sizes.

In Raman mapping experiments, the resolution of the "image" collected depends on the focussed laser spot size and the size of the step between adjacent points. Using the 50x objective, the focussed spot size is typically about 1  $\mu\text{m}$ ; in these experiments, the step size was much larger than this. Greater flexibility can be achieved with Raman as the spacing between measurements can be modified for each sample upon visual inspection through the microscope. As described further in Section 2.3.4.2 below, the spacing between points in Raman mapping did not have a significant influence on the results, so the spacing between collection of spectra were chosen to be larger than the average particle size observed.

### **2.3.3 End member classification**

Initial classification experiments were performed using the "spectral hourglass wizard" in ENVI. ATR-FTIR images of two- and three-component mixtures of caffeine, paracetamol and MCC were collected. In ENVI, both the spectral angle mapper (SAM) and spectral feature fitting (SFF) algorithms were explored. Both algorithms accurately predicted the concentrations of two component mixtures when supplied with known spectra of the individual components ('endmembers'), often yielding results with purity estimation similar to that of the true value. However, with no priori information, they usually failed to recover the correct pure endmember spectra of the components in a mixture. Instead, significant bands from both components were apparent in each of the calculated 'pure' spectra. These spectra therefore did not match any of the library spectra, and purity/composition calculations could not be carried out. This approach thus provided no advantage over other currently used

calibrating methods such as partial least squares (PLS) regression. Furthermore, it was decided that an advanced level of knowledge in spectroscopy was required in the selection of endmembers and to achieve satisfactory results. Since front-line forensic practitioners rarely possess advanced skills in spectroscopy, it was decided that the results from SAM and SFF algorithms did not meet the requirements of this project, and so this approach was not explored any further.

It was at this time that further research into hyperspectral image processing techniques was undertaken, as it was determined that more powerful techniques would be required to yield the desired results.

### **2.3.4 Classification approaches**

The sections below outline the results obtained from the use of the unsupervised chemometric techniques MCR and SIMPLISMA on ATR-FTIR and Raman hyperspectral data. The performance of each spectroscopic technique and each algorithm is compared. Overall, the two criteria used to measure the performance of each method were:

- i. the ability of the algorithm to accurately identify the correct pure compounds as determined by matching the calculated spectra with library spectra; and
- ii. the accuracy of the estimated purity of each component as determined by the algorithm and compared to the known values of the prepared mixtures.

A specialised plot was designed to visually display both aspects of the analysis. A guide to interpreting this type of plot can be found in Appendix 1.

Ultimately, the best evaluation of the benefit provided by the use of advanced spectroscopic techniques is to compare the results between this research and those obtained from currently used preliminary illicit drug identification techniques. Thus,

the samples analysed in this research were also tested with instruments currently in use by the AFP crime scene teams.

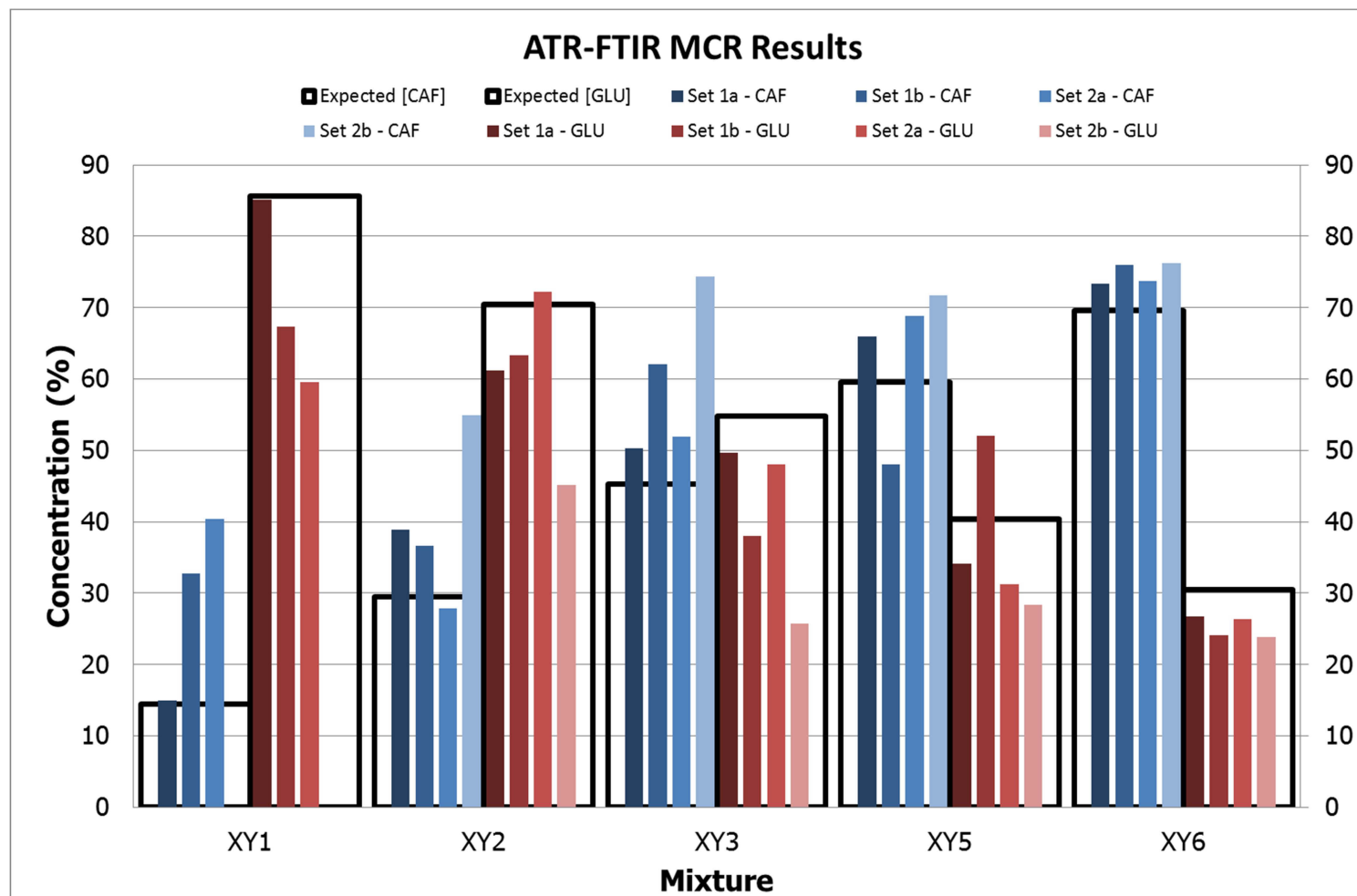
#### *2.3.4.1 ATR-FTIR*

The performance of MCR and SIMPLISMA on the analysis of ATR-FTIR hyperspectral data is presented in this section for two- and three-part powder mixtures of known concentrations, as outlined in Table 2-1.

A summary of the performance of MCR and SIMPLISMA on ATR-FTIR data is given in Figure 2-6 and Figure 2-10. Figure 2-6 below shows examples of results from a typical MCR analysis of ATR-FTIR hyperspectral imaging data. The MCR algorithm was supplied with the 4096 spectra collected per hyperspectral image, and no other information about the samples. Without user intervention, MCR was to predict the correct number of components and estimate their relative concentrations. The coloured bars show the predicted concentration for each correctly identified component and thus are only present when the algorithm has successfully identified the correct component in the test samples.<sup>§</sup>

---

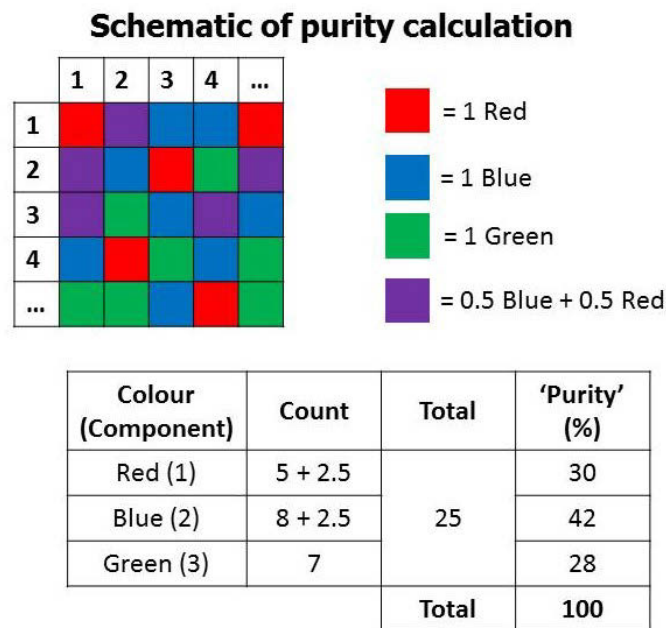
<sup>§</sup> For further detail on the interpretation of the results graphs, see Appendix 1



*Figure 2-6 MCR results for two images (a, b) of two tablets (set 1 and 2) made from the same powder mixture. i.e multiple bars for a mixture indicate replicate analyses.*

As can be seen in Figure 2-6 above, the components of the mixture were not correctly identified in the second image of the second tablet (Set 2b) for the XY1 mixture (15% caffeine, 85% glucose), and thus no predicted concentration was determined.

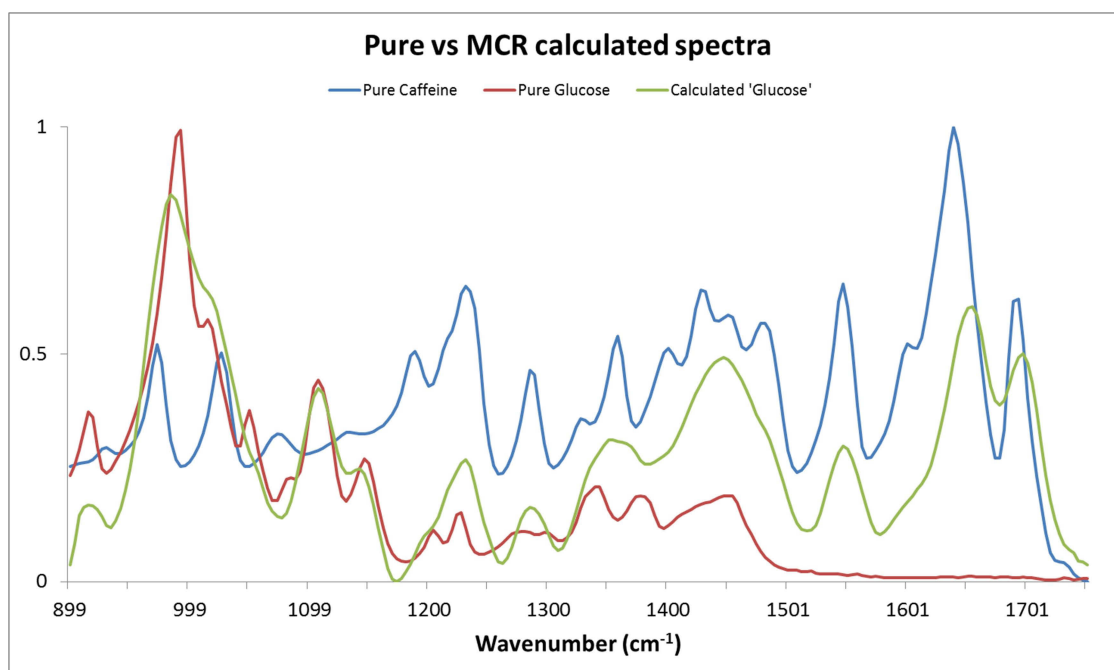
As described in section 2.3.4, the success of the method is measured in two aspects, but importantly, the purity cannot be predicted if correct and/or real spectra are not predicted for each component in the mixture. The purity calculations are inherently linked to one another, and the purities must always add to 100%. As shown diagrammatically in Figure 2-7 below, the calculation of purity by MCR and SIMPLISMA is carried out on a per pixel basis. The algorithm determines 'how much' of each of the calculated pure components is present at each pixel. The value at each individual pixel for each component is then averaged over all pixels to yield an overall purity. Thus, as the determination of one component composition relies on the other, the total of the known components will always equal 100%. This aspect of the calculation may lead to slight errors in real world scenarios due to a number of reasons including the possible presence of infrared-inactive components and low concentration components such as binders and fillers not being accounted for.



**Figure 2-7 Schematic representation of purity the calculations applied to an infrared image.**

Importantly, the correct identification of each component is a critical step of the calculation so that the correct ratio is obtained at each pixel. In saying that, the methodology was optimised in order to gain the best compromise between accuracy of predicted purity, and hit rate of true components (spectra) present. Current PIDI techniques provide no indication of purity, and thus any additional information collected on the purity of the components, even if only an estimate, provides an advantage to LEAs at the time of interception.

It can be seen in Figure 2-6 above that the predicted concentrations can range up to 30 percentage points from the true value of the test samples. As described above, the purity is calculated from the contribution of each 'pure' spectrum at each pixel, thus the determination of spectrally pure components is a critical step of the process. Through closer analysis of the spectra calculated by MCR, it became apparent that, in some instances, the MCR algorithm was not able to extract spectrally pure components. In contrast to the issues described for the endmember techniques above, these calculated spectra were still 'pure' enough to obtain a correct library match for the target compound.



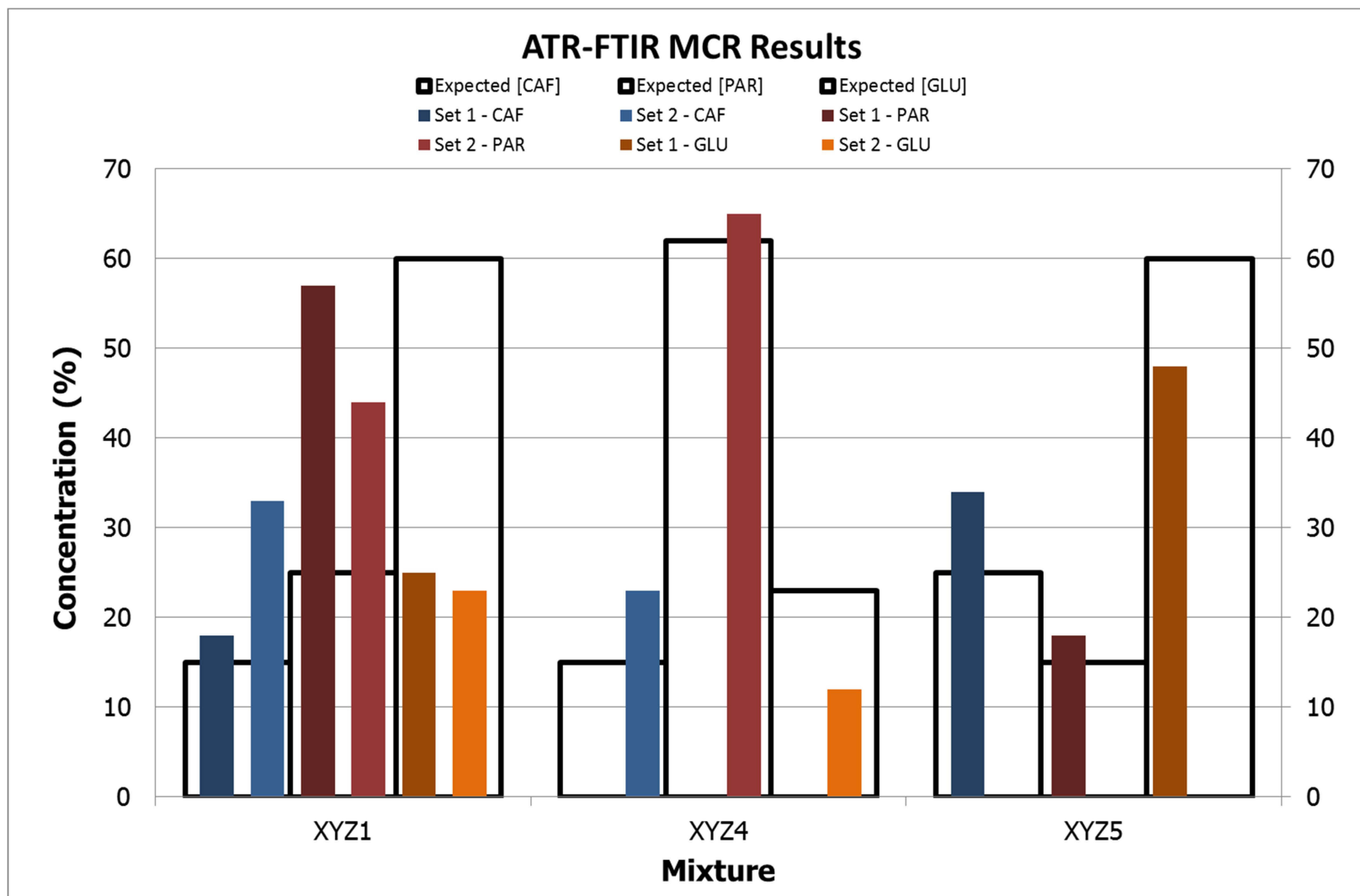
**Figure 2-8 Example of MCR-calculated spectrum vs pure FTIR spectra of caffeine and glucose.**

Figure 2-8 above depicts pure spectra of caffeine and glucose, as well as one of the calculated components from an MCR calculation on a CAF/GLU mixture. The calculated spectrum successfully gave the top library match to glucose but quite clearly has absorptions from the caffeine spectrum incorporated into it, most notably in the 1500-1700  $\text{cm}^{-1}$  region. For the calculation of concentration, this results in an over-estimation of the calculated 'glucose' contribution at each pixel as it will incorporate some of the caffeine at that pixel into the glucose concentration. As the estimated concentrations are inherently linked, this will result in an underestimation for the purity of caffeine as seen for Set 1b for the XY5 mixture in Figure 2-6 above.

The ability to supply MCR with initial estimates, that is, pure spectra of the known components, was explored. It was found that, if MCR was not going to find the correct pure components in a mixture (like in example Set 2b for XY1 mixture in Figure 2-6 above) supplying the pure spectra as initial estimates did not help the algorithm in determining the correct pure components. Furthermore, the use of initial estimates restricted the algorithm to building a model based on the number of spectra



(estimates) supplied. For example, if information about two components was supplied, the algorithm would fit a poor model to two components rather than a better fit three or four component model. It was thus decided that this feature would not meet the aims of this work and was no longer used.



*Figure 2-9 MCR results for two tablets made from the same three component powder mixture.*

Figure 2-9 above displays typical results for the analysis of three-component mixtures by ATR-FTIR hyperspectral imaging and MCR. It can be seen that MCR performed relatively poorly in predicting the correct components in the three-part mixtures. As can be seen in Figure 2-8 and described above for two-part mixtures, this was mainly due to the presence of absorptions from other components in the mixtures in the 'pure' components determined by MCR. This was more pronounced in the components predicted for the three-component mixtures. When a correct library match was obtained, the presence of these 'mixed' component spectra affected the estimation of purity and decreased the accuracy of the purity estimated by the algorithm. Modifications in the data collection, such as increasing spectral resolution to collect more data points, did not overcome this issue. It is hypothesised that for compounds with more simple spectra, this issue would not occur. This is discussed further later in this section.

The SIMPLISMA algorithm was used to analyse the same set of mixtures as above. As for MCR, the algorithm was supplied with the pre-processed image spectra, and no other information about the samples. Figure 2-10 below outlines the typical results obtained from the infrared analysis of two-component mixtures by SIMPLISMA.

As described in Section 1.2.2.4, SIMPLISMA is similar to MCR in that it aims to extract component spectra and concentrations without any prior knowledge. SIMPLISMA works on a pure variable approach. Thus, the algorithm requires that within a mixture, each component has at least one absorption frequency in its spectrum that is unique. Referring to the pure spectra of caffeine and glucose in Figure 2-8, it can be seen that caffeine has a unique absorption at  $1639\text{ cm}^{-1}$  and glucose has one at  $1107\text{ cm}^{-1}$  or (to a lesser extent) at  $991\text{ cm}^{-1}$ . Consequently, the SIMPLISMA results outlined in Figure 2-10 should, at the very least be able to resolve the two components in each of the mixtures presented to it.

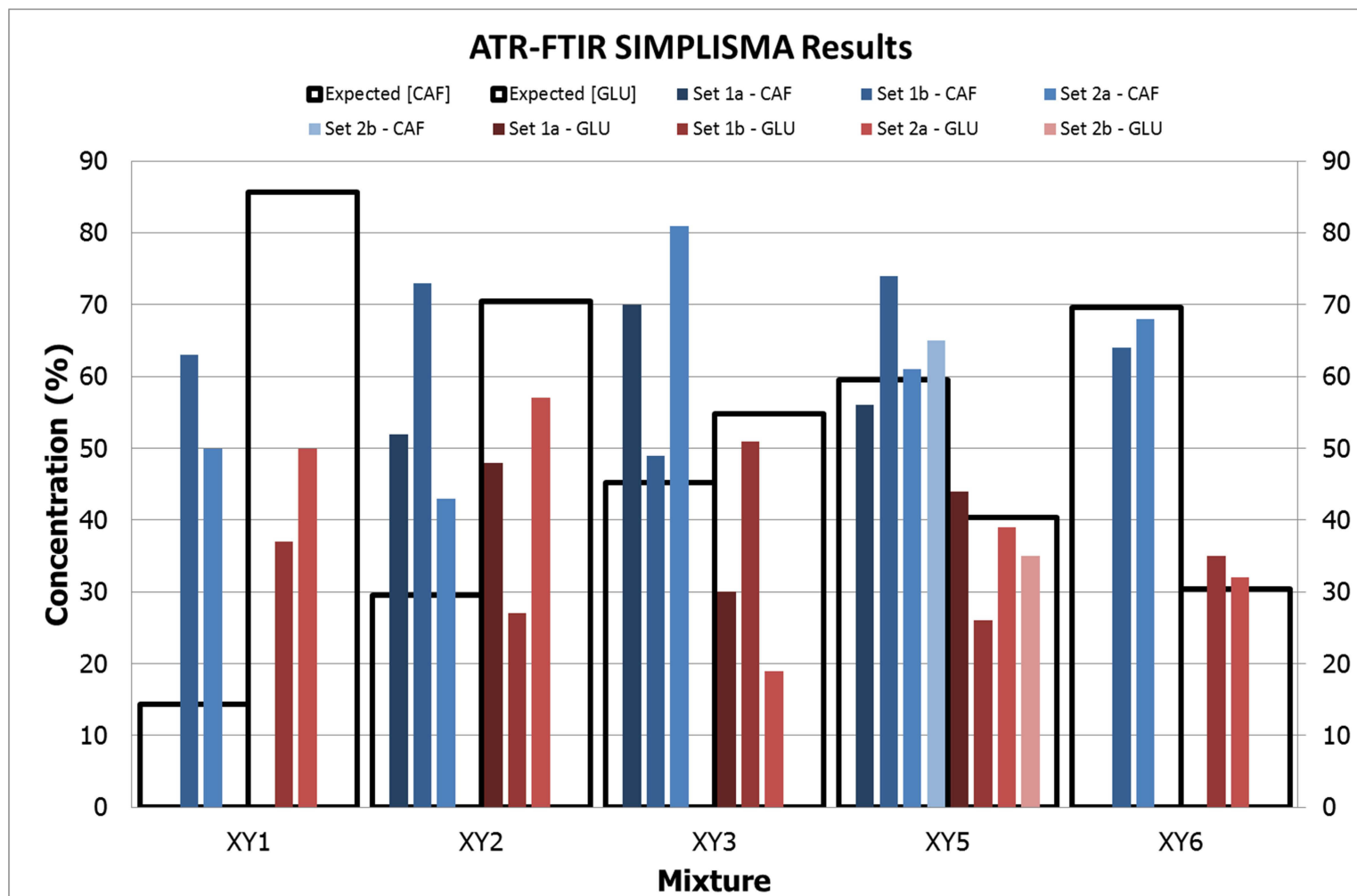


Figure 2-10 SIMPLISMA results for two images (a, b) of two tablets (set 1 and 2) made from the same powder mixture.

As the calculation of purity relies on the successful identification of pure components, the lack of data in Figure 2-10 above shows that generally, SIMPLISMA was not able to correctly identify the pure components present in many of the mixtures. Mixture XY5 is the only mixture in which SIMPLISMA was able to identify the correct components for all four images displayed in the above example. In SIMPLISMA theory, the selection of incorrect pure components translates to the algorithm not being able to attribute the correct spectrum to what it determines to be a pure variable i.e. SIMPLISMA is unable to locate a true 'pure variable' from the 4096 spectra presented to it. Furthermore, even though mixed spectra above were described for MCR (See Figure 2-8) and successfully library matched to the correct components, this was not the case for SIMPLISMA, keeping in mind that both components need to be correctly identified for a result to be displayed. Often in the SIMPLISMA analysis, the algorithm would successfully identify one of the components in the mixture, but the other spectrum found would be either a very noisy spectrum or not representative of a real substance.

So, even though in the example presented for caffeine and glucose mixtures, pure variables should exist, SIMPLISMA is either not picking the correct variables as 'pure', or, when it does find the correct pure variable, it is not working correctly and fails to calculate a spectrally pure component.

Overall, SIMPLISMA did not perform as well as MCR in determining the correct number of pure components in a mixture. When SIMPLISMA did identify the correct components, it was not as accurate as MCR in estimating the purity of the components within the mixture, with errors of up to 45 percentage points of the true value.

In a testing scenario, where the user knows the pure components in the mixture, the interactive nature of SIMPLISMA means that a user could theoretically 'force' SIMPLISMA to the correct number of components. To some extent, SIMPLISMA could also be forced to extract the correct 'pure' components by directing the algorithm to

the known pure variables, but this still does not always result in spectrally pure components.

Given that SIMPLISMA is an interactive process, with a more hands-on approach in comparison to MCR, a set of rules to guide the user through the decision making process would be ideal. The software provides visual and statistical information to aid the user in making these decisions, such as the standard deviation, mean and purity spectra\*\* for the overall dataset. The main purpose of this information is to guide the user in determining the right number of components,  $n$ , in a mixture. Determining the correct value for  $n$  is the cornerstone to a successful SIMPLISMA model. The spectrum of each component is calculated at each step of the modelling process and thus either an insufficient or excessive number of components can lead to incorrect results. While the statistics aid in the determination of the number of components, they do not necessarily aid in ensuring that the calculated components are real compounds. Attempts at developing protocols based on these statistical aids failed to produce a set of instructions that met the complexities of the calculations and resulted in reproducible and 'real' results. The main reason behind this is that the statistics are heavily dependent on decisions made in the previous step, the actual components of the mixture (which will be unknown in a real world scenario) and the quality of the spectra being analysed. For instance, when the first component is resolved by SIMPLISMA, the effect of that component is mathematically removed from the purity spectrum, affecting the statistics provided.<sup>157</sup>

Thus, while in theory no prior information about the samples is required to perform analysis by SIMPLISMA, the circumstances presented above demonstrates that both some knowledge of spectroscopy and an indication of the components present in the mixture would provide an advantage in obtaining the correct results. For the reasons outlined above, MCR was deemed to be more suitable than SIMPLISMA for the analysis of illicit drug mixtures by ATR-FTIR hyperspectral imaging.

---

\*\* The purity spectrum is defined in section 1.2.2.4 on page 19

The average %relative error was calculated to compare the performance of MCR and SIMPLISMA in estimating the correct purity across a range of samples with known concentration as per the below formula.

*% Relative Error*

$$= 100 \times \left( \frac{|Known\ purity - calculated\ purity\ (MCR\ or\ SIMPLISMA)|}{known\ purity} \right)$$

Table 2-2 below outlines the %relative error for the results presented in Figure 2-6 and Figure 2-10, the overall averages are representative of ATR-FTIR imaging data.

FTIR Mixture	Average % Relative Error	
	MCR	SIMPLISMA
XY1	60.9	171.2*
XY2	25.6	63.8
XY3	20.7	43.3
XY5	18.0	13.4
XY6	11.2	7.6
<b>Average</b>	<b>27.3</b>	<b>32.0</b>

**Table 2-2 Average %relative error for MCR Vs SIMPLISMA for examples presented in Figure 2-6 and Figure 2-10. \* not counted towards average**

The majority of algorithms, like those employed in this research, assume that the samples being analysed comply with the Beer-Lambert (Beer's) law. That is, that the absorption of light (infrared signal) is directly proportional to the concentration of the compound being analysed.<sup>177</sup> We found that the ATR spectra collected in this study did not show a linear relationship with the concentration of each component, and thus did not obey Beer's law. This non-linear relationship has also been observed in the analysis of low concentration minerals with FTIR,<sup>178</sup> and various spectral anomalies, artifacts and distortions are known for ATR spectroscopy that will cause non-linear responses.<sup>179-182</sup> Furthermore, this issue has previously been observed in our laboratory during the ATR-FTIR study of heterogeneous solids using a different ATR

accessory, and was not rectified in this study with the use of the imaging Golden Gate. This non-linear relationship is a limitation of the use of ATR-FTIR spectra for the quantitative analysis of powders. As shown in Table 2-2 above, the average % relative error for a typical MCR and SIMPLISMA analysis was 27.3% and 32.0% respectively. The table shows that MCR is the more accurate technique in the analysis of ATR-FTIR hyperspectral imaging data of solid mixtures.

Furthermore, it must be noted that the use of 'model' compounds in the field of illicit drugs can often give deceptively negative test results when more complex compounds are used than would usually be found in illicit drug samples. However, for proof of concept scenarios, the use of these compounds highlights the 'worse-case' scenario for case-work and shows the power of spectroscopy combined with chemometric techniques in being able to identify components in a mixture without the need for any sample preparation.

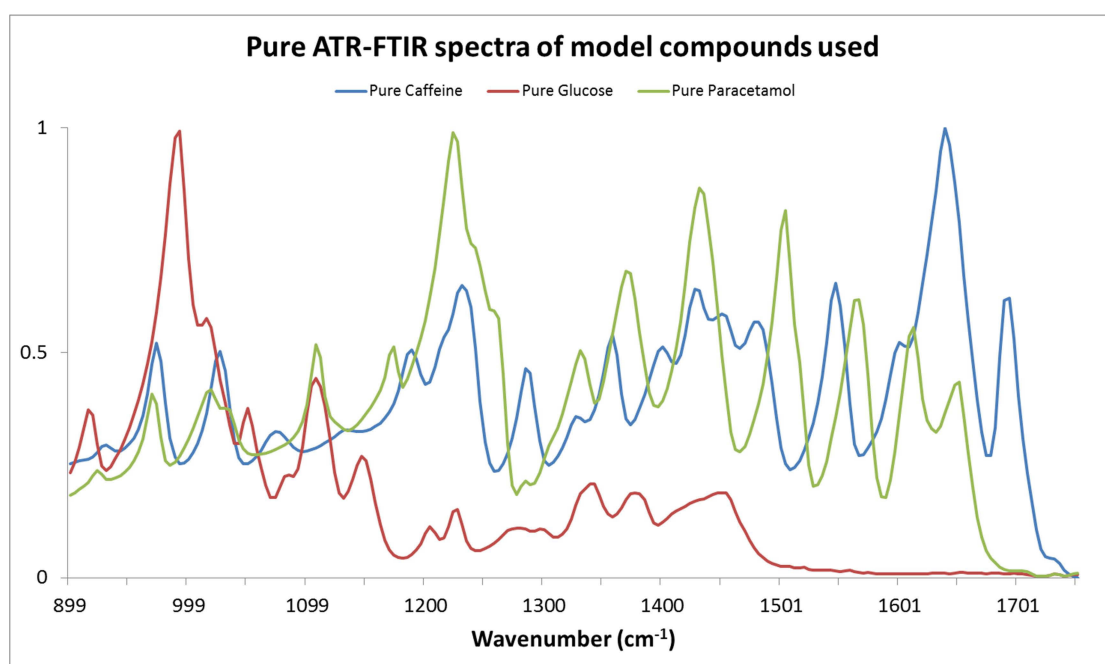


**Figure 2-11 Pure ATR-FTIR spectra of caffeine, glucose and paracetamol.**

Figure 2-11 above shows pure spectra for three components commonly used in this project, caffeine, paracetamol and glucose. It can be seen that the caffeine and



paracetamol have either completely or partly overlapping absorptions between 1600 or 1200  $\text{cm}^{-1}$ . If this is compared to Figure 2-12 below, which shows the infrared spectra of methamphetamine and dimethylsulfoxide (DMS), it can be seen that they have fewer overlapping bands in this region. DMS is a common cutting agent found in methamphetamine samples.

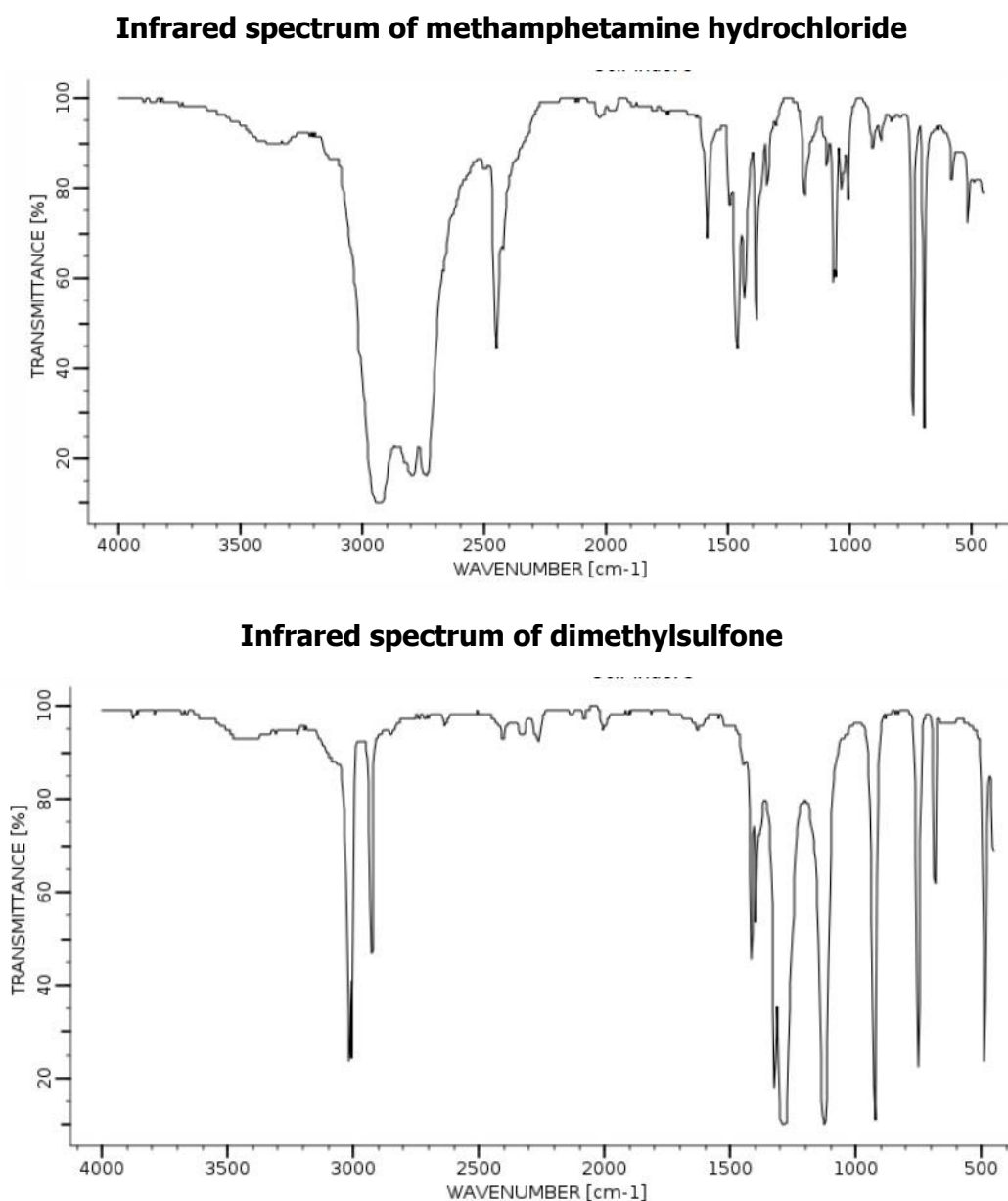


**Figure 2-12 Infrared spectra of methamphetamine hydrochloride and dimethylsulfoxide.**

As mentioned above, the choice of 'model' compounds used in research into illicit drug analysis can often complicate the analysis compared to the compounds observed

in real scenarios. Due to the lack of overlapping signals observed in the above, it is hypothesised that the chemometric technique proposed in this research would be able to extract spectrally pure components from hyperspectral data collected from a mixture of methamphetamine and DMS. Thus, the method would more accurately predict the components and relative purity of suspect illicit samples than it did with the test compounds available to the project.

#### *2.3.4.2 Raman mapping*

As in section 2.1.2 above, Raman data was subject to analysis by the MCR and SIMPLISMA algorithms. Unlike the FTIR data discussed above, satisfactory results were obtained using raw Raman data. However, a measureable improvement in the accuracy of estimated purity and the reproducibility of the results was achieved when pre-processing was performed on the data. The results below were obtained from pre-processed Raman data as described in Section 2.2.3.2 above.

Figure 2-13 and Figure 2-14 below demonstrate the typical results achieved from the application of MCR to Raman maps of powder mixtures. While the size of an ATR infrared image is fixed (by the sizes of the FPA detector and the ATR crystal), Raman mapping gives more flexibility in the number of spectra obtained and the area covered. The user has the ability to alter the size of the map and the spacing between each point, ultimately determining the number of spectra collected. Figure 2-13 below shows the difference in the results obtained from the collection of a small map (500 x 375  $\mu\text{m}^2$ ) with a smaller step size (1a and 1b, approximately 20 spectra with 125  $\mu\text{m}$  step size) and a large map with a larger step size (2a and 2b, approximately 110 spectra with 250  $\mu\text{m}$  step size) (3000 x 2250  $\mu\text{m}^2$ ) for each powder sample. As it can be seen, the correct pure components were identified by MCR in all samples in each of the maps, Figure 2-13.

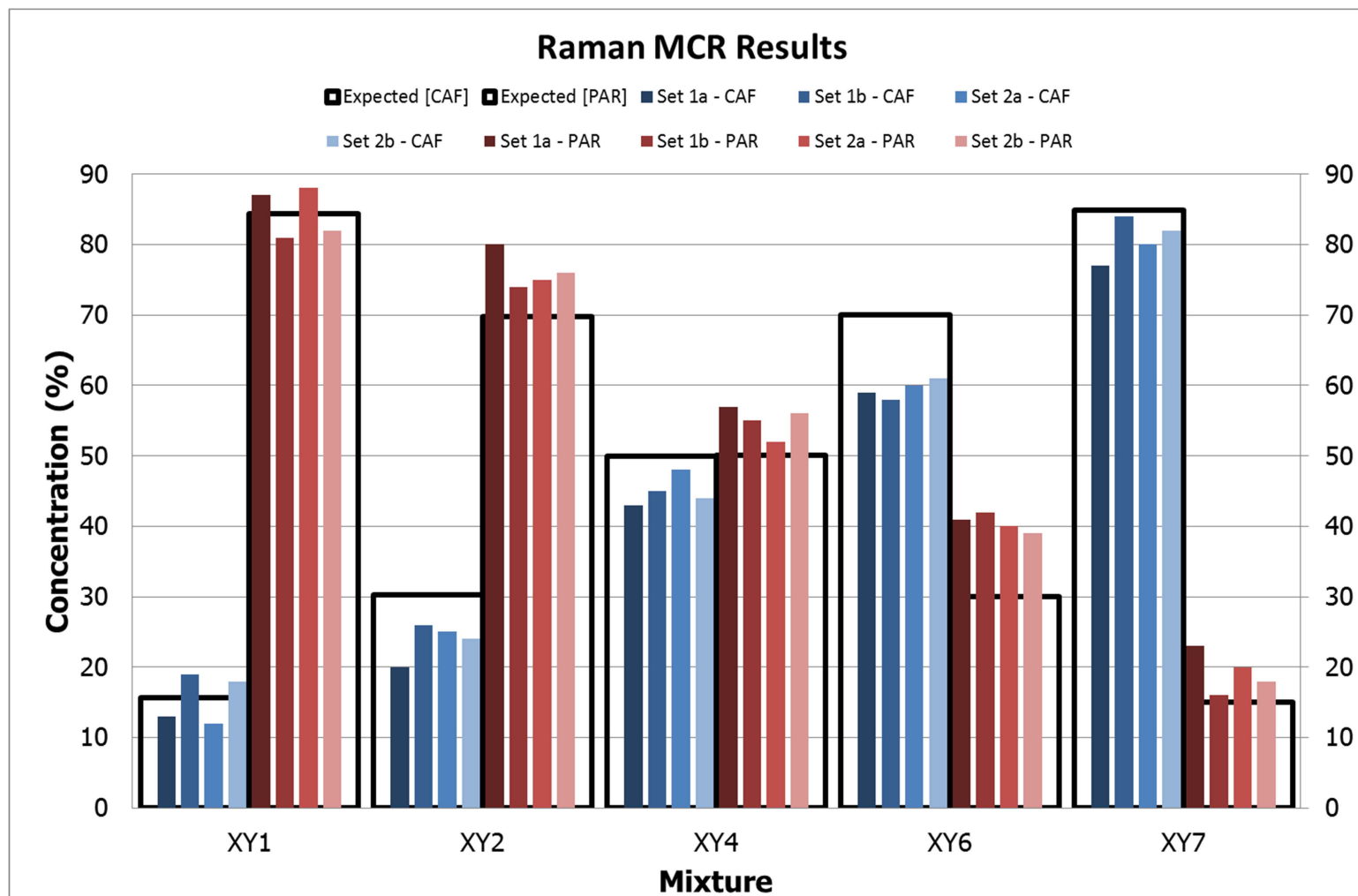
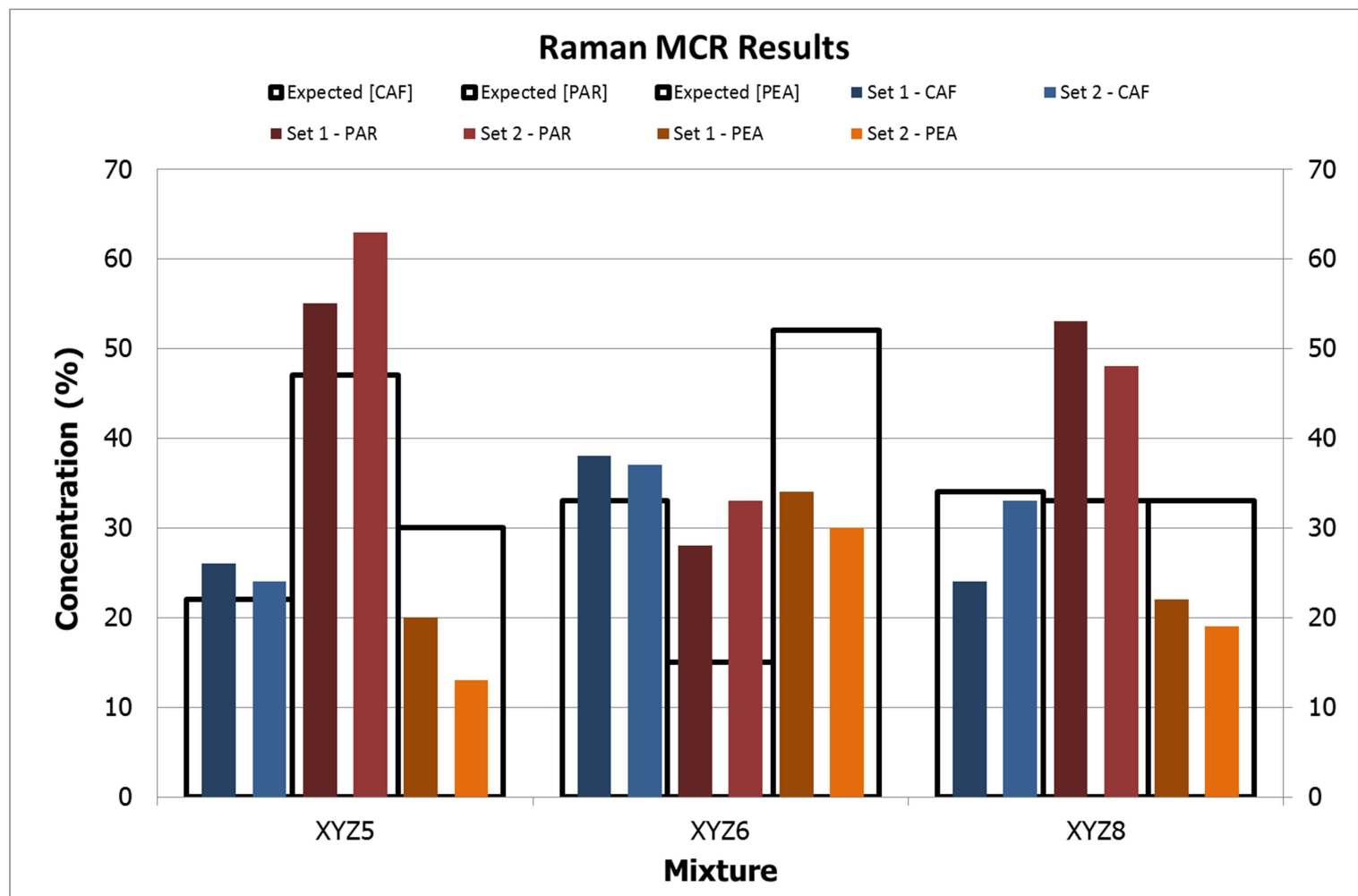


Figure 2-13 Raman MCR results. Results are displayed for two maps of each powder sample.

MCR performed exceptionally well in identifying the Raman spectra of pure components in powder mixtures it was presented with, regardless of the number of spectra in the map. In terms of estimating purity, little variation can be seen between the four Raman maps of each mixture composition. Set 1a above for the XY2 mixture has the highest error, roughly 10 percentage points from the true purity value. As mentioned previously, current techniques used by LEAs do not provide any indication of purity at all, so this is an acceptable error range for a preliminary illicit drug identification method. The similarities seen in the data presented in Figure 2-13 above show that, typically, no advantage was achieved with the collection of more spectra, or covering a larger area. It also shows that the step size between spectra was large enough to counter any issues that may arise due to the variation in the particle size of the powders analysed.

The success of MCR in identifying pure components in a mixture is further supported in the results for the three part mixtures; Figure 2-14 below shows the results of a typical analysis of three part mixtures. While MCR successfully identified the pure components in each example, there was generally greater error in comparison to the binary mixtures outlined above, with errors of up to 20 percentage points from the true value.



*Figure 2-14 Raman MCR results for three part mixture. Results are displayed for two maps of each powder sample.*

As outlined for the ATR-FTIR data above, it is hypothesised that the errors in the purity are due to the overlapping signals in the spectra of CAF, PAR and PEA (Figure 2-15) and thus MCR not successfully extracting spectrally pure components for the calculations.

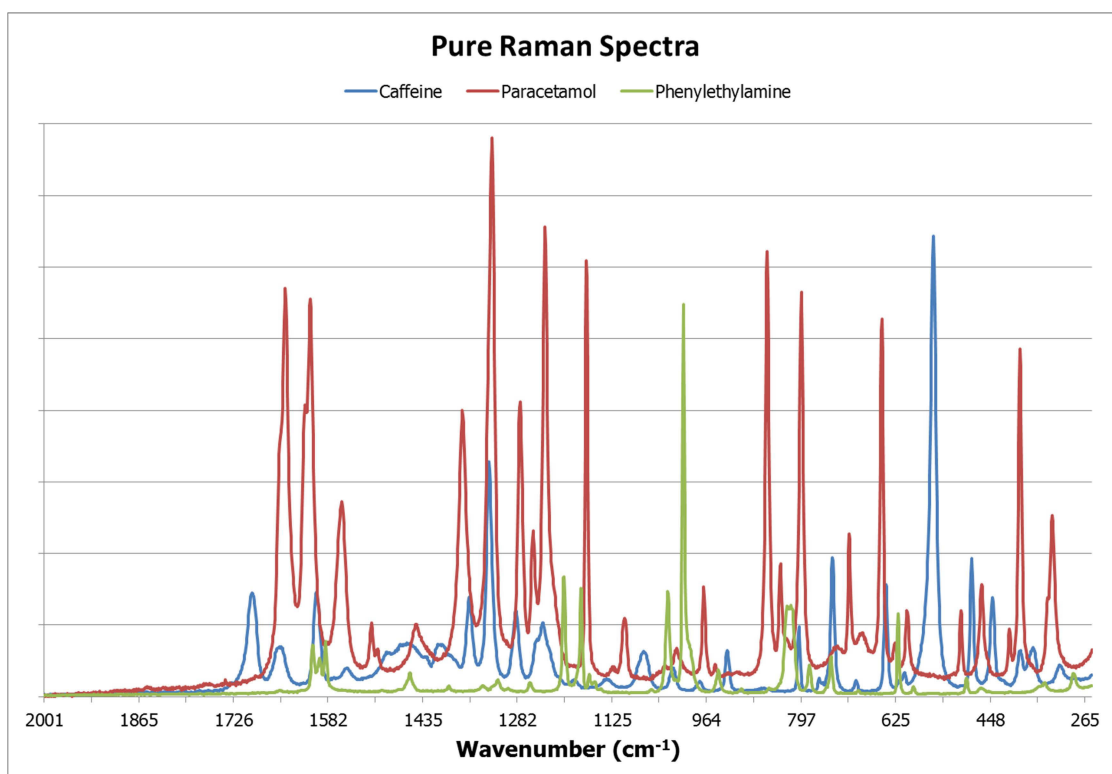


**Figure 2-15 Pure Raman spectra of caffeine (CAF), paracetamol (PAR) and phenylethylamine (PEA).**

Figure 2-16 and Figure 2-17 below show typical results from the application of SIMPLSIMA to Raman mapping data for two- and three- part mixtures. Given that caffeine (556 cm<sup>-1</sup>), paracetamol (multiple) and phenylethylamine (1004 cm<sup>-1</sup>) have 'pure variables', it is expected that analysis by SIMPLSIMA of mixtures containing these should perform as successfully as MCR in at least identifying the correct components. In the example for the two-part mixture of caffeine and paracetamol below, the correct pure components were identified in all but one sample. Importantly, it must be noted that these samples are the same as those in Figure 2-13 above, where MCR was able to correctly identify all components. Comparing the

estimated purities to those achieved with the MCR analysis, it can be seen that, while both algorithms gave similar results, MCR is again more accurate.

For the three-part mixture of caffeine, paracetamol and phenylethylamine displayed in Figure 2-17 below, SIMPLISMA was unable to identify the correct components in one set of data for one of the mixtures (XYZZ). But, when the correct component has been identified, the purity predicted by SIMPLISMA for the three-part mixtures is comparable to those observed for MCR in Figure 2-14. While in the other examples demonstrated, MCR out performed SIMPLISMA, the average %relative errors for the three-part MCR and SIMPLISMA mixtures displayed were determined to be within 0.2% of each other overall.<sup>††</sup>

---

<sup>††</sup> The %relative error is not able to be calculated when a correct component is not identified. For this example, the image whereby SIMPLISMA did not identify the correct components was excluded from the calculations.

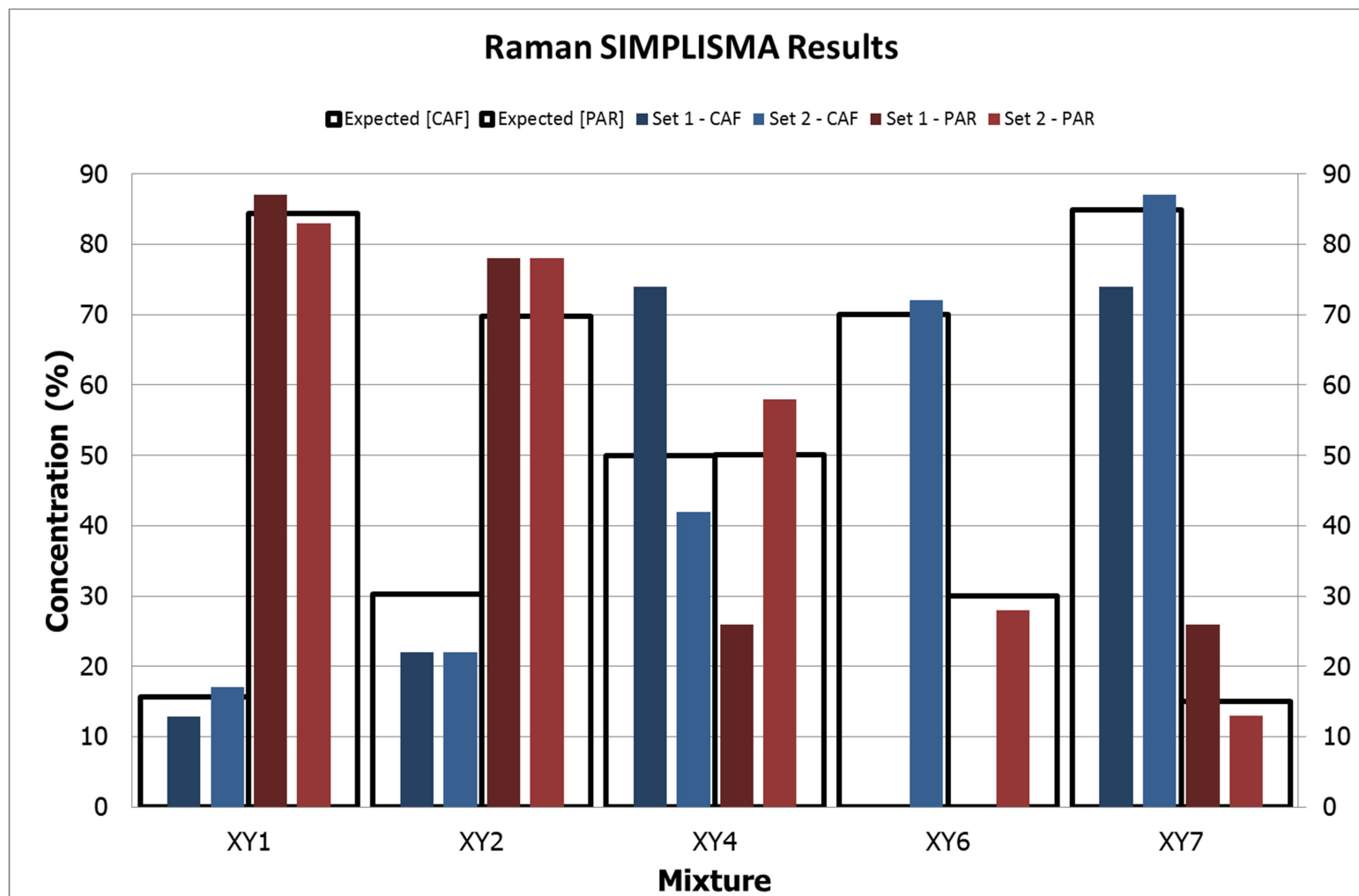


*Figure 2-16 Raman SIMPLISMA results for two-part mixtures. (two maps of each powder sample).*



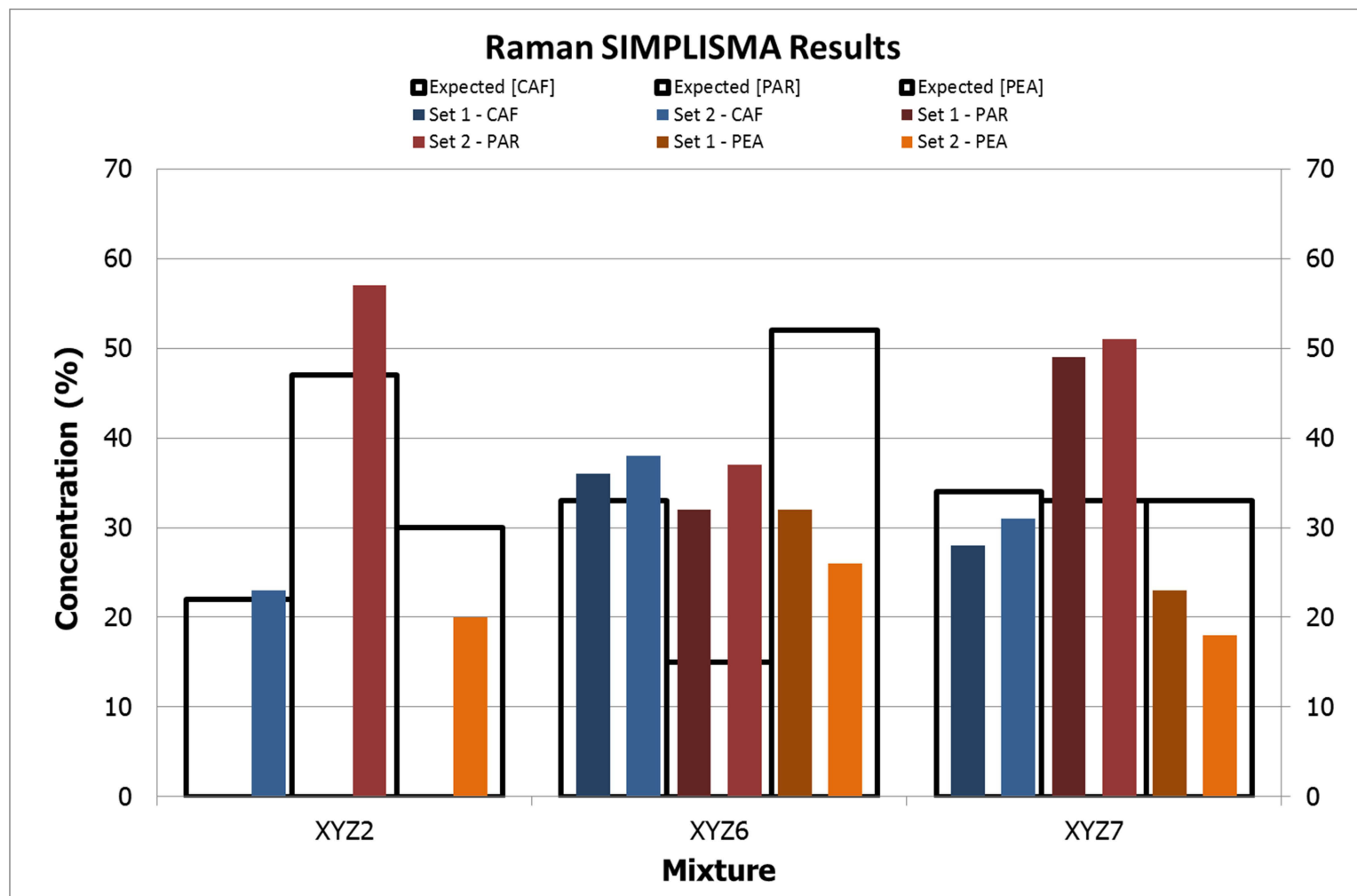


Figure 2-17 Raman SIMPLISMA results for three-part mixtures. (two maps of each powder sample).

As for the ATR FTIR data presented in Table 2-2, the average % relative error was calculated for the Raman results presented in Figure 2-13 and Figure 2-16 above. Before applying any analysis to the results, the improved accuracy and reproducibility of Raman mapping over ATR-FTIR hyperspectral data can be seen by comparing the supplied figures.

Raman Mixture	Average % Relative Error	
	MCR	SIMPLISMA
XY1	11.4	7.7
XY2	15.3	19.5
XY4	10.0	32.0
XY6	25.1	-
XY7	16.3	25.4
<b>Average</b>	<b>15.6</b>	<b>21.2</b>

**Table 2-3 Example of average %relative error for Raman analysis. Relative error calculated for data presented in Figure 2-13 and Figure 2-16.**

Given that the Raman signals are much narrower than IR absorptions, and the limitations regarding linearity and Beer's Law discussed in Section 2.3.4.1, it was hypothesised that Raman mapping would perform better than ATR-FTIR data in predicting the components of a mixture in their relative abundances. This is confirmed in Table 2-3 above, which shows that both the MCR and SIMPLISMA analysis of Raman mapping data had a smaller % relative error in comparison to the analysis of ATR-FTIR hyperspectral data, with % relative errors of 27.3% and 32.0% respectively. The average %relative error for the MCR analysis of Raman data was found to be 15.6% in the above example. This is an acceptable error for a preliminary identification technique that is supplied with no a priori information about the samples and thus no calibration. When a priori information is available, as well as the option to create calibration data using a set of mixtures that contain varying amounts of each component, partial least squares (PLS) analysis would be the preferred chemometric

technique for the analysis of this data. The use of calibrated data sets and PLS analysis would significantly improve purity estimation.

#### 2.3.4.3 *Currently used FTIR technique*

Ultimately, the best evaluation of the benefit that the advanced spectroscopic techniques provide, is to compare the results obtained with those from currently used PIDI techniques.

The infrared system made available to this research was the Smiths Detection HazMatID ATR-FTIR system that is currently in use by AFP Crime Scene teams Australia-wide. The algorithm used for the system is proprietary and thus the research takes a 'black box' approach to presenting the results.

Current procedures at the AFP require that a library match quality of 0.95<sup>††</sup> or greater is obtained for a basic user to be able to call a match. Advanced users of the FTIR system are able to perform visual comparisons to call a match at their discretion for spectra under the 0.95 match quality threshold. A search of the residual ("spectrum" obtained by subtracting the selected library spectrum from the sample spectrum) is available in the Smiths software to gain an understanding of other components that may be present. A limitation of the software is that this can only be performed once, resulting in the identification of a maximum of two components. The default method used by the AFP is set up such that if no matches above 0.80 are obtained, a "no library hit" message is shown.

The same samples analysed by the ATR-FTIR and Raman methods described above were analysed with the HazMatID system as per the procedure outlined in Section 2.2. Table 2-4 outlines the results, described in detail below.

---

<sup>††</sup> Information on the derivation of this number is proprietary to Smiths Detection.

Mixture	Result / replicate set							
	HazMATID (AFP method)				Proposed ATR-FTIR method (MCR)			
XY1	✓	✓	✓	✓	✓	✓	✓	✗
XY2	✗	✓	✗	✗	✓	✓	✓	✓
XY3	✗	✗	✗	✗	✓	✓	✓	✓
XY5	±	±	±	✗	✓	✓	✓	✓
XY6	±	±	±	±	✓	✓	✓	✓

**Table 2-4 Comparison of results for the analysis of binary mixtures with currently used FTIR technique and method proposed by this research. ✗ - No correct library matches, ± - one correct component identified, ✓ - both components correctly identified.**

For the mixtures of caffeine and glucose, no library matches (✗) were identified in 8 of the 20 samples analysed. Only caffeine (and an incorrect second component, ±) were identified in a further seven samples, and both caffeine and glucose were correctly identified (✓) in only five of the spectra collected. Four of these were from the same mixture, the 15% caffeine / 85% glucose mixture (2 spectra per tablet, 2 tablets). Interestingly, in the remaining sample, where both caffeine and glucose were identified, the first component was identified to be glucose. Following a spectral residual search, the second component was most closely matched in the library to a 1:1 mixture of caffeine and sucrose, a mixed spectrum that had been added into the on-board library. It was found that spectra of mixtures had also been added into the on-board library, such as a 1:1 mixture of caffeine and paracetamol.

The inclusion of mixed spectra in the on-board library of the HazMatID does overcome a limitation of the software in only being able to identify two components. For example, when samples of three part mixtures of caffeine, paracetamol and phenylethylamine were analysed, the 1:1 mixture of caffeine and paracetamol loaded into the on-board library was the top library match in three of the eight spectra collected from four different mixtures. PEA was only identified as an additional

component for one of those three. This was the only time that PEA was identified by this method.

### 2.3.5 Application to case samples

Tablets were provided by the AFP that had been intercepted at the Australian border by the AFP and found to contain MDMA. The exact tablets made available to the project were not tested, but samples of tablets from the same seizure and similar in appearance to those provided were analysed by NMI and reported to contain 25.7% MDMA, no further detail was provided.

Two separate tablets of this type were supplied and tested using the methods detailed above. The concentration of MDMA was determined to be 40% +/- 11% for tablets analysed by the ATR-FTIR method and subject to analysis by MCR, and 66% +/- 2% for ATR-FTIR data subject to SIMPLISMA analysis. As per the results obtained for the test samples above, multiple analyses of the tablet identified that MCR performed much better at identifying the correct component in the mixture, MDMA, and at estimating the purity.

Further to the above, microcrystalline cellulose (MCC) and N-hydroxy-3,4-MDA were also identified in the samples at 10-31% and 23-40% respectively. MCC is a common filling agent found in illicit tablets and N-hydroxy-3,4-MDA can be formed as a by-product in the synthesis of MDMA via a nitrostyrene route.<sup>183</sup>

The analysis of the supplied MDMA tablet with Raman mapping highlighted a limitation of analysis with Raman spectroscopy, namely fluorescence. The highly coloured tablet sample could not be analysed with either of the two lasers available at our laboratory due to a high level of fluorescence. However, a FT-Raman instrument made available to the project, equipped with a 1064 nm laser determined that the MDMA samples contained 44% MDMA and 55% MCC when analysed with MCR. The FT-Raman spectra collected contained almost no fluorescence signal.

## 2.4 Conclusions

The law enforcement environment is on a path to intelligence-led-policing, with an aim to gain as much information as possible and interpreting that into actionable intelligence as quickly as possible. The strategies adopted in the current work meet this principle by supplying LEAs almost instantly with information that could take up to months to gain under current protocols.

The use of unsupervised chemometric techniques could negate the need to have prior chemical information about the samples being analysed, and lends itself to the preliminary identification of illicit drugs. Although much work has been done on the classification of hyperspectral images, very few studies have focussed on using a one-hyperspectral-image-per-observation approach, especially without the use of calibration techniques such as PLS. The current work adapts the use of MCR and SIMPLISMA as unsupervised chemometric techniques to large numbers of infrared or Raman spectra in single hyperspectral images.

Currently-employed techniques follow more of a 'black box' approach than the proposed method, whereby matches to library spectra are required for most users. Also, current methods are limited (mainly by software) to only give information about one or two components. The strategies adopted in the current work demonstrate that, through the collection of hyperspectral infrared or Raman mapping data and application of MCR or SIMPLISMA, more information could be gained by LEAs. This information includes the identity of the components in a mixture and an estimation of their purity. As in the currently employed techniques, inorganic diluents that do not have a strong or characteristic FTIR or Raman signal are not detected (or only weakly detected) in the current work. Furthermore, a limitation of the current work is that components with very weak or highly overlapping spectra may not be identified. The application of the MCR algorithm can be much more automated than SIMPLISMA, and is thus better suited to use by first responders with little experience in spectroscopy.

In any case, the method that gave the best results was the MCR algorithm applied to Raman mapping data. This gave the most consistently correct pure components and most accurate estimation of purity in all the analysed mixtures. This was closely followed by the application of the MCR algorithm to ATR-FTIR hyperspectral data. The ATR-FTIR spectra collected in this study did not show a linear relationship between intensities and the concentration of each component, and thus did not obey Beer's law. The results obtained by SIMPLISMA for both the classification of pure components and estimation of purity, while acceptable and an improvement on current methods, were inferior to those obtained by MCR.

The main factor affecting the results obtained by both MCR and SIMPLISMA was the inability of the chemometric methods to extract spectrally pure components from the data. But, despite this handicap, all tested methods performed better than the single-point infrared technique currently in use by Australian LEAs. It is hypothesised that with advances in technology, ATR-FTIR hyperspectral imaging and Raman mapping could be made into commercially available *portable or handheld* instruments, like many single-point systems currently available on the market. This method needs to be tested on much larger datasets and the intricacies of the chemometric algorithms explored to determine the possibility of obtaining spectrally pure components more readily. This will ultimately improve the classification results but more likely strengthen the confidence in obtaining more precise and accurate purity estimations. The application of these chemometric systems should also be trialled on other spectral data such as proton and carbon NMR spectra of mixtures. The advancement in benchtop NMR has resulted in the method now being a cost-effective option for Australian LEAs, with the AFP recently purchasing one for testing.

***Chapter 3: Fluorescence  
landscapes and PARAFAC for the  
analysis of explosives (feasibility  
study)***



# **Chapter 3: Fluorescence landscapes and PARAFAC for the analysis of explosives (feasibility study)**

## **3.1 Introduction**

### **3.1.1 Nitro Explosives**

Open source reporting on bomb statistics in Australia reveals that the AFP fielded 567 explosive event reports from Australian policing jurisdictions during the 2013 calendar year. Of these, 144 were recorded as 'bombings'.<sup>184</sup> Globally, events involving explosives are on the rise, with terrorist organisations commonly using improvised explosive devices (IEDs) to cause disturbance to western civilisation.

Many of the explosives used commercially, by the military, or illegally by individuals and terrorist groups are nitro-containing compounds. The main nitro-containing explosives fall into three main categories: nitroaromatics, nitrate esters and nitramines, and an example of each type is shown in Figure 3-1 below.

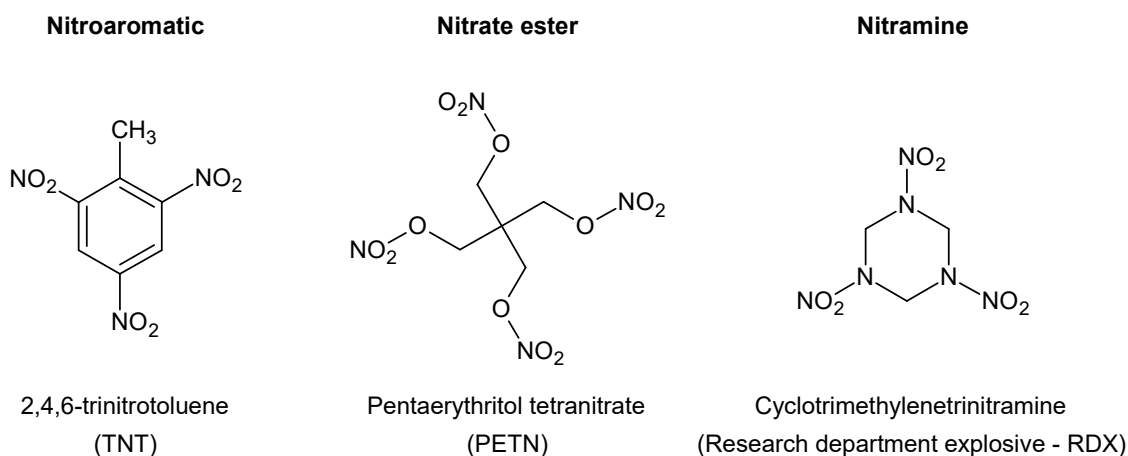


**Figure 3-1 Chemical names and structures for some common nitro-containing explosives TNT, PETN and RDX.**

One of the earliest known nitroaromatic explosives is picric acid (trinitrophenol), which was used in place of blackpowder from 1888 in British munitions. Following further research into explosives, TNT was discovered and became the main explosive charge in World War I. The potential of both RDX and PETN were discovered after World War I and were utilised throughout World War II by themselves and in mixtures with TNT. Today RDX, TNT and PETN are still widely used as explosives, and are commonly mixed with plasticisers to reduce their sensitivity to shock or friction.<sup>185</sup>

The explosives analysed in this work are referred to as secondary (or high) explosives. While they have a higher explosive charge than primary explosives, they usually require detonation by an external source.<sup>185</sup> This is important from a forensic perspective as often residual unexploded secondary explosives can be identified in post-blast scenes.

### 3.1.2 Current detection

Police and intelligence agencies invest heavily in the investigation of incidents involving explosives; this generally involves identification of the explosive compounds and devices used. This is especially true when these attacks have been acts of

terrorism. Typically, these investigations will involve collecting debris that may have been close to the explosive device and thus may contain residue, but also can also include bulk, unexploded components. While there are many techniques available for the detection of explosives, fluorescence spectroscopy is a sensitive technique as a strong signal is obtained from small quantities of material. It is thus ideal for the analysis of trace material such as explosive residues.

A number of analytical methods exist for the detection and analysis of nitro-containing explosive compounds.<sup>186-188</sup> Aside from the more popular separation-based approaches, which are often combined with mass spectrometry (MS),<sup>189</sup> explosive detection methods commonly include ion mobility spectrometry (IMS),<sup>190</sup> infrared<sup>187,191,192</sup> or Raman<sup>191,193</sup> spectroscopy and colorimetric tests.<sup>187,194,195</sup> Methods have also been proposed for the detection of specific compounds, such as TNT<sup>196</sup> and RDX.<sup>197</sup> Detector dogs have also been used to detect explosive compounds.<sup>198</sup> A summary of some other common analytical methods used to detect organic, nitro-containing explosives is presented in Table 3-1 below.

Analytical method	Detection limit	Advantages	Disadvantages
Thin Layer Chromatography (TLC)	µg to sub-µg	Simple and inexpensive	Low resolution
Gas Chromatography-Electron Capture Detector (GC-ECD)	pg	Rapid, selective and highly sensitive for nitro containing compounds	Requires volatile analytes
Gas Chromatography-Thermal Energy Analyser (GC-TEA)	pg	Sensitive and selective for nitro compounds	Requires volatile analytes, limited to nitro-containing
High Pressure Liquid Chromatography (HPLC)-Ultra Violet (UV) or Diode Array (DA)	ng	Sensitive	Low selectivity
Liquid Chromatography-Mass Spectrometry (LC-MS)	pg to ng	Analysis of non-volatiles	Requires interface between HPLC and MS

**Table 3-1 Some analytical methods for the analysis of organic explosives adopted from Royds et al.<sup>187</sup>**

There has been extensive research into the use of chemiluminescence<sup>199</sup> including fluorescence sensors and other fluorescence-based methods for the detection of organic explosives<sup>200-202</sup> due to the improved safety offered by stand-off detection systems. The vast majority of research has focussed on the fluorescence quenching qualities of nitroaromatic compounds for detection,<sup>201-204</sup> most recently using lab-on-a-chip technology.<sup>205</sup> The majority of these methods offer a screening technique, rather than a confirmatory analysis like those reported in Table 3-1 above. Although less common, the promotion of fluorescence has also been used for the detection of explosives.<sup>206,207</sup>

Recently, excitation-emission matrix (EEM) fluorescence spectroscopy (fluorescence landscapes) has been used to assess the removal of pollutants from wastewater of an explosive manufacturing plant.<sup>208</sup> However, no published work on the collection of fluorescence landscapes for the analysis of explosives in a forensic context has been identified.

As evidenced by research into fluorescence quenching properties, nitro-containing explosives generally lack the fluorescence required for analysis by fluorescence spectroscopy. This, combined with the lack of options to derivatise nitro-containing compounds into fluorescence products, directed this research to the reduction of nitro groups to their corresponding amines and the subsequent derivatisation as explained in Sections 3.1.4 and 3.1.5 below.

### 3.1.3 Fluorescence landscapes

A potential application of EEMs or fluorescence landscapes is the identification of nitro-containing explosive mixtures that have been reduced to amines and derivatised.

As outlined in Section 1.1.3, the use of fluorescence landscapes improves the selectivity achieved by regular fluorescence spectroscopy by providing a more characteristic signal for each sample. This provides an advantage for the analysis of explosives, which are commonly detected in low concentrations, often at trace levels. The simultaneous collection of excitation and emission spectra across a determined range of wavelengths provides the user with a larger dataset for interpretation. This is especially important for the analysis of mixtures, as fluorescence signals are often broader than those in infrared or Raman spectra, and thus will often have overlapping signals.<sup>81</sup>

In a forensic context the use of fluorescence landscapes has mainly been limited to environmental applications, looking at dissolved organic matter (DOM)<sup>209,210</sup> and bioaerosol<sup>211</sup> detection; other applications include the detection of doping agents in urine<sup>212</sup> and the analysis of fibres<sup>213</sup>.

Owing to the simplicity of the technique and minimal moving parts in the instrumentation, this technique has the potential for in-field or portable laboratory applications. This is advantageous in the analysis of explosives, as it can be conducted at the scene without the need for transportation of dangerous chemicals or devices.

### 3.1.4 Reduction to amine groups

The reduction of nitro groups to amines is well-documented in synthetic chemistry literature.<sup>214-219</sup> The majority of the reported methods use some type of catalytic hydrogenation to aid in the reduction of the nitro groups to their corresponding amines.

Bandstra *et al.*<sup>219</sup> outline the reduction of TNT to 2,4,6-triaminotoluene (TAT) using granular iron in a sealed environment. The authors note a very brief appearance of mono- and di-amino intermediates as per the schematic in Figure 3-2.<sup>219</sup>

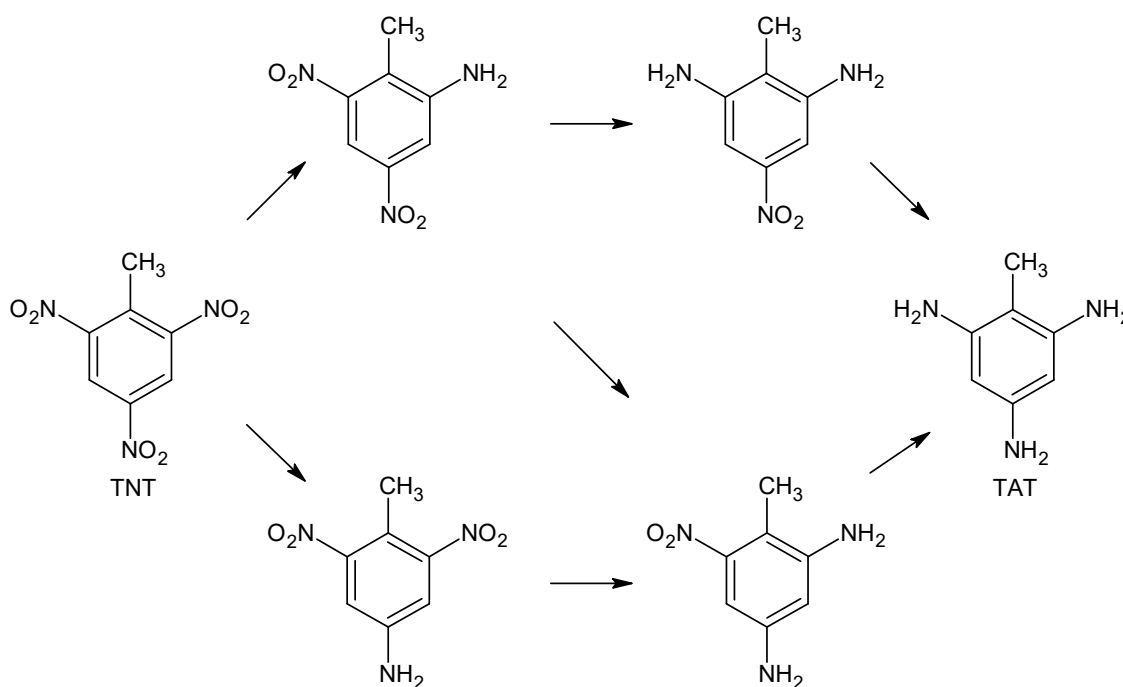


**Figure 3-2 Schematic outlining reduction pathway from TNT to TAT, adopted from Bandstra.<sup>219</sup>**

Like Bandstra *et al.*, Jafarpor *et al.*<sup>220</sup> outline the use of iron for the reduction of dinitrotoluene isomers with only a brief appearance of the intermediates. Other studies on the reduction of nitro aromatics using iron,<sup>221,222</sup> tin<sup>223,224</sup> and zinc<sup>225</sup> note

similar findings and report a reduction time of up to 90 minutes for full conversion to the amine.

The use of ammonium formate for the mild reduction of aromatic and aliphatic nitro compounds has been reported to produce fewer by-products than the methods outlined above.<sup>216,226-228</sup> Furthermore, these methods have been reported to be highly chemoselective, preserving other functional groups present. While some studies use gold<sup>226</sup> or copper<sup>227</sup> nanoparticles, others use the more conventional palladium on carbon (Pd-C) approach.<sup>228</sup> Pd-C has also been used in combination with sodium borohydride in THF to reduce nitroaromatic compounds to their corresponding amines at room temperature within 60 minutes.<sup>217</sup>

Oh et al. showed that the attempted reduction of RDX and HMX with elemental iron resulted in relatively constant yields of formaldehyde, but also inconsistent levels of N<sub>2</sub>O and NH<sub>4</sub><sup>+</sup> and other soluble by-products.<sup>221</sup>

Some of the colorimetric tests used for detection of explosives (See Section 3.1.2) utilise the reduction of nitro groups to amines prior to tagging with a reagent which induces fluorescence.<sup>194,229</sup> While these methods are quite sensitive, detecting explosives down to nanogram amounts, they are often not selective.

To be operationally viable and for ease of use in the field, the reduction technique is required to be simple, relatively quick and inexpensive. Existing methods for the rapid reduction of nitro groups can often be too harsh and lead to undesired reductions of other functional groups, or cause the analyte to breakdown. Herein lies the challenge: the development of a single technique which is both strong enough to reduce nitroaromatic, nitramine, and nitrate ester functional groups in solution to their primary amines, but at the same time gentle enough to preserve the molecules and not form undesired by-products. While systems exist that are successful in targeting



specific functional groups,<sup>218-220</sup> developing a “one size fits all” approach applicable to nitroaromatics, nitramines and nitrate esters, may be problematic.

### 3.1.5 Derivatisation of amino groups

The transformation of nitro compounds to their corresponding amines is an important reaction in organic chemistry as the amine group serves as a site for further derivatisation.<sup>216</sup> Using amine-specific reagents to produce intense colours is well-documented in fingerprint development literature<sup>230</sup> and for the detection of amines on TLC plates.<sup>231,232</sup> For example, ninhydrin is a well-known amine-specific reagent that upon reaction with amino acids, such as those present in fingerprint deposits, forms an intense colour that can be photographed.<sup>230</sup>

While the sensitivity of ninhydrin and similar compounds is sufficient for fingerprint deposits, a tagging compound with greater sensitivity and selectivity is required for the trace analysis of explosives. Additionally, a key criteria for the selection of a derivatising agent is that it incorporates itself into the final fluorescent compound, thus leading to fluorophores with potentially unique landscapes. Ninhydrin is not suitable for this purpose because the fluorophore is always Ruhemann’s purple regardless of the analyte amine.<sup>233</sup>

Much like the reduction parameters described above, the chosen derivatisation method should be simple, quick and relatively cheap for routine use in the field. Three amine-specific reagents that may meet the required criteria are *o*-phthalaldehyde (OPA), naphthalene-2,3-dicarboxaldehyde (NDA) and diphenylmaleic anhydride (DPMA).

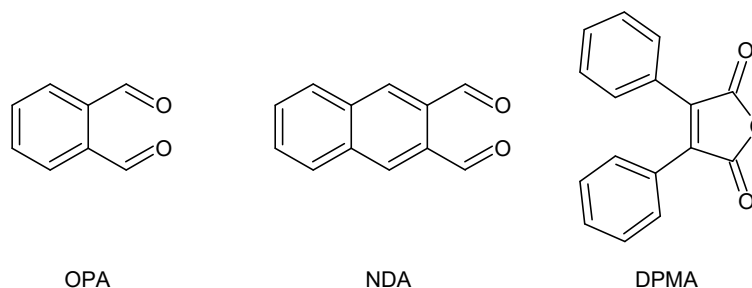


**Figure 3-3 Structures of derivatising agents OPA, NDA and DPMA.**

Roth<sup>234</sup> observed that OPA reacted with amino acids in the presence of 2-mercaptoethanol to give rise to strongly fluorescing compounds within five minutes at room temperature. Since the work of Roth, OPA has featured in a number of research articles and is a commonly used derivatising agent for not only primary amines and amino acids<sup>235-239</sup> but also other functional groups. Zuman<sup>240</sup> notes 175 references in his review of OPA reactions, including the addition of water and hydroxide ions to alcohols, thiols and other sulphur-containing compounds.<sup>240</sup> A common application of OPA is in the fluorometric determination of suitable analytes post-separation with ion chromatography<sup>239</sup> or HPLC.<sup>241</sup> Benson described the use of OPA for the derivatisation of amino acids as far superior to ninhydrin and fluorescamine.<sup>242</sup>

Carlson *et al.*<sup>243</sup> built on the work by Roth by synthesising NDA for the derivatisation of amines. They described the use of sodium cyanide rather than 2-mercaptoethanol as the nucleophile for the derivatisation of amines with NDA.<sup>243</sup> It has been demonstrated that the products of the corresponding derivatisation with NDA were more stable in solution than those with OPA, though the derivatisation with NDA was noted to take up to two hours.<sup>243,244</sup> Comparative studies between OPA, NDA and the anthracene derivative (ADA) show an increase in fluorescence with conjugation i.e. the products from the derivatisation with ADA are more fluorescent than those using NDA and so on.<sup>236</sup>

The use of DPMA has been demonstrated for the derivatisation of primary and secondary amines to increase the sensitivity and selectivity of HPLC analysis.<sup>245</sup> Pawlowska *et al.* noted a three-minute reaction time at room temperature.<sup>245</sup>

### 3.1.6 Parallel Factor Analysis (PARAFAC)

The main application of PARAFAC in the literature has been in the analysis of fluorescence landscapes (or EEMs). PARAFAC has the power to decompose the landscapes into individual components and recover true spectra. This relies on the correct selection of the number of components and an appropriate signal-to-noise ratio.<sup>85,165</sup> The PARAFAC model is constructed using multiple landscapes collected for mixtures of known or unknown composition. Conventionally, these datasets consist of tens or hundreds of landscapes, but, in a real-world forensic scenario this may not always be possible or appropriate. Successful PARAFAC modelling has been demonstrated with datasets of fewer than ten samples.<sup>246,247</sup>

Like the other previously noted applications of PARAFAC, the forensic applications to date have mainly been in the analysis of EEMs, with demonstrated applications in the area of forensic marine science,<sup>91,209,210</sup> the analysis of fibres<sup>213</sup> (where EEMs and PARAFAC were used to differentiate between visually indistinguishable fibres), and for the analysis of steroids in cosmetics.<sup>248</sup> The use of PARAFAC and fluorescence data has also been used for the detection of doping agents in urine.<sup>249</sup>

The use of PARAFAC in forensic science has also extended to other instrumental techniques, including the use of gas chromatography paired with various mass spectrometry techniques for the analysis of diesel fuel<sup>250</sup> and impurity profiling of chemical weapon precursors.<sup>251</sup> To our knowledge, no reports have applied PARAFAC to the analysis of organic explosives.

The ability of PARAFAC to recover the true spectra (landscapes) of the components in a mixture relies heavily on the correct selection of the number of components. The DOMFLUOR toolbox for MATLAB contains a number of functions that can assist in the development of accurate PARAFAC models, including the selection of the correct number of components. The *OutlierTest* is one such function which, although it aims (as the name suggests) to identify outliers in a large set of data, can also be a vital tool in determining the correct number of components. The *OutlierTest* calculates a series of PARAFAC models, using from 2 to  $f$  factors, where  $f$ , the maximum number of components to model, is defined by the user.<sup>89</sup> The results from these runs can then be evaluated to estimate the correct number of components in the dataset. This decision is made by the user, and requires a basic understanding of fluorophores. In essence, as the number of components increases, the user needs to identify the point at which the spectra identified by the model still represent organic fluorophores, and not noise or scatter, which may be represented by narrow, sharp bands.

Another powerful tool that can be used to determine the correct number of components in PARAFAC is the core consistency diagnostic (CORCONDIA).<sup>159</sup> This can be calculated independently or together with PARAFAC using the N-WAY toolbox. The CORCONDIA will return the degree of consistency, with a max value of 100%. A CORCONDIA value below 90% is indicative of a poorly fitted model, suggesting that an incorrect number of components (too few or too many) have been modelled.<sup>159</sup>

Although its use may be limited in this application of PARAFAC, *SplitHalfAnalysis* is another useful tool available to users of PARAFAC. For the technique to be effective, a large dataset of samples, containing the same analytes at different concentrations, (known or unknown) needs to be analysed and combined. The technique splits the data, performs PARAFAC modelling of the data *halves*, and then compares the models to determine if a valid model is formed.<sup>89</sup> This method would be suited to testing scenarios but is not applicable to real world scenarios, where the makeup of the

sample is unknown, and (for example) the amounts of each explosive in a mixture, cannot be controlled.<sup>89</sup>

### 3.1.7 Aims

This study focusses on the use of fluorescence landscapes to detect and quantify trace levels of explosive compounds by analysis with PARAFAC. The nitro-containing explosives firstly require reduction to their corresponding amines by a method that is fast and field deployable. The reduced compounds can then be derivatised to highly fluorescent products prior to collection of fluorescence landscapes. PARAFAC will then be used to analyse the fluorescence data and yield information about the mixtures.

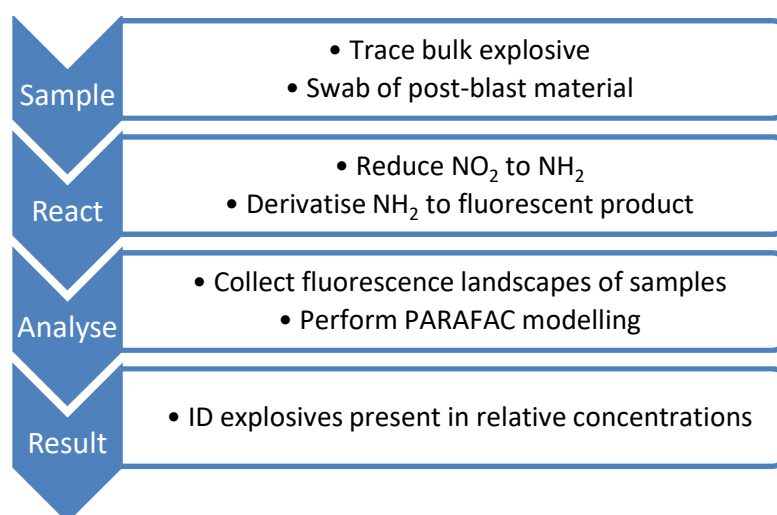


**Figure 3-4 Work flow diagram for the analysis of explosives.**

Figure 3-4 above outlines that following the collection of suspected nitro-containing explosive compounds, the nitro (-NO<sub>2</sub>) groups of organic explosives are reduced to amines (-NH<sub>2</sub>), which are subsequently derivatised in solution to form a fluorescent product. A fluorescent landscape is collected for each of the resulting solutions. The landscapes are then combined into a dataset and the data is pre-processed and subjected to PARAFAC analysis as a set. The end result is an identification of the explosives present in each of the mixtures and an indication of their relative ratios.

## 3.2 Experimental

### 3.2.1 Sample preparation

#### 3.2.1.1 Compounds

A number of test compounds were selected as a representation of the most popular nitro-containing organic explosives. Compounds 2,4-dinitrotoluene, 2,6-dinitrotoluene, picric acid (2,4,6-trinitrophenol) and 2,4-diaminotoluene were purchased from Sigma-Aldrich and used as received. 2,4-diaminotoluene (2,4-DAT) was purchased in order to compare the results from a commercially prepared amine versus the results from amines made from the reduction of nitroaromatic compounds. Reagents, catalysts and derivatising agents 2-mercaptoethanol, ammonium formate, elemental zinc, iron and tin, *o*-phthalaldehyde (OPA), diphenylmaleic anhydride (DPMA), naphthalene-2,3-dicarboxaldehyde (NDA) were purchased from Sigma-Aldrich or Fluka chemicals and used as received. Samples of (non-explosive) aromatic amines were also obtained to test the performance of the derivatisation methods.



**Figure 3-5 Samples of commercial explosive samples as supplied by the AFP.**

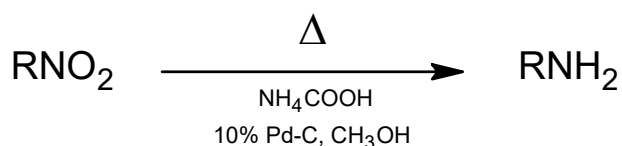
Samples of commercial explosives were supplied by the AFP for testing, but some of these samples (sample numbers 4, 5 and 9 - Figure 3-5) fell outside the scope of this research as they did not contain nitro groups. Explosive samples were stored and handled under the conditions set out in the Workcover NSW exemption under clause 93 of the *Explosive Regulation 2005*.

Sample #	Commercial name	Nitro containing explosive component
1	Primasheet	RDX
2	PE4 military explosive	RDX
3	Detonator cord	PETN
4	ANFO	-
5	Orica senatel magnum	-
6	UEE Booster - 26	PETN, TNT
7	Anzomex D Primer	PETN, TNT
8	Orica Pentex PPP booster	PETN, RDX, TNT
9	Black powder	-

**Table 3-2 Explosive samples supplied by the AFP - Sample numbers relate to number in Figure 3-5.**

### 3.2.1.2 Reduction

The mild reduction of nitro groups in the organic explosives was performed as a modification of the method outlined by Ram.<sup>228</sup> For testing, the method involved dissolving 100 mg of organic explosive in approximately 10 mL of dry methanol. The solution was heated to 40°C with moderate stirring while 30-40 mg of 10% Pd-C was added. Anhydrous NH<sub>4</sub>COOH (ammonium formate) was added at a mole ratio of 1:12 organic explosive:NH<sub>4</sub>COOH.



Generally, a colour change from pale yellow/orange to colourless indicated completion for most compounds. Nevertheless, the reaction was monitored with thin-layer



chromatography (TLC). Once TLC indicated completion (30-50 mins), the 10% Pd-C was removed by filtration and the methanol was evaporated. In most cases, the derivatisation was performed on the crude product, without further purification. In some cases, water was added to the residue and the product was extracted into a suitable organic solvent. The solution was then dried over Na<sub>2</sub>SO<sub>4</sub> before evaporation of the organic solvent gave the isolated amino derivative.

### 3.2.1.3 Derivatisation

The derivatisation of the amino compounds with *o*-phthalaldehyde (OPA) was performed as per the method outlined by Roth.<sup>234</sup> OPA (10 mg/mL in ethanol, 1.5 mL) and 2-mercaptoethanol solution (5 μL/mL in ethanol, 1.5 mL) were added to 90 mL of a 0.05 M borate buffer (adjusted to pH 9.5). The amine solution (10<sup>-4</sup> to 10<sup>-3</sup> M, 100 μL) was added to 3 mL of the buffered reagent solution and the fluorescence landscape was collected 5 to 15 minutes after mixing at room temperature.

To confirm that the desired isoindole derivatives were formed, high-resolution mass spectrometry was used to analyse the solutions. The spectra were obtained with an Agilent Technologies 6520 Q-TOF LC/MS. Separation was performed using a Zorbax SB-C18 column (Agilent Technologies) with an isocratic mobile phase containing 70:30 acetonitrile:H<sub>2</sub>O + 0.1% formic acid.

## 3.2.2 Collection of landscapes

Fluorescence landscapes were collected on a Varian Cary Eclipse fluorescence spectrophotometer. An excitation range of 270-500 nm with 10 nm steps was used with emission spectra collected from 270-600 nm at steps of 5 nm. Both excitation and emission slits were set at 5 nm. A fast scanning rate of 3000 nm min<sup>-1</sup> was used. Landscapes were collected in under four minutes each. The data was exported as .csv files that were directly imported into MATLAB for PARAFAC analysis.

### 3.2.3 Data analysis - PARAFAC

The fluorescence landscapes were analysed by PARAFAC to retrieve landscapes of each component in the mixture. PARAFAC, CORCONDIA and associated pre-processing was performed in MATLAB 2008b (The MathWorks, Inc.) using the DOMFLuor,<sup>89</sup> N-way<sup>159</sup> and drEEM<sup>161</sup> toolboxes.

The landscapes to be analysed were concatenated in MATLAB prior to analysis by PARAFAC. Scattering was removed using the inbuilt EEMCut functionality of the DOMFLuor toolbox or the *smootheem* functionality of the drEEM toolbox. The effect of normalisation was trialled using *normeem* in the drEEM toolbox. The ideal number of PARAFAC components was selected based on several techniques including the examination of residuals, *OutlierTest* and CORCONDIA values of the PARAFAC model. The fluorescence landscape of each component was reconstructed in MATLAB and compared to landscapes of the known individual components.

## 3.3 Results and Discussion

As previously outlined, the aim of this research was not only to assess the potential of this methodology in successfully identifying trace explosive compounds, but also to develop a process that can be realistically performed in the field. With that in mind, restrictions were placed on the wet chemistry components of the method, i.e. the reduction of nitro groups to their corresponding amines and the derivatisation of the amines to fluorescence products. These restrictions involved:

- minimising the use of hazardous chemicals;
- using 'one-pot' style reactions where possible to minimise the need for extraction and/or filtering;

- reactions that were insensitive to the atmosphere (i.e. do not need to be performed in an inert environment such as nitrogen or argon gas); and
- keeping the time taken for the entire process to a minimum.

### 3.3.1 Reduction of nitro aromatics

A number of reduction conditions were tested with limited success. Gowda<sup>215</sup> reported reduction of 2,4-dinitrotoluene to the resulting amine in five minutes at 90% yield. This claim was tested under a range of conditions, including modifications of the reagents and reaction conditions, but could not be replicated. Monitoring of the reaction by TLC and analysis of the final product by NMR revealed an abundance of intermediate compounds and starting product, with minimal conversion to the amine. A mixture of tin and HCl in 50:50 acetonitrile:methanol and heated to 40°C gave complete conversion in approximately 40 min, but with a range of by-products present in the crude product. Following unsuccessful trials with this method and other reactions, including the use of NaBH<sub>4</sub> and charcoal,<sup>217,218</sup> the method proposed by Ram<sup>228</sup> was tested.

Starting Product(s)	Expected finished product(s) identified	Reaction time (min)
2,4-DNT	Yes	20
2,6-DNT	Yes	20
TNT	Yes	40
Picric acid*	Yes	35
PETN	No	†
RDX	No	†
2,4-DNT + 2,6-DNT	Yes	20
2,4-DNT + TNT	Yes	40
2,4-DNT + 2,6-DNT + TNT	Yes	40
Orica Pentex PPP booster (PETN + RDX + TNT)	TAT identified**	40

**Table 3-3 Outline of desired products and average reaction time for the reduction of target compounds. \*picric acid was not tried in mixtures with other explosive compounds due to the known instability of this compound. †reaction times from 5 minutes to 48 hours were trialled with limited success. \*\*see comments below regarding reduction products of RDX and PETN.**

A modified version of the reaction proposed by Ram was determined to be suitable for the reduction of nitroaromatic compounds. No single method was identified that successfully reduced nitroaromatic, nitramine, and nitrate ester functional groups simultaneously. Therefore this modified technique is proposed for nitroaromatic explosives only. Interestingly, studies on post blast residue from controlled explosions containing TNT, PETN and RDX show that, on average, TNT is generally found in higher concentrations in post blast residue compared to PETN and RDX.<sup>252</sup> This is likely due to TNT being a more stable compound with a likelihood of persistence that can be influenced by the efficiency of the detonation. Table 3-3 also shows that, nitroaromatics (such as TNT), in the presence of PETN and RDX, are still successfully reduced to their corresponding amine.

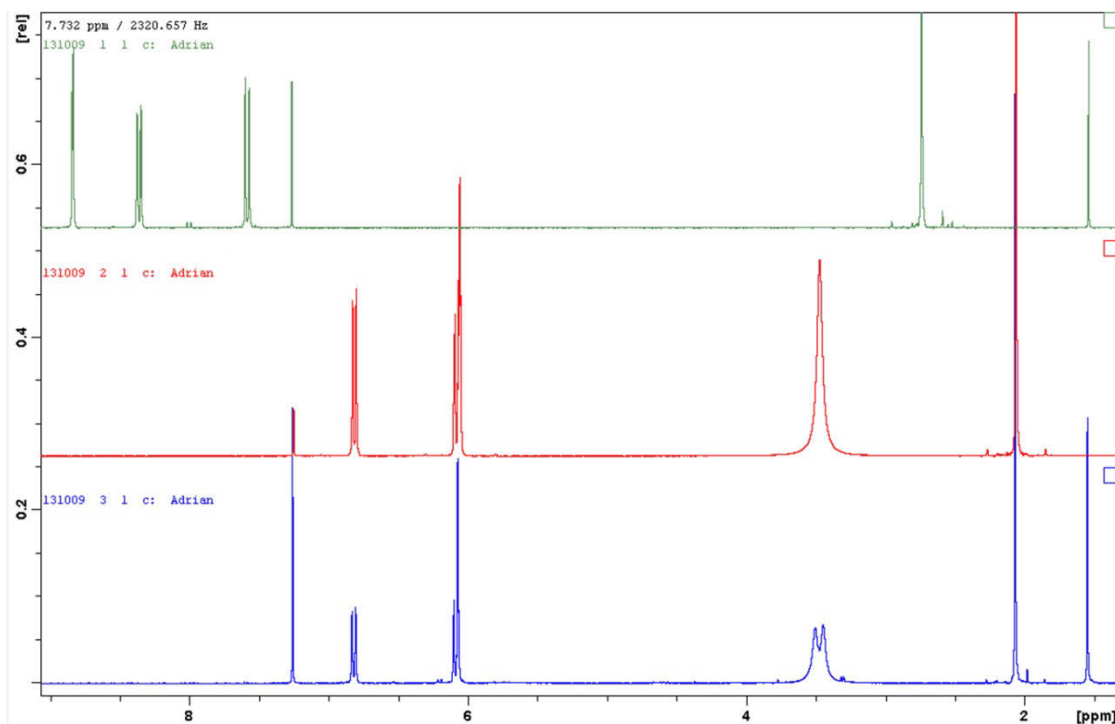


**Figure 3-6**  $^1\text{H-NMR}$  spectra of pure 2,4-DNT (green), pure 2,4-DAT (red) and 2,4-DAT from a reduced sample of 2,4-DNT, demonstrating a full conversion to the amine.

The nitroaromatic compounds 2,4-DNT, 2,6-DNT and TNT, either individually or in mixtures, were successfully converted to their amino derivatives in a reasonable time frame and under conditions that could be implemented in the field. Table 3-3 above shows the average time taken to completely reduce the compounds in solution from the time the palladium was added. The reaction times in Table 3-3 above demonstrate that, on average, the reduction of TNT took longer than the corresponding di-nitro compounds. This is expected with the increasing number of nitro groups on an aromatic compound.

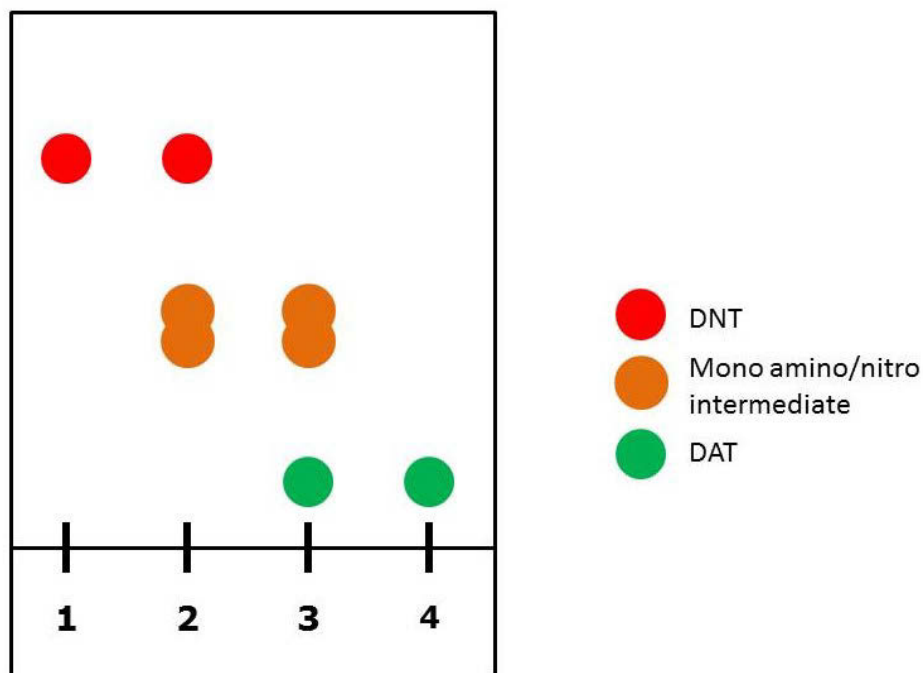


**Figure 3-7 Schematic of TLC reaction monitoring, showing the reduction of 2,4-DNT to 2,4-DAT. 1 = DNT, at start of reaction. 2= intermediate and DNT present within minutes of reaction starting. 3 = disappearance of DNT and appearance of DAT (sometimes DAT/DNT co-exist) 4 = full conversion to DAT with no intermediate or DNT present.**

The reduction reactions were monitored by  $^1\text{H-NMR}$  (Figure 3-6) and TLC (Figure 3-7).  $^1\text{H-NMR}$  showed that the reduction from nitroaromatic to aromatic amine with the proposed method resulted in a full conversion with no formation of by-products. The TLC schematic in Figure 3-7 above demonstrates the typical results obtained during the reduction. This example shows the reduction of 2,4-DNT to 2,4-DAT and confirms that the intermediates appear and disappear throughout the reduction; the structures of these intermediates are shown in Table 3-4 below. This aligns with the process outlined in Figure 3-2 as demonstrated by Brandstra et al.<sup>219</sup> for the reduction of TNT to TAT.

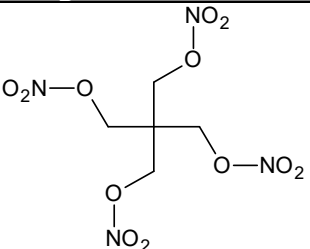
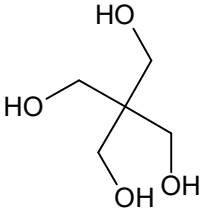
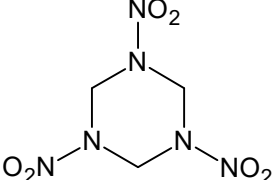
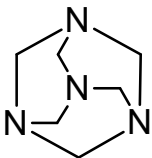
Starting Product	Intermediates	Expected Finished Product
TNT	See Figure 3-2 Schematic outlining reduction pathway from TNT to TAT, adopted from Bandstra. <sup>219</sup>	
Picric Acid		
2,4-DNT		
2,6-DNT		

**Table 3-4 Intermediates and products obtained from the reduction of nitroaromatic explosives TNT, 2,4-DNT and 2,6-DNT.**

While the method described is suitable for mixtures of nitroaromatic explosives, a limitation is that the reductions of PETN and RDX were not successful. Thus as described above, the technique is proposed for nitroaromatic explosives only. However, for commercial explosives that contained mixtures of TNT with PETN and/or RDX, the TNT was successfully converted to TAT, even though the reduction of PETN and RDX to their corresponding amines was not successful.

Following the attempted reduction of samples containing PETN, RDX, or mixtures of these, <sup>1</sup>H-NMR and GC-MS analysis confirmed that the reduction products of PETN and RDX were 2,2-bis(hydroxymethyl)-1,3-propanediol (pentaerythritol) and

hexamine respectively. Previous research has shown ammonia and formaldehyde to be the products of the reduction of RDX.<sup>221</sup> Furthermore, both ammonia and formaldehyde can be formed as by-products in the proposed reduction reaction and can react further to form hexamine. Neither ammonia nor formaldehyde were seen among the products of the reductions, supporting the hypothesis that the exposure of RDX to these reaction conditions led to further reaction to form hexamine. Pentaerythritol and hexamine are fluorescent themselves and cannot be derivatised with OPA.

	Starting Product	End product
PETN		
RDX		

**Table 3-5 End products obtained from the reduction of explosives PETN and RDX.**

### 3.3.2 Derivatisation

Prior to the derivatisation of samples of nitro aromatics that had been reduced to amines, the outlined method (Section 3.2.1.3) was performed on mixtures of pure aromatic amines. In these instances, the derivatisation was demonstrated by a change in the collected fluorescence landscape as shown in Figure 3-8, Figure 3-9 and Figure 3-10 below.



## o-Phthalaldehyde (OPA) buffer solution

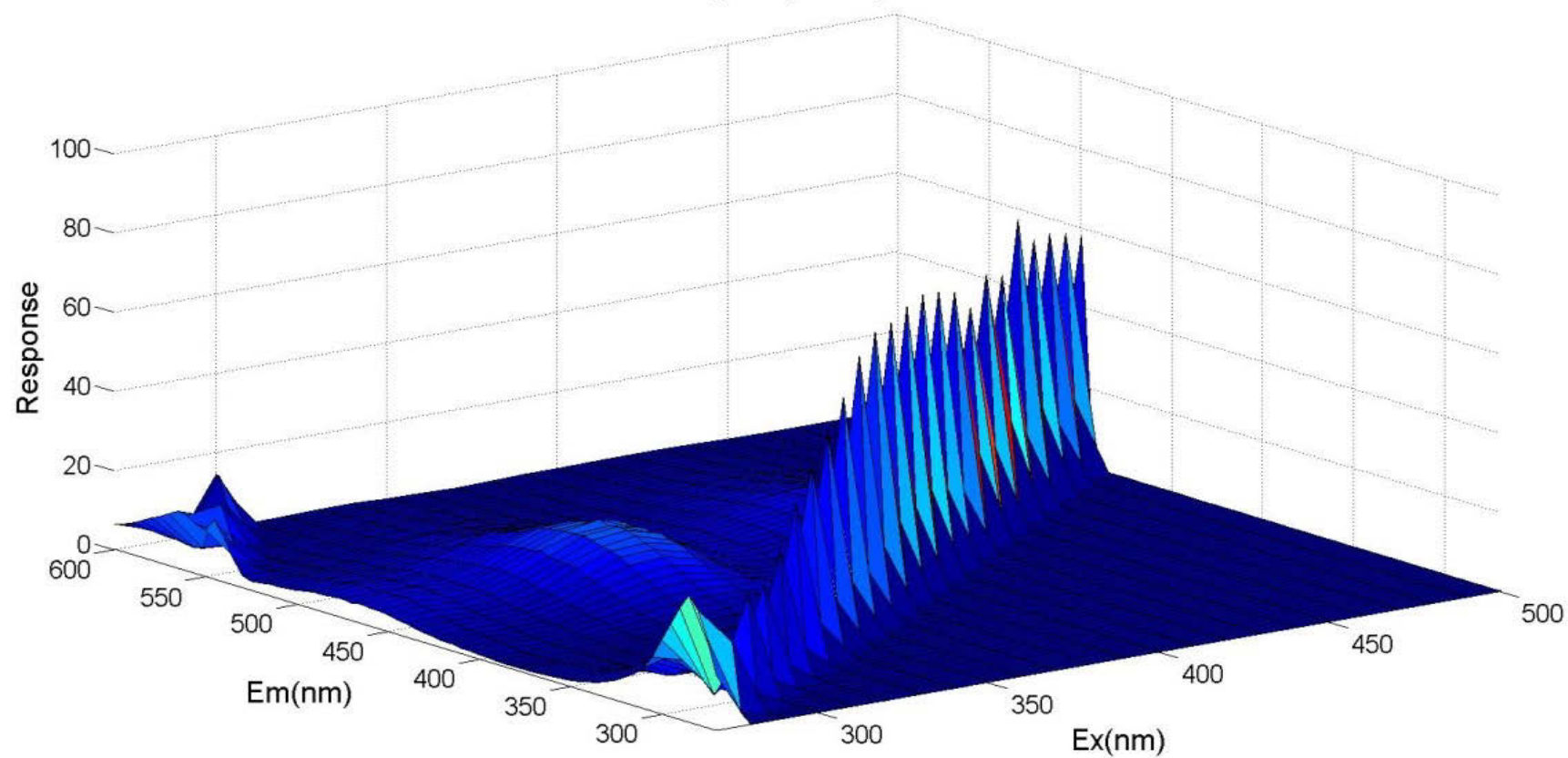


**Figure 3-8** Fluorescence landscape of blank OPA buffer solution showing minimal fluorescence.

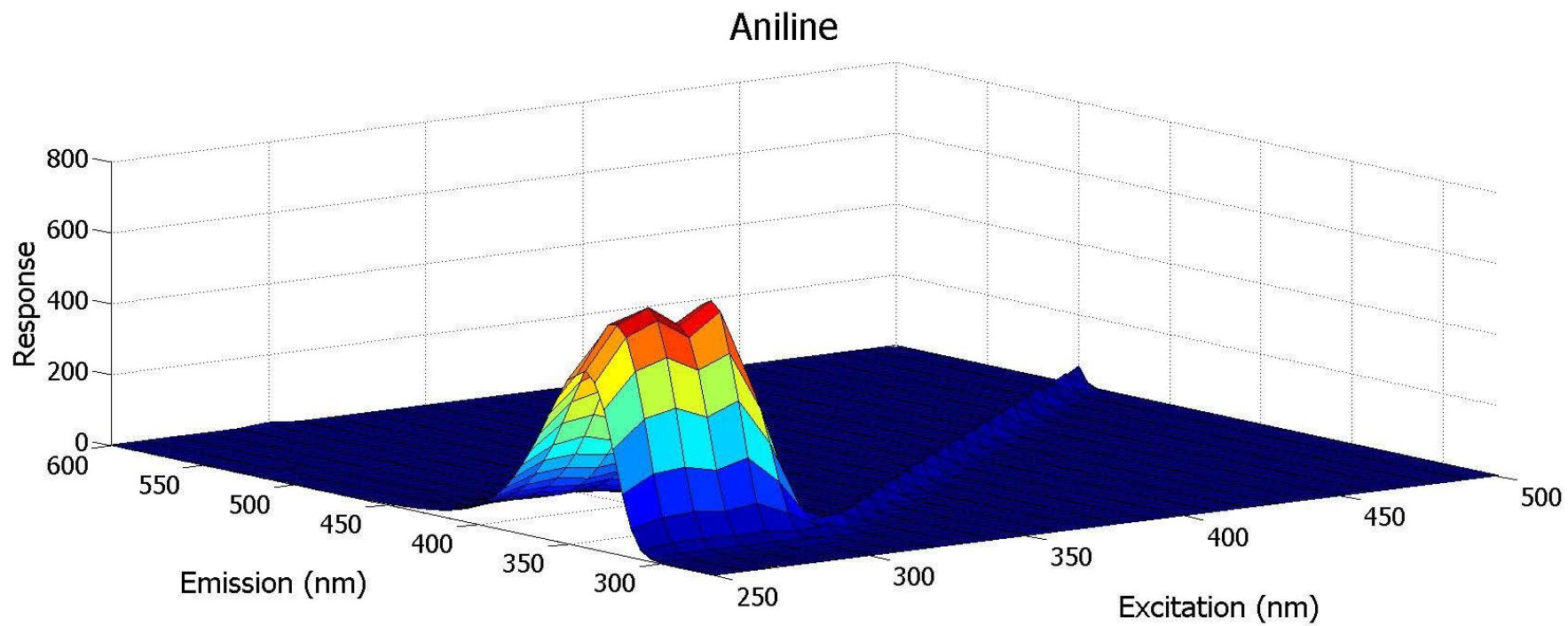


**Figure 3-9** Fluorescence landscape of aniline solution. Note change in scale relative to that in Figure 3-8 and Figure 3-10.

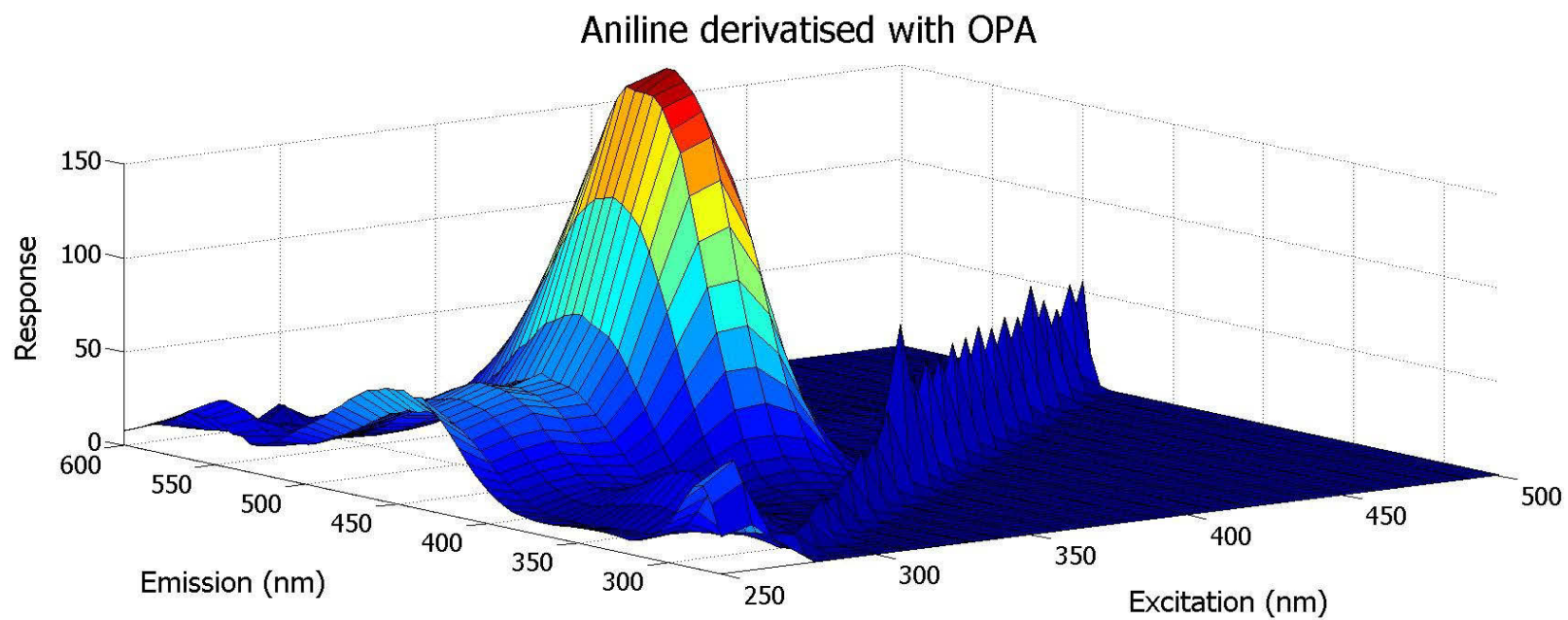


**Figure 3-10** Fluorescence landscape of Aniline derivatised with OPA.

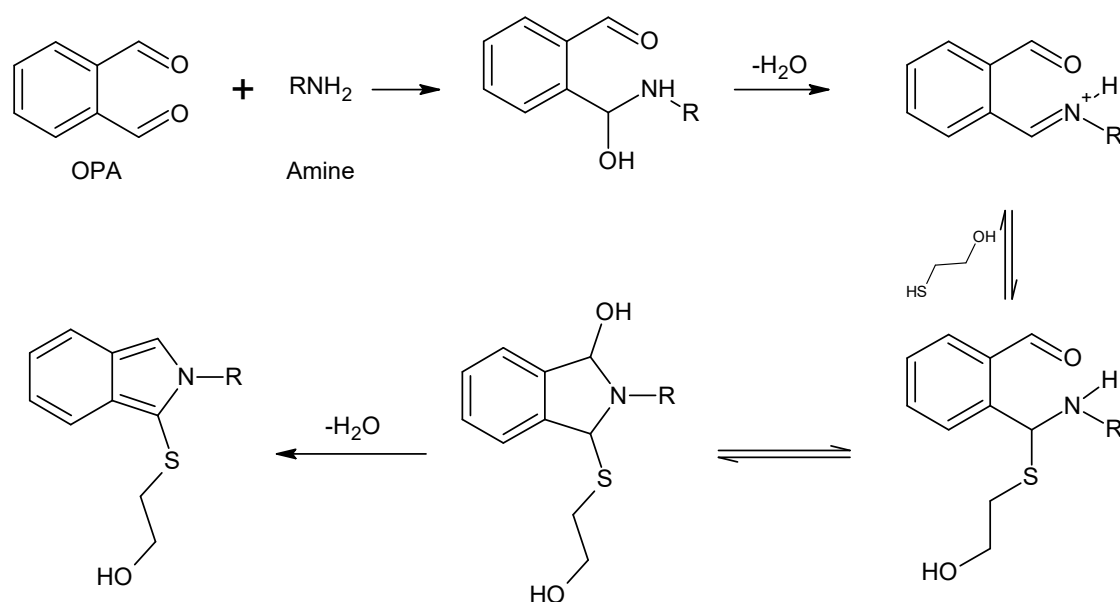
The Rayleigh and Raman scattering mentioned previously can be seen in Figure 3-8, Figure 3-9 and Figure 3-10 above. It occurs in regions where the excitation and emission values are similar. This scatter is seen as a diagonal line of very narrow peaks; it can be more intense than the fluorescence of interest and is removed prior to the analysis of landscapes.

Figure 3-8 shows that the OPA buffer solution has a very weak signal, which is significantly amplified following the derivatisation as shown by the landscape for derivatised aniline in Figure 3-10. Conversely, Figure 3-9 and Figure 3-10 show that the fluorescence profile of aniline is substantially changed, and somewhat reduced in intensity, once it is derivatised with OPA. Notably, a very slight colour change was observed when the amine was added to the derivatising buffer solution. These results are further explored in Section 3.3.4 below.

The derivatisation of amines was not affected by the use of the crude reaction products from the reduction of nitroaromatics. This is important for field deployable techniques as it negates the requirement for the purification of material prior to testing, which ultimately saves time and reduces the need for chemicals and equipment. The only complicating factor in using crude product is the inability to accurately measure how much amine is present. As outlined in Section 3.2.1.3, 100  $\mu\text{L}$  of the amine solution ( $10^{-4}$  to  $10^{-3}$  M) is added to the buffer, resulting in a final concentration of approximately 20 ppm of amine in the OPA/buffer solution. As with other amines, the derivatisation of the reduced nitroaromatics induced a slight colour change in the solution. At higher concentrations of amine, the fluorescent adduct precipitated out of solution, and could not be accurately analysed as the resulting solid interfered with the collection of the fluorescence data. Prior to collecting the fluorescence landscape, it is possible to dilute the derivatised solution further to dissolve this product. More accurate results were achieved if the amine solution was diluted prior to the derivatisation step. No advantage was gained from longer

derivatisation times, mild heating, or performing the derivatisation in an inert atmosphere (under nitrogen or argon).

A mechanism for the generation of the fluorescent product with OPA is proposed in Figure 3-11. The mechanism shows that a primary amine is required for the desired product to be formed. This is consistent with previous research on the derivatisation of amines with OPA.<sup>241,242</sup>



**Figure 3-11 Proposed mechanism for OPA derivatisation of primary amine.**

High-resolution time-of-flight mass spectrometry (TOF-MS) confirmed the formation of isoindole derivatives for the crude amine derivatives of 2,4-DNT, 2,6-DNT and TNT. Figure 3-12 below demonstrates the structures of the 2,4-DAT, 2,6-DAT and TAT isoindole adducts that were confirmed by TOF-MS. The identification of these structures support the mechanism outlined in Figure 3-11 above. Sample mass MS spectra of the OPA adducts are given below in Figure 3-13, Figure 3-14 and Figure 3-15.

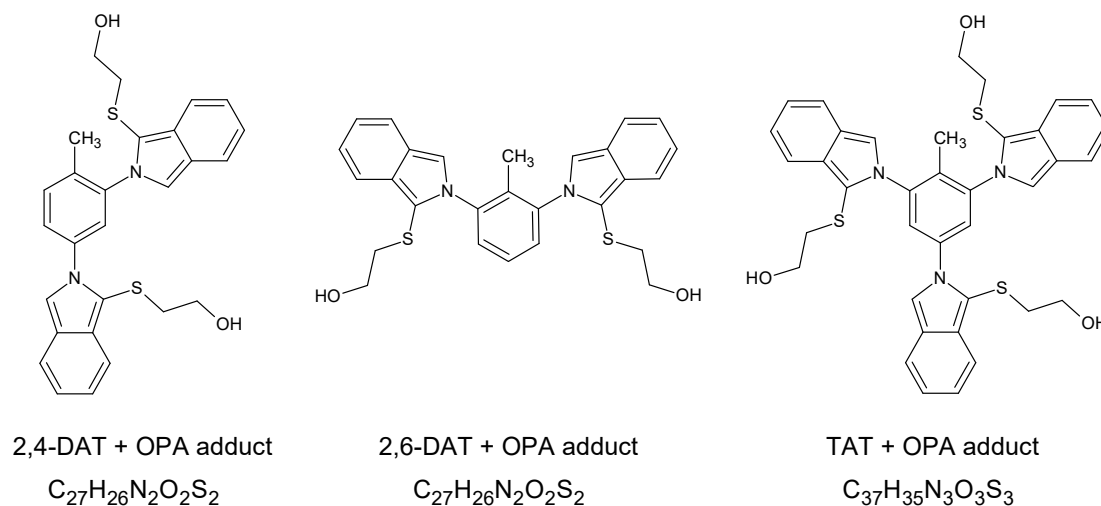


**Figure 3-12 Isoindole adducts identified by LCMS. These are the expected products for the diaminotoluene and triaminotoluene derivatisation with *o*-phthalaldehyde.**

Analysis by TOF-MS also proved 100% conversion for the derivatisation of 2,4-DAT, 2,6-DAT and TAT. No remaining starting material and no mono-, or di- (in the case of TAT) substituted OPA adducts were identified.

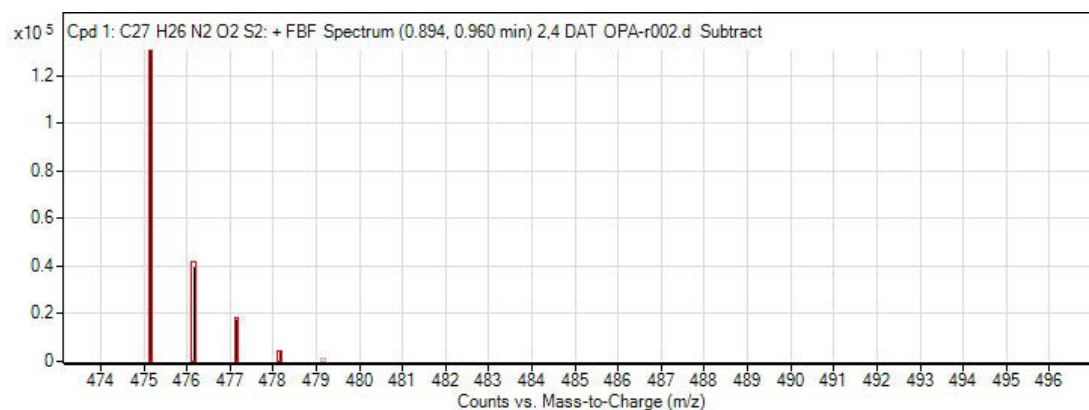


**Figure 3-13 Mass spectrum of pure 2,4-DAT derivatised with OPA. The red outline of the signal shows the expected library splitting pattern for the formula provided.**

Figure 3-13 and Figure 3-14 show the spectra for the OPA adducts of pure 2,4-DAT and crude 2,4-DAT respectively. The comparison of the expected (red) and obtained (black) splitting patterns in these spectra proves that using the crude product does not affect the end derivatisation product obtained.

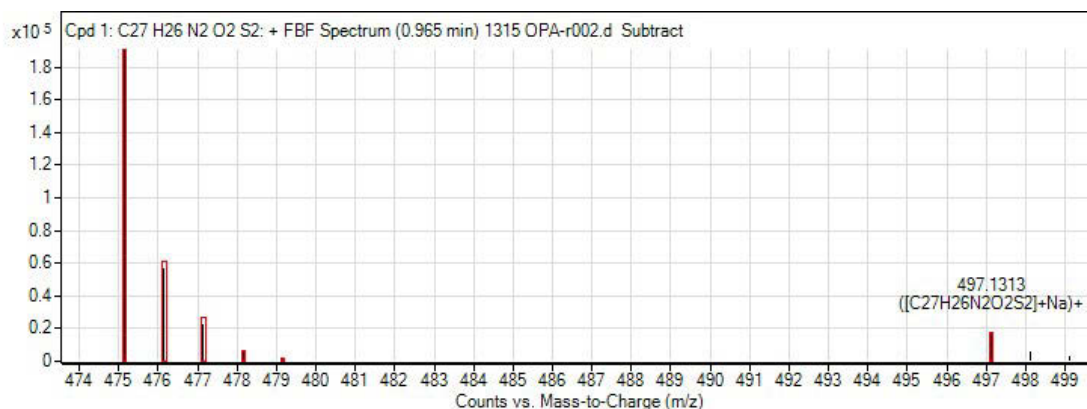


**Figure 3-14** Mass spectrum of crude 2,4-DAT (reduced from 2,4-DNT without purification) derivatised with OPA. The red outline of the signal shows the expected library splitting pattern for the formula provided.

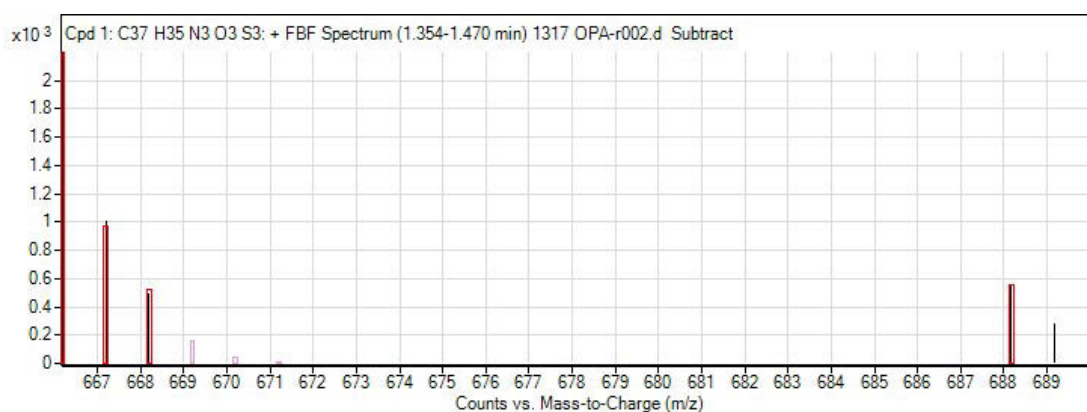


**Figure 3-15** Mass spectrum of crude TAT derivatised with OPA. The red outline of the signal show the expected library splitting pattern for the formula provided.

Both naphthalene-2,3-dicarboxaldehyde (NDA) and diphenylmaleic anhydride (DPMA) were also trialled as potential derivatising agents for aromatic amines. The reaction conditions set out by Carlson *et al.*<sup>243</sup> for the derivatisation of amines with NDA were deemed unsuitable for use outside of a laboratory setting. Furthermore, the suggested use of cyanide rather than 2-mercaptoethanol as the nucleophile for this reaction presented additional safety concerns. Various reaction times from five minutes to two hours were reported for the derivatisation to go to completion, in contrast to the quite uniform 15 minutes for the OPA derivatisation. The noted potential advantage of NDA over OPA was the stability of the derivatised products.

However, the reported instability of the amines derivatised by OPA was not found to be an issue in this work. It is hypothesised that product stability was not an issue as the fluorescence landscapes were collected in solution, 15 minutes from the time that the amine was introduced to the OPA buffer solution, and this is supported by stability studies of aniline derivatised with OPA.<sup>253</sup>

The increased conjugation offered by the extra aromatic ring in NDA in comparison to OPA could assist in the differentiation of highly overlapping fluorescence signals. This was not observed and the resulting landscapes collected from amines derivatised with NDA were also highly overlapping. Thus, NDA did not provide an advantage over OPA in the derivatisation of aromatic amines and was not investigated any further.

Pawlowska *et al.*<sup>245</sup> found that that the derivatisation of aliphatic and aromatic amines with DPMA occurred at room temperature in roughly three minutes. The method proposed by Pawlowska *et al.* was followed as described with successful derivatisation of 2,4-DAT (both the commercially sourced amine and 2,4-DAT formed via the reduction of 2,4-DNT) and TAT. However, the detection of amines via DPMA derivatisation was found to be orders of magnitude less sensitive than using OPA, with very little fluorescent signal when measured at the same detector voltage. In comparison to OPA, DPMA was also found to be less selective, with fluorescence landscapes of mixtures not showing the distinguishing features that were observed with OPA.

### 3.3.3 Collection of landscapes

The collection of fluorescence landscapes from quartz cuvettes was fast and straightforward. Each collection took approximately 4 minutes. Occasionally, solutions of amine that were highly concentrated (but not concentrated enough for the fluorescent adduct to precipitate out of the solution) would cause an emission



response above the range of the fluorescence detector. When this occurred, the amine solutions were diluted and the derivatisation step was repeated.

### 3.3.4 PARAFAC

PARAFAC is a powerful tool in the analysis of fluorescence EEMs. In practice, a PARAFAC model is usually calculated based on hundreds of landscapes of the samples of interest. For the in-field application of this work, where the samples being analysed are unknowns, large datasets are often not practical; not only because of the time taken to sample and process the results, but because of the limited amount of material that is likely to be available for testing. Furthermore, the limitations of this method in only being able to detect nitroaromatic explosives limit the possible variation in landscapes that will make up a dataset. Given this, the largest dataset examined in any one PARAFAC analysis consisted of twenty-one landscapes. As discussed in Section 3.1.6 above, previous research has demonstrated PARAFAC models can be developed with fewer than ten landscapes.

While PARAFAC is commonly used to model fluorescence landscapes, or EEMs, the data analysis is complicated by the presence of Rayleigh and Raman scattering. A function built into the DOMFluor, EEMCut, removes the scattering and sets the value of the response on the outer bounds of the scattering as zero. An example is given in Figure 3-16 below.

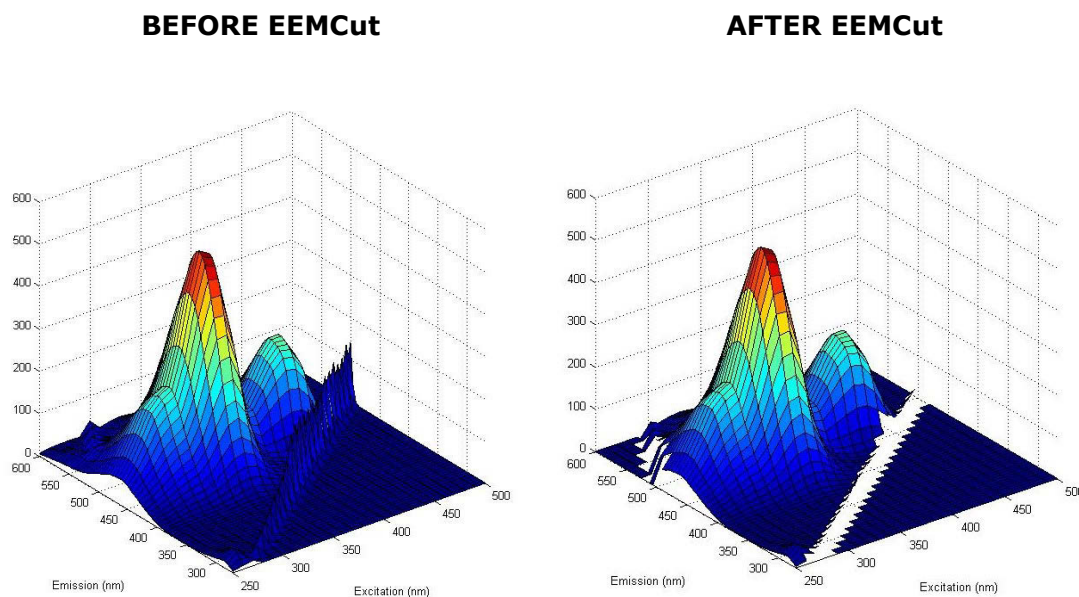


**Figure 3-16** Sample fluorescence landscapes before (left) and after removal of scattering using EEMCut (right).

As with the EEMCut function, the *smootheem* function in the drEEM toolbox can be used to remove the scattering. The *smootheem* function differs slightly from the EEMCut function in that it offers the option to interpolate across the excised scatter peaks.<sup>161</sup> Interpolation was not required in this work as the scattering was not interfering with the signal of the OPA adducts being analysed.

As described in Section 3.3.2, initial testing on the derivatisation of aromatic amines was performed with a range of compounds. The example for aniline and 4-aminobenzoic acid is shown below.

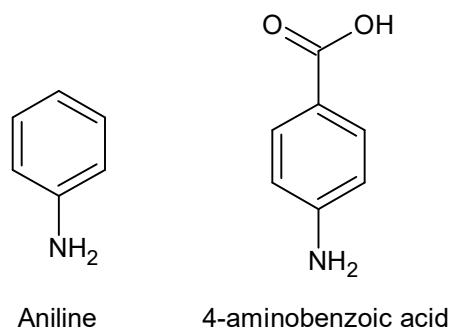


**Figure 3-17 Chemical structures of Aniline and 4-aminobenzoic acid**

Figure 3-18 below shows the XY or 'birdseye' view of the EEMCut-processed fluorescence landscape obtained for a 1:1 (molar ratio) mixture of aniline and 4-aminobenzoic acid derivatised by OPA. Two distinct signals at  $\lambda_{\text{Ex}} = 345 \text{ nm}$ ,  $\lambda_{\text{Em}} = 455 \text{ nm}$  and  $\lambda_{\text{Ex}} = 285 \text{ nm}$ ,  $\lambda_{\text{Em}} = 345 \text{ nm}$  can be seen for the OPA-derivatised aniline and 4-aminobenzoic acid respectively.

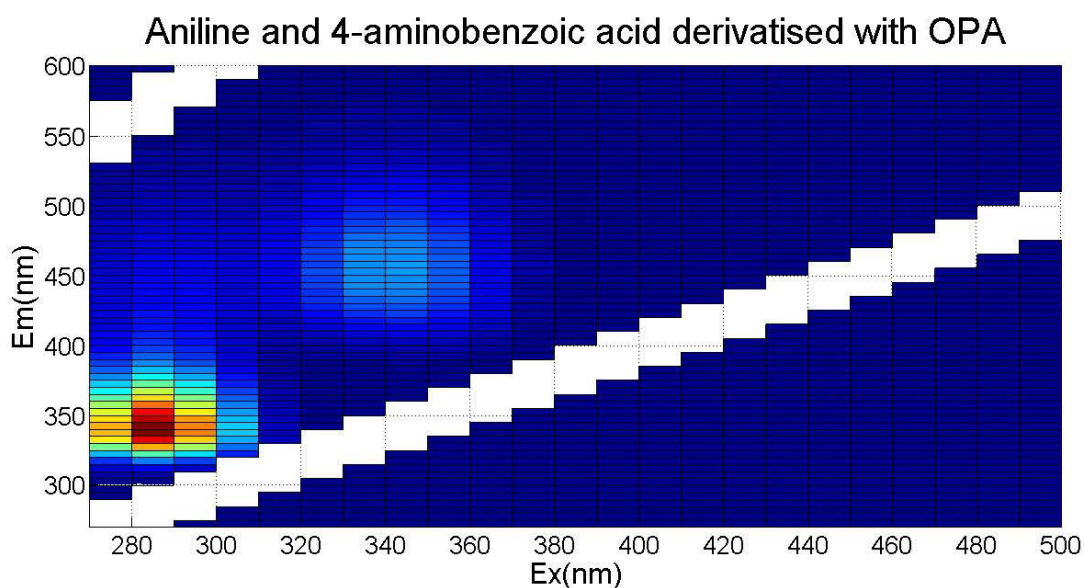


**Figure 3-18 Fluorescence landscape for a 1:1 mixture of aniline and 4-aminobenzoic acid derivatised with OPA (EEMCut performed).**

Figure 3-19 shows the XY view of the EEMCut-processed fluorescence landscape of the OPA buffer solution. Due to the relative nature of these plots, the colour scale

(dark blue (low) to dark red (high)) can only be used to compare intensities within a given plot, not between plots.

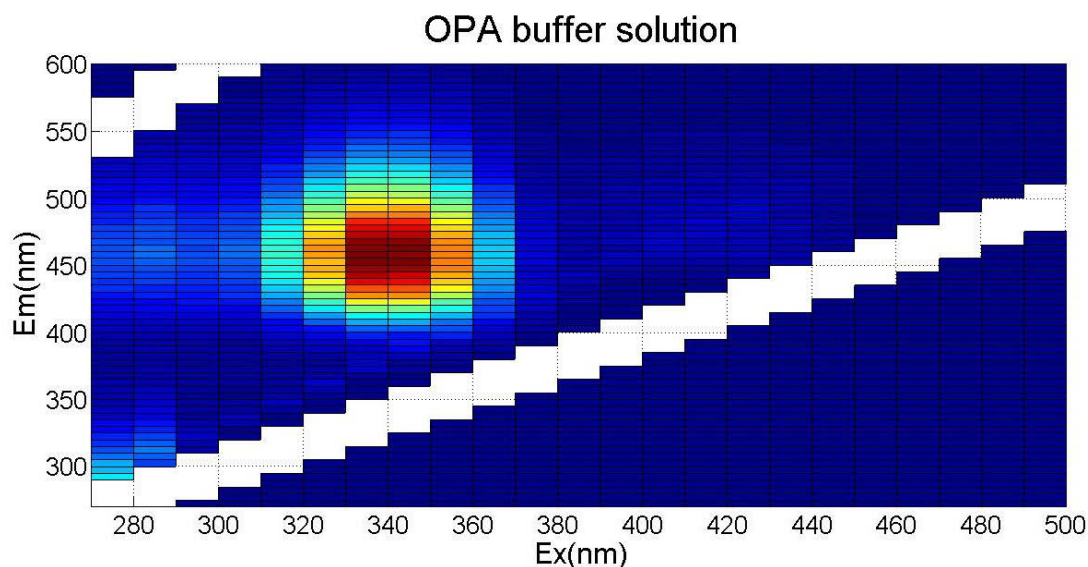


**Figure 3-19 Fluorescence landscape of OPA buffer solution prior to addition of amine (EEMCut performed).**

Figure 3-20 shows the result of the *OutlierTest* conducted during the PARAFAC analysis for the model amines shown in Figure 3-17, derivatised with OPA. The dataset contained landscapes of the mixture, the individual components and the blank OPA solution. The results for two- and three-component models are displayed. The CORCONDIA values for these and a four-component model of the same data is shown in Table 3-6.

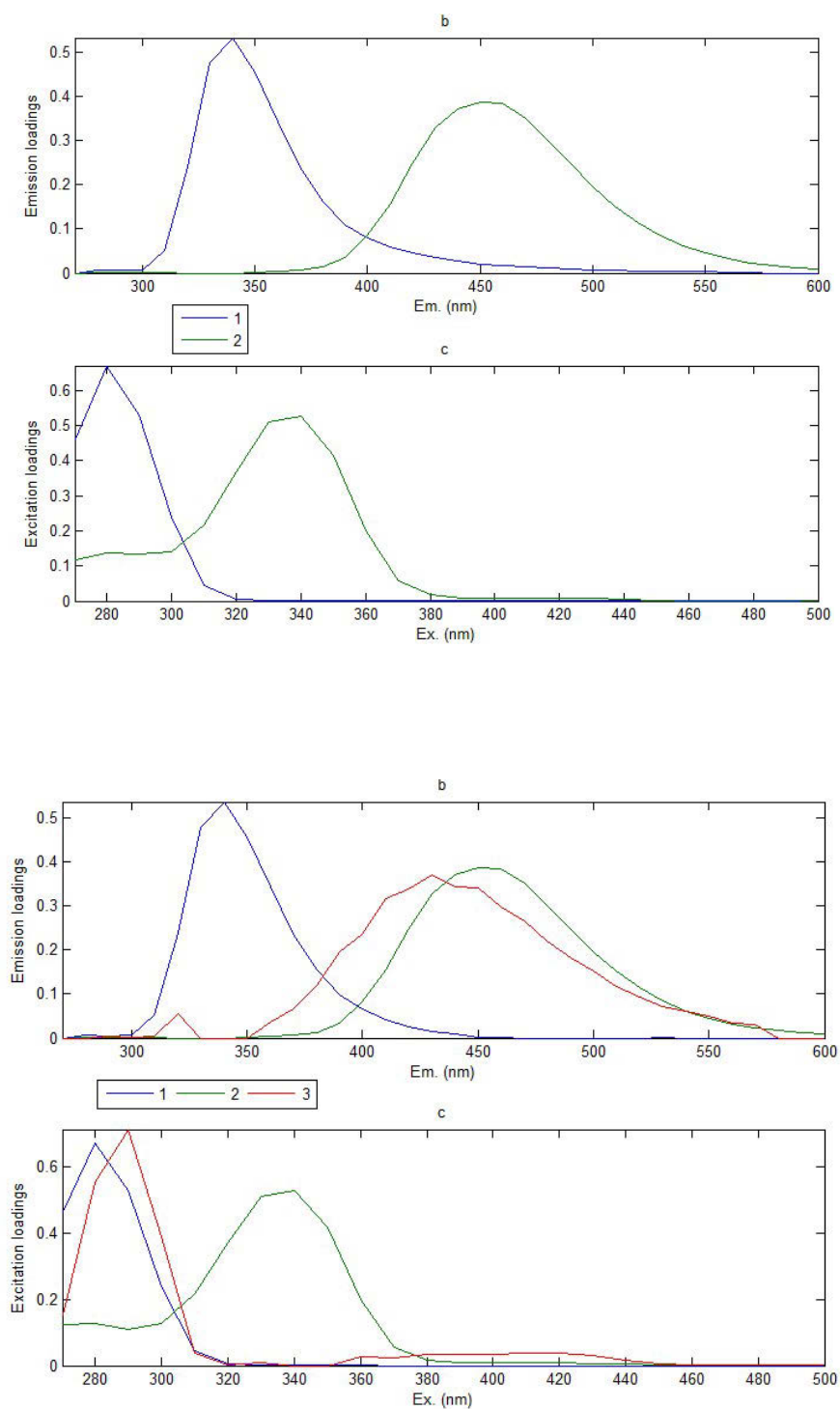


**Figure 3-20** Loading and leverage plots for two (top) and three (bottom) component PARAFAC models as predicted by the OutlierTest for the derivatised mixture of aniline and 4-aminobenzoic acid.

Core consistency diagnostic values	
Number of components	Value
2	99.9997
3	3.6787
4	2.6973

**Table 3-6 Core consistency diagnostic (CORCONDIA) values for PARAFAC models of aniline and 4-aminobenzoic acid mixtures derivatised with OPA.**

As described previously, the correct number of components predicted by the *OutlierTest* and CORCONDIA is the maximum number that yields spectra consistent with 'fluorescence like' signals and yields a CORCONDIA value close to 100. Analysis of the above shows that PARAFAC predicts two (2) components form the ideal solution.

The loadings for the two component PARAFAC model resemble what is expected from fluorescing isoindoles, i.e. relatively smooth, broad signals. While this is true for both the two- and three-component solutions shown in Figure 3-20, we see that the shape of the third (red) component is not as smooth, and is more irregular in shape than the first two components. When a fourth component is modelled (not shown), sharp, narrow bands are apparent in both the emission and excitation loadings; these are unlikely to represent fluorescence data and this is reflected in the poor CORCONDIA score of approximately 2.7 shown in Table 3-6 above. Notably, even though the loadings appear on the same scale, the scores when the PARAFAC model is run will determine the final intensity of these landscapes. As the scores are not helpful in determining the correct number of components, they are not shown at this stage of the analysis. Importantly, the excitation and emission loadings, the scores, and thus the resulting landscapes of the individual components are only estimations in the *OutlierTest*, these are refined when the PARAFAC model is built and can be seen in Figure 3-21.

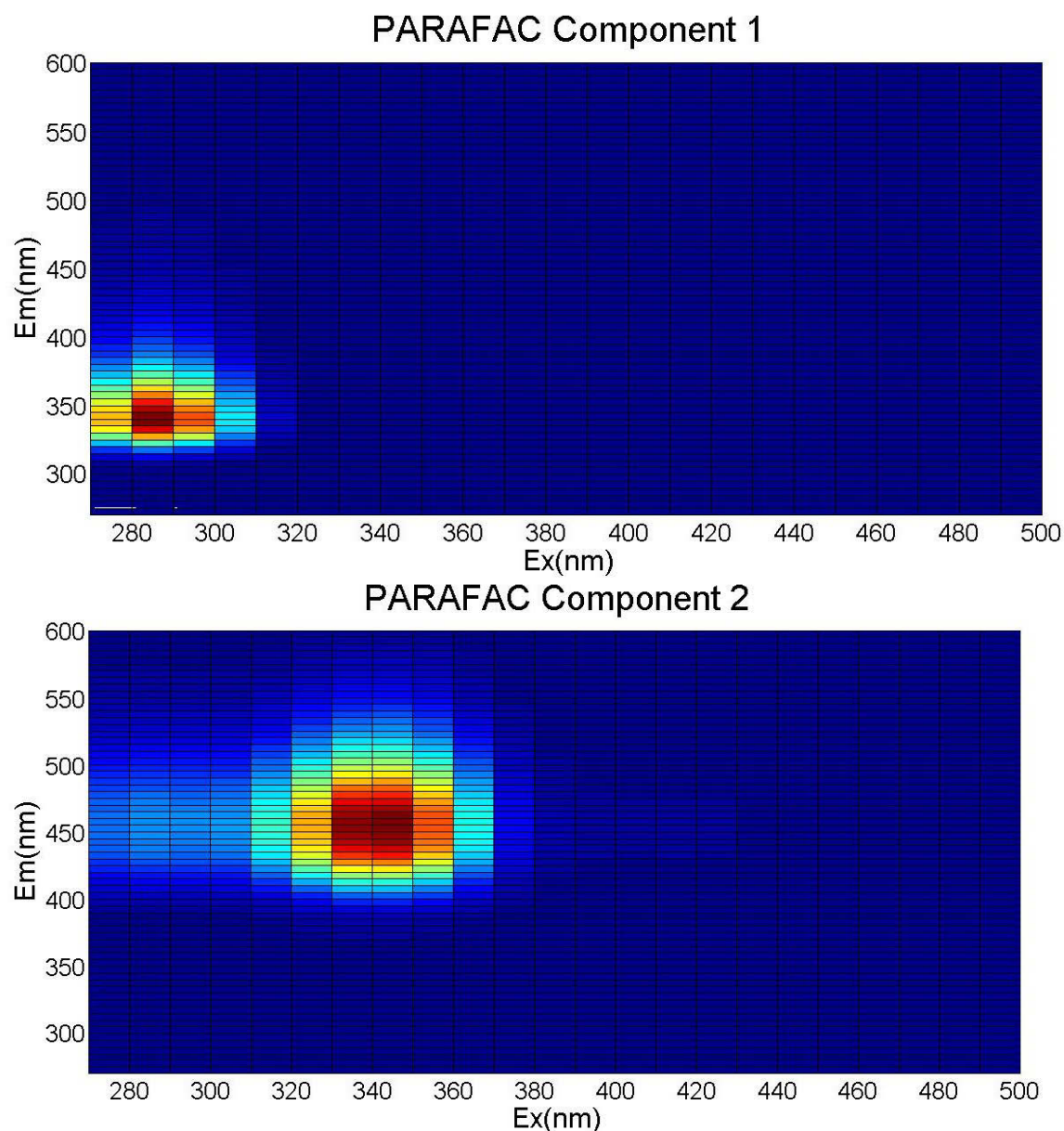


**Figure 3-21** Fluorescence landscapes for components 1 (top) and 2 (bottom) as predicted by PARAFAC for aniline and 4-aminobenzoic acid.

The results of a two-component PARAFAC model are shown in Figure 3-21 above. Components 1 and 2 predicted by PARAFAC resemble the landscapes of the 4-aminobenzoic acid and aniline OPA adducts respectively. Figure 3-22 below shows that the differences in intensity that are observed in the landscape shown in Figure 3-18 are preserved in the results of the PARAFAC model. The original ratio of the  $\lambda_{\max}$  values of 4-aminobenzoic acid to aniline was 70:30 for the 1:1 molar mixture. The

PARAFAC model demonstrated has predicted a  $\lambda_{\max}$  ratio of 68:32. This demonstrates that the relative concentration of each component in a mixture can also be estimated by PARAFAC.

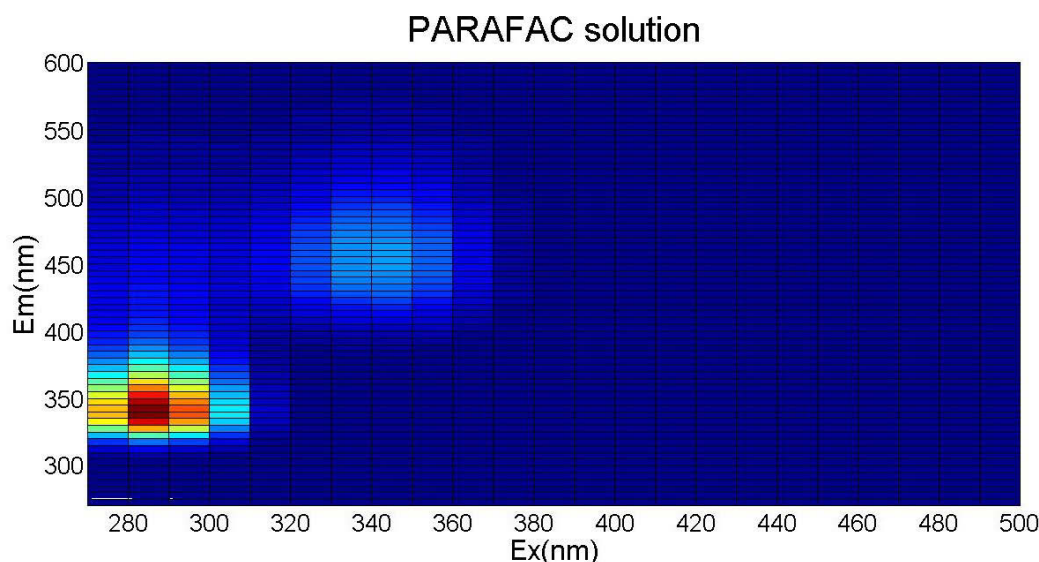


**Figure 3-22 PARAFAC solution for mixture of aniline and 4-aminobenzoic acid derivatised with OPA.**

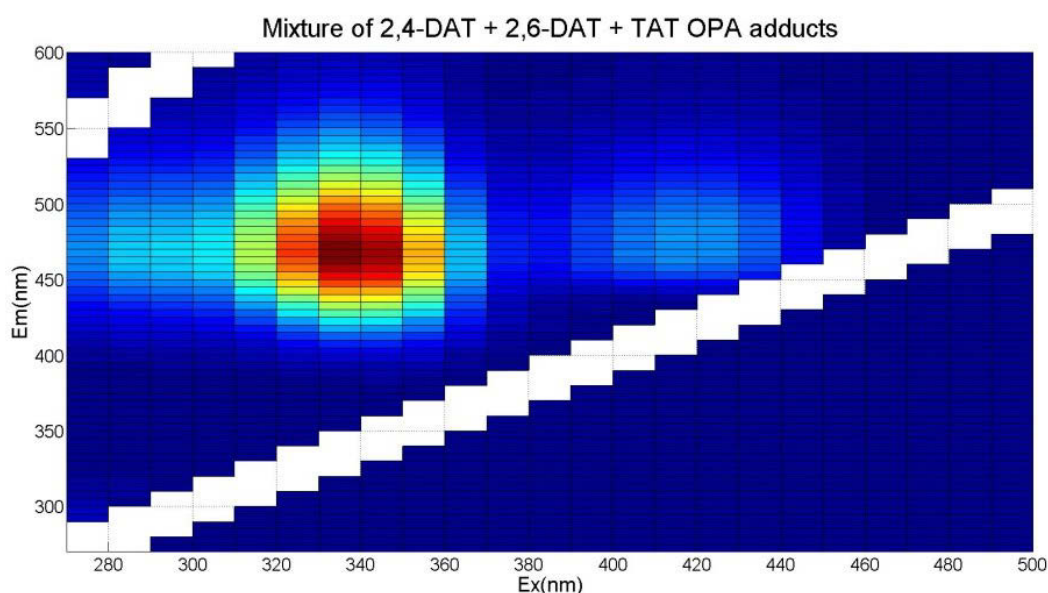
On average, OPA is present in a molar excess of up to 60 times (depending on the mono-, di- or tri- substitution) in the derivatisation reaction. Roth proposed this excess to achieve an effective derivatisation and to force the process to completion, with other authors also describing the use of excess OPA.<sup>235,236</sup> It was hypothesised that this excess of OPA might affect the PARAFAC modelling. To avoid this, options were explored to remove the potential for interference from OPA. These included using less OPA for the derivatisation, or performing multiple derivatisations of the same mixture using a varying amount of OPA. The latter should help the PARAFAC model to identify the OPA and separate it from other components. Other options explored included subtracting the OPA signal from the final landscapes (like a quasi-background subtraction) and expecting OPA as an extra component in the PARAFAC model. Fortunately, as previously demonstrated (Figure 3-8 and Figure 3-10) the fluorescence of the blank OPA solution is significantly less intense than that of the



OPA adducts, and it was not observed to interfere with the modelling of the derivatised amine data.

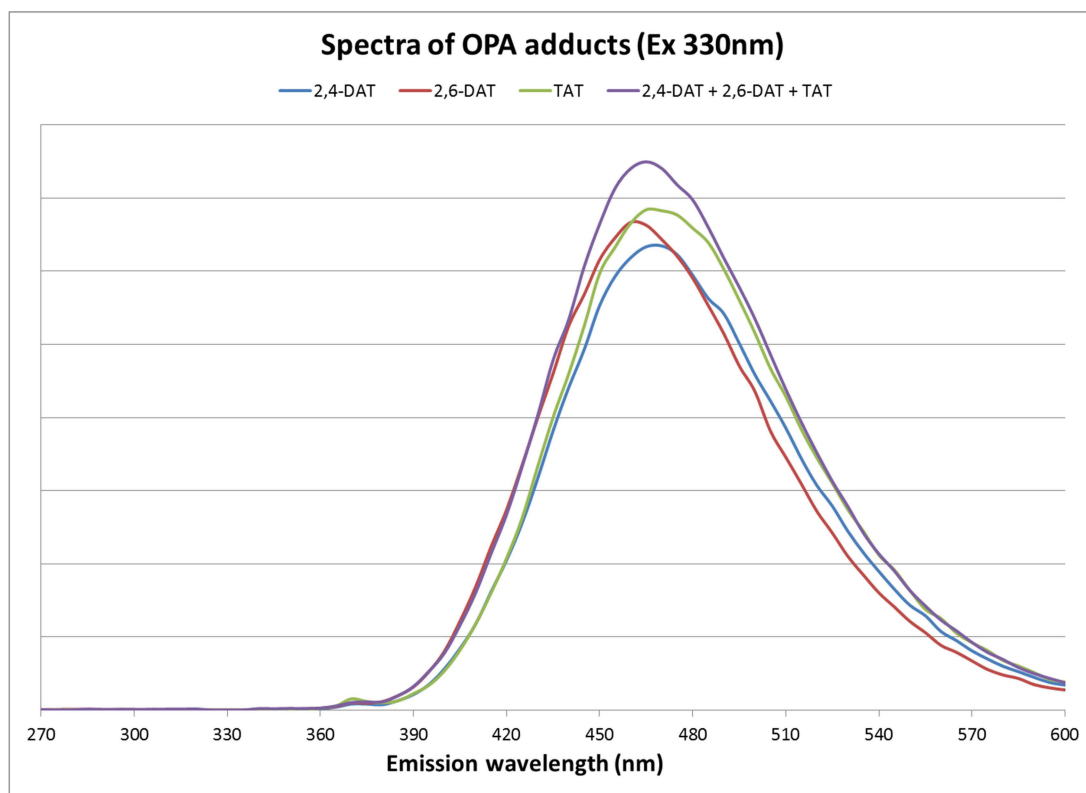
Following the successful trials on model amines, PARAFAC was performed on landscapes of the reduced and derivatised products of nitroaromatic explosives.

Figure 3-23 below shows an example fluorescence landscape for a mixture of 2,4-DAT, 2,6-DAT and TAT that was reduced as per the procedure in Section 3.2.1.2 from a mixture of 2,4-DNT, 2,6-DNT and TNT and then derivatised (crude) with OPA.



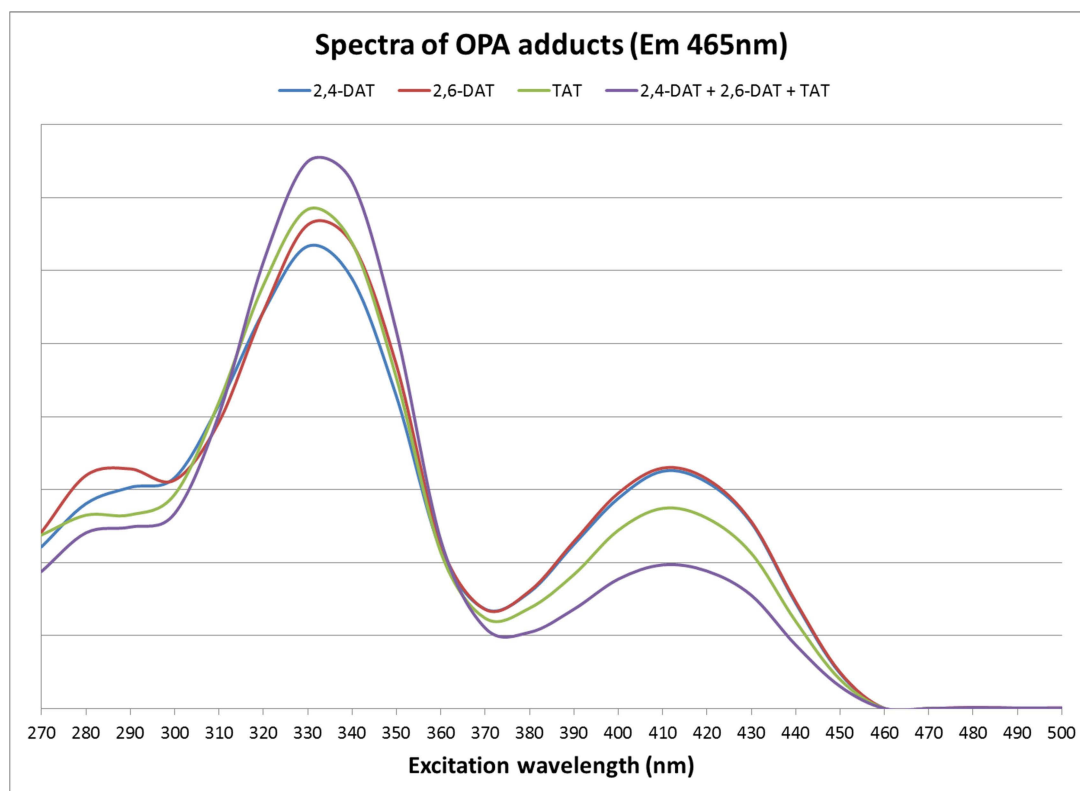
**Figure 3-23 Fluorescence landscape of 2,4-DAT, 2,6-DAT and TAT derivatised with OPA (EEMCut performed).**

Figure 3-24 and Figure 3-25 below show the emission and excitation spectra for OPA adducts of 2,4-DAT (reduced from 2,4-DNT), 2,6-DAT (reduced from 2,6-DNT), TAT (reduced from TNT) and a mixture of the three.



**Figure 3-24 Emission Spectra of 2,4-DAT, 2,6-DAT, TAT and a mixture of the three derivatised with OPA (EEMCut performed).**

The emission spectra in Figure 3-24 above show that all species share an almost identical emission profile at an excitation wavelength of 330 nm.



**Figure 3-25 Excitation spectra of 2,4-DAT, 2,6-DAT, TAT and a mixture of the three derivatised with OPA (EEMCut performed).**

While the above spectra show that the OPA adducts for the di- and tri-amine aromatic compounds share similar excitation signals at  $\sim\lambda_{\text{Ex}} = 330 \text{ nm}$  and  $420 \text{ nm}$ , it also shows that they differ somewhat in the relative intensities and ratios of these two signals. Figure 3-25 above highlights that, as expected, the excitation spectra for 2,4-DAT and 2,6-DAT are the most similar, with some differences at 280 nm. Looking at the landscapes for the OPA adducts of 2,4-DAT and TAT shown in Figure 3-26 below, it can be seen that the ratio of the signals in each are approximately 2:1 and 3:1 respectively.

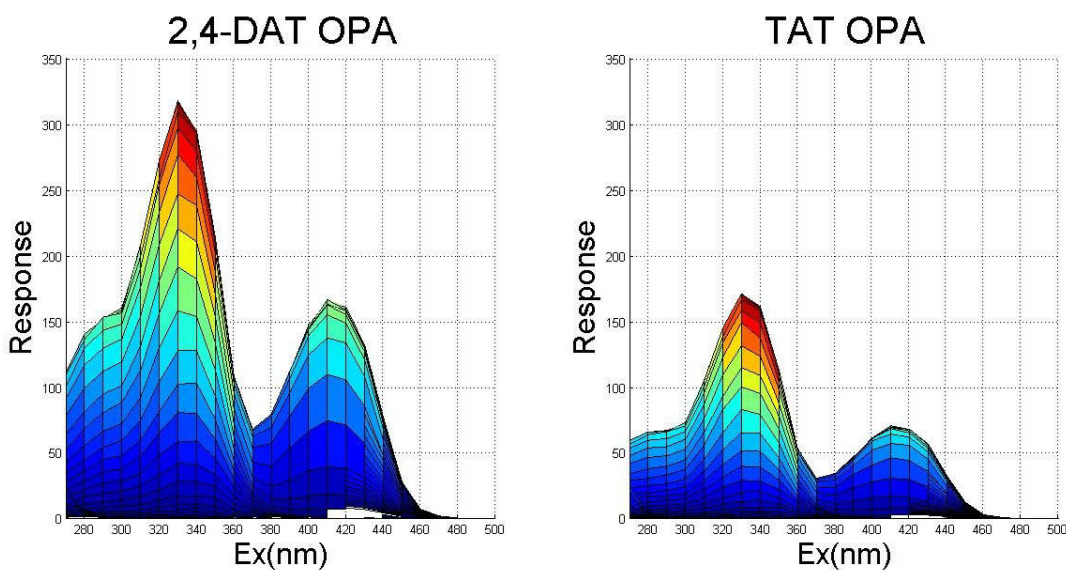


**Figure 3-26 Fluorescence landscapes of 2,4-DAT and TAT derivatised with OPA (EEMCut performed).**

For the three-part mixtures, PARAFAC was performed on up to twenty-one landscapes as per Table 3-7 below, as well as a landscape of the OPA buffer solution. As mentioned above, the OPA landscape did not affect the PARAFAC modelling. But, it was included in the analysis as a control to ensure that the components calculated by PARAFAC were not influenced by the OPA signal. This was confirmed by analysis of the scores for the PARAFAC-determined components as well as comparing the results of PARAFAC models with and without the OPA signal included.

Soln.	Ratio of each component (%)		
	2,4-DAT	2,6-DAT	TAT
1	100	-	-
2	-	100	-
3	-	-	100
4	100*	-	-
5	-	100*	-
6	-	-	100*
7	50	50	-
8	50	-	50
9	-	50	50
10	50	25	25
11	25	50	25
12	25	25	50
13	10	70	20
14	20	10	70
15	70	20	10
16	90	5	5
17	5	90	5
18	5	5	90
19	40	30	30
20	30	40	30
21	30	30	40

**Table 3-7 Ratios of 2,4-DAT, 2,6-DAT and TAT in mixtures and derivatised with OPA and analysed vis PARAFAC. \*these samples were at half concentration.**

As in the example presented above for the model amine compounds, CORCONDIA and the *OutlierTest* were performed in order to predict the appropriate number of components for the PARAFAC model. As shown in Table 3-8 below, the CORCONDIA values for two-, three- and four-component PARAFAC models fall within eleven points of each other and are all relatively close to 100 in comparison with the value of 9.5 for the five-component model. Thus, according to the CORCONDIA diagnostic alone, the PARAFAC model could have two, three or four components.

Core consistency diagnostic values	
Number of components	Value
2	90.7741
3	79.8108
4	84.0873
5	9.4824

**Table 3-8** Core consistency diagnostic (CORCONDIA) values for PARAFAC models of 2,4-DAT, 2,6-DAT and TAT derivatised with OPA.

Analysis of the scores and loadings calculated by the *OutlierTest* for the derivatised mixture of 2,4-DAT, 2,6-DAT and TAT showed that a three-component PARAFAC model best represented the dataset. The loadings for both the two- and three-component models were adequate but the scores for the fourth component in the four-component test model showed that it was modelling noise and not a true fluorescence signal.

Given the above results for the *OutlierTest* and CORCONDIA, PARAFAC has correctly found the number of components to be three. However, as outlined in more detail below, the excitation and emission loadings that PARAFAC has predicted for each of the three components do not match those of the original components (see Figure 3-27 and Figure 3-28).

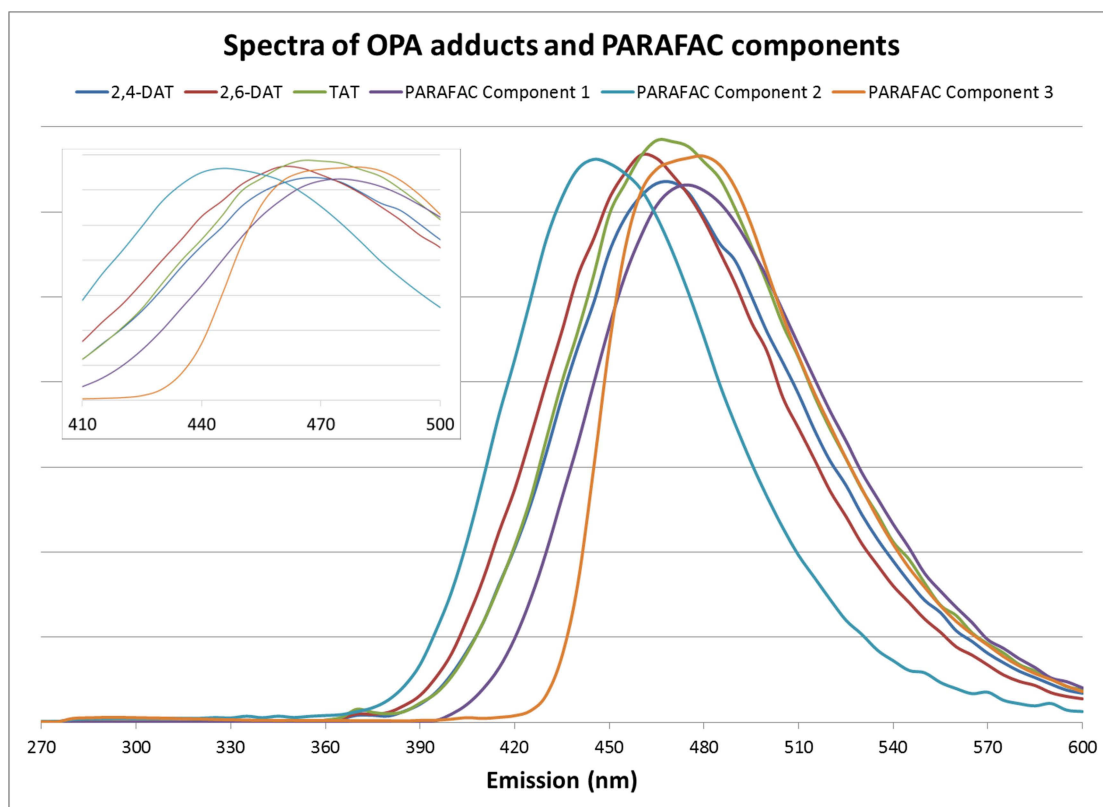


**Figure 3-27 Emission spectra of OPA adducts and components as predicted by PARAFAC.**

Figure 3-27 shows the emission spectra shown in Figure 3-24 for 2,4-DAT, 2,6-DAT and TAT OPA adducts plotted together with the three components predicted by PARAFAC for the mixture. It can be seen from the above plot that the  $\lambda_{\max}$  values for the three PARAFAC components are different to each of the real chemical components. PARAFAC has (incorrectly) determined that the signal in the twenty-one landscapes presented to it in the range 390-450 nm is a product of two species and as such has separated them into two components, evidenced by the sharp rise in signal for component 3 (relative to all other signals) after 420 nm and the shift of  $\lambda_{\max}$  value for PARAFAC component 2 to a shorter wavelength.

Figure 3-28 below shows the excitation spectra presented in Figure 3-25 for 2,4-DAT, 2,6-DAT and TAT OPA adducts plotted together with the components that have been predicted by PARAFAC for a three-component model.

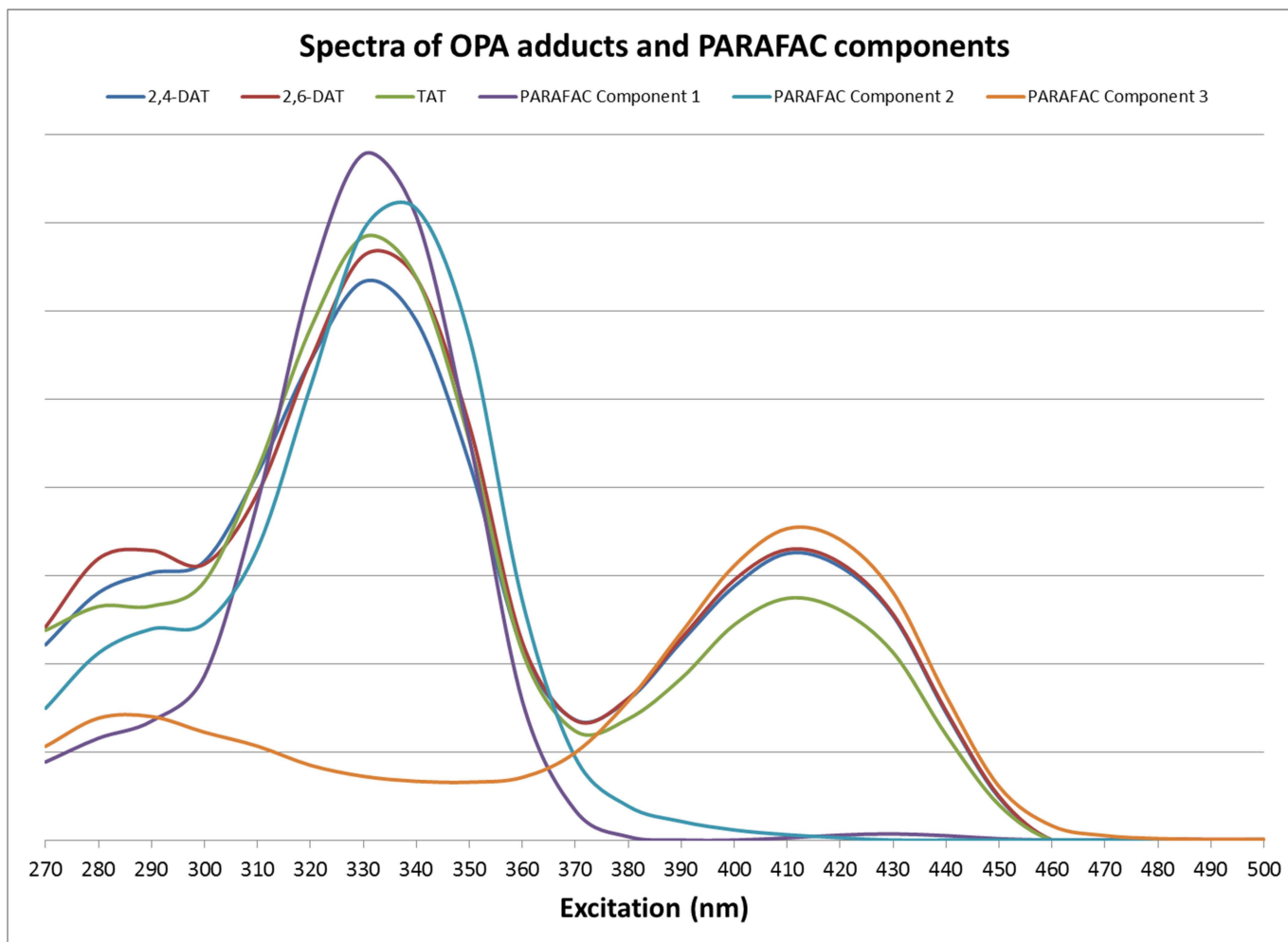


**Figure 3-28** Excitation spectra of OPA adducts and components predicted by PARAFAC.



The figure above highlights where PARAFAC has not been able to resolve the subtle differences in the landscapes of the OPA adducts of the reduced nitroaromatic explosive compounds. As seen above and as previously demonstrated, the collected excitation spectra for 2,4-DAT, 2,6-DAT and TAT OPA adducts each have two peaks, at 330 nm and 420 nm. The above graph shows that the excitation spectra for PARAFAC components 1 and 2 show only a peak near 330 nm while the spectrum for the third modelled component contains only the peak at 420 nm.

The PARAFAC algorithm has not been able to detect that each of the OPA adducts in the mixture has two peaks. The inclusion of samples containing different ratios of the chemical components (as outlined in Table 3-7) into one dataset is designed to aid the algorithm in identifying the individual components. It is hypothesised that even with these samples, the fluorescence landscapes of the three species are too similar for PARAFAC to separate. As for the emission spectra of the components predicted by PARAFAC, the excitation spectra for components 1 and 2 have slightly different  $\lambda_{\max}$  values in comparison to the spectra for the OPA adducts.

Given PARAFAC's failure to separate the data over a large spectral range, spectral truncation was performed on the data for all samples outlined in Table 3-7 in order to exploit the area of the dataset with the most variation between the species in the mixture. Figure 3-25 shows the excitation spectra of 2,4-DAT, 2,6-DAT, TAT and the mixture of the three OPA adducts. From this it can be seen that the range of greatest variation in shape between the signals appears at the 270-310 nm range, and so this was the area chosen for the spectral truncation. However, the PARAFAC analysis still proved unsuccessful in separating the true chemical components.

Finally, in an attempt to combat any potential covariance that has arisen in the data due to samples with stronger signals or differences in concentration, the landscapes were normalised with the *normeem* function in the drEEM toolbox. This should allow the model to focus on the chemical variations between the samples rather than the

magnitude. It was also hypothesised that any minor variations between the landscapes that may be present would be revealed following normalisation and assist PARAFAC in determining the correct spectra for the three components. Using the normalised data, PARAFAC again predicted the correct number of components, but with the same issues that have been outlined above.

### 3.4 Conclusions

This investigation has demonstrated that the trace analysis of nitroaromatic explosives using fluorescence landscapes and PARAFAC may have some potential, but further developmental work is required in order to determine how the landscapes of the reduced and derivatised species can be resolved. This could include exploration of other chemometric techniques. The initial aim of the project was to determine a field-deployable, 'one-size-fits-all' approach to explosives detection, but in reality the reduction method was found to be suitable only for nitroaromatic explosives, of which there is a limited number routinely encountered in case work.

The overall process involves subjecting samples suspected to contain nitroaromatic explosive compounds to a reaction whereby they are reduced to their corresponding amine compounds. Following the reduction, a derivatisation with *o*-phthalaldehyde (OPA) is performed to form fluorescent isoindoles; these two steps have been optimised in this research and can be completed in less than 60 minutes. They both meet the aims of the project as they have been assessed to be field-deployable.

Using HRMS, isoindole derivatives were identified for the reduced products of 2,4-DNT, 2,6-DNT and TNT, confirming the success of the reduction and derivatisation reaction. Following the collection of fluorescence landscapes, DOMFLuor, NWay and drEEM toolboxes written for MATLAB were used to implement data pre-processing and PARAFAC analysis. Techniques were utilised to predict the number of components and hence the landscapes of individual components in mixtures of aromatic amine

compounds derived from nitroaromatics. Further work is needed to investigate other mild reduction techniques, where the more sensitive nitrate ester and nitramine compounds are not degraded. Literature methods for the conversion of these compounds to appropriate amines are not available. Furthermore, it is hypothesised that the 'expected' products outlined in Section 3.3.1 will not be achieved for these groups due to their instability, no matter how mild a reduction is performed.

The potential of different derivatising agents and for quantitative analysis with this technique should also be explored. For this method to be operationally viable, libraries of landscapes are required to be able to identify explosives without any prior knowledge of the sample. Furthermore, the effect of matrix effects in post-blast samples such as fluorescent contaminants in soil or water must also be tested and known, although it is hypothesised that these would fluoresce at wavelengths away from the explosive compounds and can be easily identified and disregarded by PARAFAC.

Analysis of the results obtained from the PARAFAC modelling has showed that the landscapes of the isoindole OPA adducts were too similar for the PARAFAC analysis to correctly separate and thus identify them. Importantly, PARAFAC routinely predicted the correct number of components, but the spectra of the predicted components did not represent the known components in the mixture. Further investigation into PARAFAC or other chemometric techniques suited to fluorescence data is recommended to determine whether there exists a methodology under which these mixtures can be separated.

The noted similarities in the fluorescent signals of the isoindole OPA adducts highlights an opportunity for single-wavelength detection systems such as lab-on-a-chip technology that could be developed for the detection and separation of organic nitro containing explosive compounds. Lab-on-a-chip methods offer a sensitive

analysis technique that can be set-up on the scene with minimal equipment and use of solvents.

If successful PARAFAC modelling is achieved, investigation is warranted to determine whether the amount of user interaction (required to determine the correct number of components for a model) can be reduced by automation. Front line officers may not have the knowledge of fluorescence spectroscopy required to determine if the correct number of components recommended by the *OutlierTest* and CORCONDIA should be relied upon. The determination of the correct number of components is an integral step in the development of a PARAFAC model. This may involve the application of a third party application or an additional chemometric technique to assist in the decision making process.

***Chapter 4: Conclusions and  
Further work***

---

## Chapter 4: Conclusions and Further work

The policing environment is on a path to intelligence-led-policing, with an aim to gain as much information as possible and interpreting that into actionable intelligence as quickly as possible. The focus on this information is not necessarily how accurate it is, but in what intelligence it can provide. The strategies adopted in the current work meet this principle by supplying information to LEAs almost instantly. For the work on illicit drugs, information about mixtures and purity could take months to gain under current procedures. In the area of explosive analysis, there is always a need for field deployable methodology that does not require the acquisition of expensive equipment.

Within the field of forensic science, there remains a desire to maintain specialist knowledge by using hands-on techniques, rather than those that rely on *black box* technologies like many of the handheld devices currently on the market for both drug and explosive analysis. The pure *black box-type* instruments appeal to policing members with little or no scientific knowledge. Currently, some LEAs in Australia use these *black box-type* instruments to indicate that a banned substance may be present, and warrant further investigation and analysis by a forensic team.

The techniques explored in this research fall somewhere in between requiring synthetic and analytical chemistry knowledge and being able to operate a *black box* with no scientific input. Thus, the target user group would be members of forensic science departments within LEAs, who are likely to have some scientific knowledge or training. Ideally experience with vibrational spectroscopy would be ideal, but with the further developments of the methodology that is suggested in this research, this may not be necessary in the long term.

For the first main topic in this research, ATR-FTIR hyperspectral imaging and Raman mapping were explored for the preliminary identification and quantitation of illicit

drugs. Single-point ATR-FTIR instruments are currently used by the Australian Federal Police (AFP) crime scene (CS) teams as part of their PIDI procedures. It was demonstrated that the methods in this research are more successful in identifying components within a mixture than current methods, and that, our methods give information on the purity of those components, which current methods do not provide. In situations where the components of a drug mixture are known (but their relative concentrations are not) other chemometric techniques, such as partial least squares (PLS) would be used to construct a calibration model for spectroscopic data. However, this project was designed to address the situation where samples contain unknown drugs and cutting agents in unknown amounts – hence the use of multivariate curve resolution (MCR). The application of MCR analysis to Raman mapping data gave the best and most consistent results, followed by the application of MCR analysis to ATR-FTIR hyperspectral data.

The accuracy of purity estimations calculated by MCR and SIMPLISMA were affected by the algorithms' inability to extract spectrally pure components in each set of data. For ATR-FTIR data, error rates were increased as the spectra collected did not obey Beer's law i.e. the ATR-FTIR spectra did not have a linear relationship with the concentration of each component.

This approach needs to be tested on much larger datasets of seized and tested material, which were not available during this research, to more accurately assess its performance in comparison to currently used methodologies. The intricacies of the chemometric algorithms MCR and SIMPLISMA should be explored further and modified to determine the possibility of obtaining spectrally pure components more readily. This will ultimately improve the classification results but more likely strengthen the confidence in obtaining more precise and accurate purity estimations.

Further to the above, it should be noted that ATR-FTIR hyperspectral imaging is a much quicker and easier (in terms of the collection of spectra) technique than Raman mapping and more likely to be adopted operationally. If future development of FTIR

hyperspectral data collection methods for powder or tablets can resolve the identified linearity issue, it would be a very powerful technique for the preliminary identification and quantitation of illicit drugs and other unknown powders. An added advantage in the development of FTIR methods is that it is already an accepted and widely used preliminary identification technique. Forensic and law enforcement agencies are also familiar with FTIR. Finally, the application of these chemometric systems should be trialled on other spectral data such as the proton and carbon NMR spectra of mixtures. The advancement in benchtop NMR has resulted in the method now being a cost-effective option for Australian LEAs, with the AFP recently purchasing one for testing. The FT-Raman mapping method identified in this project should be explored further in relation to the collection of Raman spectra from coloured illicit tablets. Also, a 'fast' Raman mapping option is now available from some manufacturers which significantly decreases the time taken to collect hyperspectral Raman data, making it more practical for operational use.

In the other main area of this project, a feasibility study was conducted on the application of parallel factor analysis (PARAFAC) to fluorescence landscapes for the analysis of explosives. This project identified that a 'one-size-fits-all' approach to the reduction of nitro-containing explosives to their relevant amines was not possible. Therefore, a method was proposed only for the reduction of nitroaromatic compounds, which still proved to be successful when nitroaromatic explosives were found in mixtures with other commonly found nitro-containing explosives such as PETN and RDX. The subsequent derivatisation of the amines with *o*-phthalaldehyde (OPA) was proven to be successful for all compounds via high resolution mass spectrometry (HRMS).

Fluorescence landscapes of model amine compounds derivatised with OPA were used to demonstrate the PARAFAC process and how it can be used to successfully predict pure components and their relative concentrations without any prior knowledge of the sample. PARAFAC was performed using toolboxes built for MATLAB.



The collection of fluorescence landscapes of the OPA adducts of 2,4-DAT, 2,6-DAT and TAT that had been reduced from the corresponding nitroaromatics showed that the fluorescence landscapes for all of the compounds are very similar. Each of the compounds had peaks at  $\lambda_{\text{Ex}} = 330$  and 420 nm, but with different relative intensities. Various analyses of the data with PARAFAC highlighted the inability of the chemometric method to successfully resolve the landscapes of each of the components. Using the *OutlierTest* and core consistency diagnostic (CORCONDIA) PARAFAC successfully predicted the correct number of components for two- and three-part mixtures of reduced and derivatised nitroaromatic compounds, but failed to correctly separate the spectra of each of the components.

Further research would involve re-visiting the reduction technique with an aim to developing a method that would reduce nitroaromatics, nitrate esters and nitramine explosives. Furthermore, options for creating species that would have more variety in their fluorescence landscapes should be explored; ideally, these could be incorporated into the derivatisation step and maintain the field deployable nature of this work.

# ***Appendices***

# Appendix 1

## **Interpretation of results**

As described in section 2.3.4, the results of this analysis are measured in two ways:

1. initially a 'real' and 'true' spectrum must be identified for each of the components;
2. once a spectrum has been identified, the purity at each pixel is then used to estimate an overall purity.

The diagram below outlines how the graphs used to display the results should be interpreted.

The black outline is the expected concentration i.e. the concentration of each component in the test samples.

The thinner, coloured bars show the calculated purities for each mixture. Multiple bars represent replicate analyses.

It must be noted that for each 'set' the calculated concentrations will add to 100.

If no true or real spectrum is identified by the algorithm (MCR or SIMPLISMA) then no calculation of purity will be performed, and there will be a blank space in the graph.

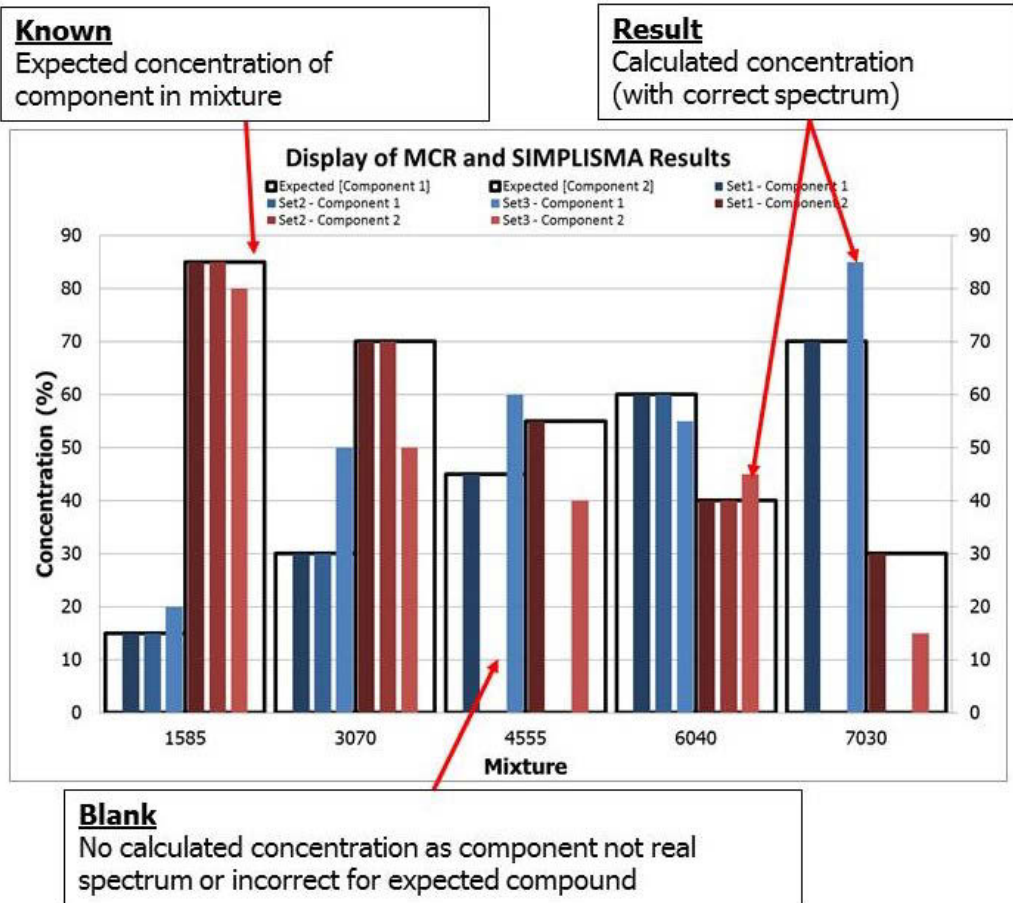


*Figure 4-1 Example graph to demonstrate how result are to be interpreted*

# ***References***

---

## References

1. Crispino, F.; Rossy, Q.; Ribaux, O.; Roux, C., Education and training in forensic intelligence: a new challenge. *Australian Journal of Forensic Sciences* **2015**, 47 (1), 49-60.
2. Australian Federal Police, Strategix Context Paper - AFP Future Directions 2015. In 2015.
3. Griffiths, P. R. Infrared and Raman Instrumentation for Mapping and Imaging. In *Infrared and Raman Spectroscopic Imaging*; Salzer Reiner.; Siesler Heinz W., Eds.; Wiley-VCH: Weinheim, 2009.
4. Griffiths, P. R.; Haseth de, J. A. *Fourier Transform Infrared Spectrometry*, 2nd ed.; John Wiley & Sons: New Jersey, 2007.
5. Pavia Donald L.; Lampman Gary M.; Kriz George S. *Introduction to Spectroscopy*, 3rd ed.; Brooks/Cole: USA, 2001.
6. Skoog, D. A.; Leary, J. J. *Principles of Instrumental Analysis*, 4th ed.; Saunders College Publishing: USA, 1992.
7. Stuart, B. H. Molecular Spectroscopy. In *Analytical Techniques in Materials Conservation*; John Wiley & Sons, Ltd: 2007; pp 109-208.
8. Kaur, H. *Spectroscopy*; Pragati Prakashan: Meerut, IND, 2009.
9. Bhargava Rohit; Levin Ira W. Fourier transform mid-infrared spectroscopic imaging. In *Spectrochemical Analysis Using Infrared Multichannel Detectors*; Bhargava Rohit; Levin Ira W., Eds.; Blackwell Publishing: Oxford, UK, 2005.
10. Levin, I. W.; Bhargava, R., Fourier Transform Infrared Vibrational Spectroscopic Imaging: Integrating Microscopy and Molecular Recognition. *Annual Review of Physical Chemistry* **2005**, 56 (1), 429-474.
11. Koenig, J. L.; Wang, S.-Q.; Bhargava, R., FTIR Images. *Analytical Chemistry* **2001**, 73 (13), 360 A-369 A.
12. Lewis, E. N.; Levin, I. W., Real-time, mid-infrared spectroscopic imaging microscopy using indium antimonide focal-plane array detection. *Applied Spectroscopy* **1995**, 49 (5), 672-8.
13. Lewis, E. N.; Levin, I. W., Vibrational Spectroscopic Microscopy: Raman, Near-Infrared and Mid-Infrared Imaging Techniques. *Microscopy and Microanalysis* **1995**, 1 (01), 35-46.
14. Lewis, E. N.; Treado, P. J.; Reeder, R. C.; Story, G. M.; Dowrey, A. E.; Marcott, C.; Levin, I. W., Fourier Transform Spectroscopic Imaging Using an Infrared Focal-Plane Array Detector. *Analytical Chemistry* **1995**, 67 (19), 3377-81.

15. Lewis, E. N.; Kidder, L. H.; Arens, J. F.; Peck, M. C.; Levin, I. W., Si:As focal-plane array detection for Fourier transform spectroscopic imaging in the infrared fingerprint region. *Applied Spectroscopy* **1997**, 51 (4), 563-567.
16. Koenig, J. L. FTIR imaging of multicomponent polymers. In *Spectrochemical Analysis Using Infrared Multichannel Detectors*; Rohit, B.; W., L. I., Eds.; Blackwell Publishing: Oxford, UK, 2005.
17. Babrah, J.; McCarthy, K.; Lush, R. J.; Rye, A. D.; Bessant, C.; Stone, N., Fourier transform infrared spectroscopic studies of T-cell lymphoma, B-cell lymphoid and myeloid leukaemia cell lines. *Analyst (Cambridge, U. K.)* **2009**, 134, 763-768.
18. Krafft, C.; Codrich, D.; Pelizzo, G.; Sergo, V., Raman and FTIR imaging of lung tissue: Methodology for control samples. *Vib. Spectrosc.* **2008**, 46, 141-149.
19. Kuimova, M. K.; Chan, K. L. A.; Kazarian, S. G., Chemical imaging of live cancer cells in the natural aqueous environment. *Appl. Spectrosc.* **2009**, 63, 164-171.
20. Rutledge, H. T.; Reedy, B. J., Classification of heterogeneous solids using infrared hyperspectral imaging. *Applied Spectroscopy* **2009**, 63 (2), 172-179.
21. Tahtouh, M.; Kalman, J. R.; Roux, C.; Lennard, C.; Reedy, B. J., The detection and enhancement of latent fingerprints using infrared chemical imaging. *Journal of Forensic Sciences* **2005**, 50 (1), 64-72.
22. De Grazia, A.; Mikhael, M.; Stojanovska, N.; Reedy, B.; Shimmon, R.; Tahtouh, M., Diacetylene copolymers for fingerprint development. *Forensic Science International* **2012**, 216 (1-3), 189-197.
23. Bhargava, R.; Schwartz Perlman, R.; Fernandez, D. C.; Levin, I. W.; Bartick, E. G., Non-invasive detection of superimposed latent fingerprints and inter-ridge trace evidence by infrared spectroscopic imaging. *Analytical and Bioanalytical Chemistry* **2009**, 394 (8), 2069-2075.
24. Ng, P. H. R.; Walker, S.; Tahtouh, M.; Reedy, B., Detection of illicit substances in fingerprints by infrared spectral imaging. *Analytical and Bioanalytical Chemistry* **2009**, 394 (8), 2039-2048.
25. Flynn, K.; O'Leary, R.; Lennard, C.; Roux, C.; Reedy, B. J., Forensic applications of infrared chemical imaging: Multi-layered paint chips. *Journal of Forensic Sciences* **2005**, 50 (4), 832-841.
26. Kalasinsky, K. S.; Magluilo Jr, J.; Schaefer, T., Hair analysis by infrared microscopy for drugs of abuse. *Forensic Science International* **1993**, 63 (1-3), 253-260.
27. Maric, M.; van Bronswijk, W.; Lewis, S. W.; Pitts, K.; Martin, D. E., Characterisation of chemical component migration in automotive paint by

- synchrotron infrared imaging. *Forensic Science International* **2013**, 228 (1–3), 165-169.
28. Banas, A.; Banas, K.; Breese, M. B. H.; Loke, J.; Heng Teo, B.; Lim, S. K., Detection of microscopic particles present as contaminants in latent fingerprints by means of synchrotron radiation-based Fourier transform infrared micro-imaging. *Analyst (Cambridge, U. K.)* **2012**, 137, 3459-3465.
  29. Sommer, A. J.; Tisinger, L. G.; Marcott, C.; Story, G. M., Attenuated total internal reflection infrared mapping microspectroscopy using an imaging microscope. *Applied Spectroscopy* **2001**, 55 (3), 252-256.
  30. McCreery, R. L. Introduction and Scope. In *Raman Spectroscopy for Chemical Analysis*; John Wiley & Sons, Inc.: 2005; pp 1-14.
  31. Krafft, C.; Steiner, G.; Beleites, C.; Salzer, R., Disease recognition by infrared and Raman spectroscopy. *Journal of biophotonics* **2009**, 2 (1-2), 13-28.
  32. Kazarian, S. G.; Chan, K. L. A.; Tay, F. H. ATR-FT-IR Imaging for Pharmaceutical and Polymeric Materials: From Micro to Macro Approaches. In *Infrared and Raman Spectroscopic Imaging*; Reiner, S.; W, S. H., Eds.; Wiley-VCH: Weinheim, 2009.
  33. Esaki, Y.; Yokokawa, K.; Araga, T. Accessory and crystalline element for ATR infrared spectroscopy. US Patent 5216244, 1993.
  34. Lewis, L. L.; Sommer, A. J., Attenuated Total Internal Reflection Infrared Mapping Microspectroscopy of Soft Materials. *Applied Spectroscopy* **2000**, 54, 324-330.
  35. Patterson, B. M.; Havrilla, G. J., Attenuated Total Internal Reflection Infrared Microspectroscopic Imaging Using a Large-Radius Germanium Internal Reflection Element and a Linear Array Detector. *Applied Spectroscopy* **2006**, 60, 1256-1266.
  36. Patterson, B. M.; Havrilla, G. J.; Marcott, C.; Story, G. M., Infrared Microspectroscopic Imaging Using a Large Radius Germanium Internal Reflection Element and a Focal Plane Array Detector. *Applied Spectroscopy* **2007**, 61, 1147-1152.
  37. Chan, K. L. A.; Kazarian, S. G., ATR-FTIR spectroscopic imaging with expanded field of view to study formulations and dissolution. *Lab on a Chip* **2006**, 6 (7), 864-870.
  38. Chan, K. L. A.; Kazarian, S. G., Macro FTIR imaging in transmission under a controlled environment. *Vibrational Spectroscopy* **2006**, 42 (1), 130-134.
  39. Specac, Golden Gate ATR DataSheet. In 2015.
  40. Salzer, R.; Siesler, H. W. *Infrared and Raman Spectroscopic Imaging*, 2 ed.; Wiley: Hoboken, 2014.



41. Kazarian, S. G.; Chan, K. L. A., Micro- and macro-attenuated total reflection Fourier transform infrared spectroscopic imaging. *Applied Spectroscopy* **2010**, 64 (5), 135A-152A.
42. Chan, K. L. A.; Hammond, S. V.; Kazarian, S. G., Applications of Attenuated Total Reflection Infrared Spectroscopic Imaging to Pharmaceutical Formulations. *Analytical Chemistry* **2003**, 75 (9), 2140-2146.
43. Chan, K. L. A.; Kazarian, S. G., New Opportunities in Micro- and Macro-Attenuated Total Reflection Infrared Spectroscopic Imaging: Spatial Resolution and Sampling Versatility. *Appl. Spectrosc.* **2003**, 57 (4), 381-389.
44. Kazarian, S. G.; Chan, K. L. A., Applications of ATR-FTIR spectroscopic imaging to biomedical samples. *Biochim. Biophys. Acta, Biomembr.* **2006**, 1758 (7), 858-867.
45. Chan, K. L. A.; Elkhider, N.; Kazarian, S. G., Spectroscopic Imaging of Compacted Pharmaceutical Tablets. *Chemical Engineering Research and Design* **2005**, 83 (11), 1303-1310.
46. Chan, K. L. A.; Kazarian, S. G., Fourier Transform Infrared Imaging for High-Throughput Analysis of Pharmaceutical Formulations. *Journal of Combinatorial Chemistry* **2005**, 7 (2), 185-189.
47. Ewing, A. V.; Wray, P. S.; Clarke, G. S.; Kazarian, S. G., Evaluating drug delivery with salt formation: Drug disproportionation studied in situ by ATR-FTIR imaging and Raman mapping. *Journal of Pharmaceutical and Biomedical Analysis* **2015**, 111 (0), 248-256.
48. Ewing, A. V.; Wray, P. S.; Clarke, G. S.; Kazarian, S. G., Evaluating drug delivery with salt formation: Drug disproportionation studied in situ by ATR-FTIR imaging and Raman mapping. *J. Pharm. Biomed. Anal.* **2015**, 111, 248-256.
49. Ricci, C.; Eliasson, C.; Macleod, N. A.; Newton, P. N.; Matousek, P.; Kazarian, S. G., Characterization of genuine and fake artesunate anti-malarial tablets using Fourier transform infrared imaging and spatially offset Raman spectroscopy through blister packs. *Analytical and Bioanalytical Chemistry* **2007**, 389 (5), 1525-1532.
50. Kazarian, S. G.; Chan, K. L. A., Sampling approaches in fourier transform infrared imaging applied to polymers. *Progress in Colloid & Polymer Science* **2006**, 132, 1-6.
51. Chan, K. L. A.; Kazarian, S. G., Detection of trace materials with Fourier transform infrared spectroscopy using a multi-channel detector. *Analyst* **2006**, 131 (1), 126-131.
52. Ricci, C.; Phiriyavityopas, P.; Curum, N.; Chan, K. L. A.; Jickells, S.; Kazarian, S. G., Chemical Imaging of Latent Fingerprint Residues. *Applied Spectroscopy* **2007**, 61, 514-522.

53. Ricci, C.; Bleay, S.; Kazarian, S. G., Spectroscopic Imaging of Latent Fingermarks Collected with the Aid of a Gelatin Tape. *Anal. Chem. (Washington, DC, U. S.)* **2007**, 79 (15), 5771-5776.
54. Ricci, C.; Chan, K. L. A.; Kazarian, S. G., Combining the Tape-Lift Method and Fourier Transform Infrared Spectroscopic Imaging for Forensic Applications. *Applied Spectroscopy* **2006**, 60, 1013-1021.
55. Ricci, C.; Chan, K. L. A.; Kazarian, S. G. Fourier Transform Infrared Spectroscopic Imaging for the Identification of Concealed Drug Residue Particles and Fingerprints. In *Society of Photo-Optical Instrumentation Engineers (SPIE) Conference Series*; Lewis, C.; Owen, G. P., Eds.; 2006; Vol. 6402.
56. Lanzarotta, A.; Lakes, K.; Marcott, C. A.; Witkowski, M. R.; Sommer, A. J., Analysis of Counterfeit Pharmaceutical Tablet Cores Utilizing Macroscopic Infrared Spectroscopy and Infrared Spectroscopic Imaging. *Anal. Chem. (Washington, DC, U. S.)* **2011**, 83, 5972-5978.
57. Bojko, K.; Roux, C.; Reedy, B. J., An examination of the sequence of intersecting lines using attenuated total reflectance-Fourier transform infrared spectral imaging. *Journal of Forensic Sciences* **2008**, 53 (6), 1458-1467.
58. Mou, Y.; Rabalais, J. W., Detection and identification of explosive particles in fingerprints using attenuated total reflection-Fourier transform infrared spectromicroscopy. *Journal of Forensic Sciences* **2009**, 54 (4), 846-850.
59. Bueno, J.; Lednev, I. K., Attenuated Total Reflectance-FT-IR Imaging for Rapid and Automated Detection of Gunshot Residue. *Analytical Chemistry* **2014**, 86 (7), 3389-3396.
60. Stuart, B. H. *Analytical Techniques in Materials Conservation*; John Wiley & Sons Ltd.: West Sussex, 2007.
61. Stewart, S.; Priore, R. J.; Nelson, M. P.; Treado, P. J., Raman imaging. *Annu. Rev. Anal. Chem.* **2012**, 5, 337-360.
62. Ferraro, J. R.; Nakamoto, K.; Brown, C. W. *Introductory Raman Spectroscopy*; Academic Press: Burlington, US, 2003.
63. Bell, S. E. J.; Stewart, S. P.; Speers, S. J. Raman Spectroscopy of Drugs of Abuse. In *Infrared and Raman Spectroscopy in Forensic Science*; Chalmers, J. M.; Edwards, H. G. M.; Hargreaves, M. D., Eds.; John Wiley & Sons: 2011.
64. Faulds, K.; Smith, W. E. Detection of Dugs of Abuse Using Surface Enhanced Raman Scattering. In *Infrared and Raman Spectroscopy in Forensic Science*; Chalmers, J. M.; Edwards, H. G. M.; Hargreaves, M. D., Eds.; John Wiley & Sons: 2011.
65. Lee, E. Imaging Modes. In *Raman Imaging: Techniques and Applications*; Zoubir, A., Ed.; Springer: Berlin, 2012.

66. Francis W.L. Esmonde-White; Morris, M. D. Raman Imaging and Raman Mapping. In *Emerging Raman Applications and Techniques in Biomedical and Pharmaceutical Fields*; Pavel Matousek; Morris, M. D., Eds.; Springer: Berlin Heidelberg, 2010.
67. Tres, F.; Patient, J. D.; Williams, P. M.; Treacher, K.; Booth, J.; Hughes, L. P.; Wren, S. A. C.; Aylott, J. W.; Burley, J. C., Monitoring the Dissolution Mechanisms of Amorphous Bicalutamide Solid Dispersions via Real-Time Raman Mapping. *Mol. Pharmaceutics* **2015**, 12, 1512-1522.
68. Wray, P. S.; Sinclair, W. E.; Jones, J. W.; Clarke, G. S.; Both, D., The use of in situ near infrared imaging and Raman mapping to study the disproportionation of a drug HCl salt during dissolution. *Int. J. Pharm. (Amsterdam, Neth.)* **2015**, 493, 198-207.
69. Bernard, S.; Beyssac, O.; Benzerara, K., Raman Mapping Using Advanced Line-Scanning Systems: Geological Applications. *Applied Spectroscopy* **2008**, 62, 1180-1188.
70. Stadelmann, R.; Hughes, B.; Orlovskaya, N., Guideline of mapping parameters for Raman mapping of ZrB<sub>2</sub>-SiC ceramic composites. *Adv. Appl. Ceram.* **2016**, 115 (1).
71. Vanco, L.; Kadlecikova, M.; Breza, J.; Belanyiova, E.; Michniak, P.; Rehakova, M.; Ceppan, M., Raman mapping as a tool for discrimination of blue writing inks and their cross lines. *Vib. Spectrosc.* **2015**, 79, 11-15.
72. Stojanovska, N.; De Grazia, A.; Tahtouh, M.; Shimmon, R.; Reedy, B., Refining Fingerprint Development using Diacetylene Copolymers on Difficult Surfaces. *J. Forensic Sci.* **2015**, 60, 619-626.
73. Tripathi, A.; Emmons, E. D.; Guicheteau, J. A.; Christesen, S. D.; Wilcox, P. G.; Emge, D. K.; Fountain, A. W., III, Trace explosive detection in fingerprints with Raman chemical imaging. *Proc. SPIE* **2010**, 7665, 76650N/1-76650N/6.
74. Widjaja, E., Latent fingerprints analysis using tape-lift, Raman microscopy, and multivariate data analysis methods. *Analyst (Cambridge, U. K.)* **2009**, 134, 769-775.
75. Almeida, M. R.; Correa, D. N.; Zacca, J. J.; Logrado, L. P. L.; Poppi, R. J., Detection of explosives on the surface of banknotes by Raman hyperspectral imaging and independent component analysis. *Analytica Chimica Acta* **2015**, 860, 15-22.
76. Bueno, J.; Lednev, I. K., Raman microspectroscopic chemical mapping and chemometric classification for the identification of gunshot residue on adhesive tape. *Anal. Bioanal. Chem.* **2014**, 406, 4595-4599.
77. Lakowicz, J. R. *Principles of Fluorescence Spectroscopy*, 3rd edition ed.; Springer US: 2006.

78. Rendell, D. *Fluorescence and Phosphorescence Spectroscopy*; John Wiley & Sons: London, 1987.
79. Di Bartolo, B.; Collins, J. luminescence spectroscopy. In *Handbook of applied solid state spectroscopy*; Vij, D. R., Ed.; Springer: New York, 2006.
80. Albani, J. R. *Principles and Applications of Fluorescence Spectroscopy*; Wiley: Chichester, GBR, 2008.
81. Gatto, E.; Malik, M. A.; Di Natale, C.; Paolesse, R.; D'Amico, A.; Lundstrom, I.; Filippini, D., Polychromatic fingerprinting of excitation emission matrices. *Chemistry--A European Journal* **2008**, 14 (20), 6057-6060.
82. Malik, M. A.; Gatto, E.; Macken, S.; Di Natale, C.; Paolesse, R.; D'Amico, A.; Lundstroem, I.; Filippini, D., Imaging fingerprinting of excitation emission matrices. *Analytica Chimica Acta* **2009**, 635 (2), 196-201.
83. Bahram, M.; Bro, R.; Stedmon, C.; Afkhami, A., Handling of Rayleigh and Raman scatter for PARAFAC modeling of fluorescence data using interpolation. *Journal of Chemometrics* **2007**, 20 (3-4), 99-105.
84. Alves, J. C. L.; Poppi, R. J., Simultaneous determination of acetylsalicylic acid, paracetamol and caffeine using solid-phase molecular fluorescence and parallel factor analysis. *Analytica Chimica Acta* **2009**, 642 (1-2), 212-216.
85. Bro, R., PARAFAC. Tutorial and applications. *Chemometrics and Intelligent Laboratory Systems* **1997**, 38, 149-171.
86. Andersen, C. M.; Bro, R., Practical aspects of PARAFAC modeling of fluorescence excitation-emission data. *Journal of Chemometrics* **2003**, 17 (4), 200-215.
87. Nikolajsen Rikke P.H.; Åse Marie Hansen; Bro, R., Attempt to separate the fluorescence spectra of adrenaline and noradrenaline using chemometrics. *Luminescence* **2001**, 16 (2), 91-101.
88. Vaitkuvienė, A.; Gegzna, V.; Juodkaziš, S.; Jursenas, S.; Miasojedovas, S.; Kurtinaitienė, R.; Rimienė, J.; Vaitkus, J., Fluorescence spectrum and decay measurement for HSIL vs normal cytology differentiation in liquid pap smear supernatant. *AIP Conference Proceedings* **2009**, 1142 (Laser Florence 2008--Bridge to the Laser Medicine World), 21-25.
89. Stedmon, C. A.; Bro, R., Characterizing dissolved organic matter fluorescence with parallel factor analysis: a tutorial. *Limnol. Oceanogr.: Methods* **2008**, 6 (Nov.), 572-579.
90. Miller, C.; Gordon, K. G.; Kieber, R. J.; Willey, J. D.; Seaton, P. J., Chemical characteristics of chromophoric dissolved organic matter in rainwater. *Atmospheric Environment* **2009**, 43 (15), 2497-2502.

91. Hua, B.; Yang, J.; Deng, B.; Veum, K.; Jones, J., Parallel factor analysis of fluorescence EEM spectra for identifying THM precursors in lake waters. *Abstracts of Papers, 236th ACS National Meeting, Philadelphia, PA, United States, August 17-21, 2008* **2008**, ENVR-176.
92. Gendrin, C.; Roggo, Y.; Collet, C., Pharmaceutical applications of vibrational chemical imaging and chemometrics: A review. *Journal of Pharmaceutical and Biomedical Analysis* **2008**, 48 (3), 533-553.
93. de Juan, A.; Maeder, M.; Hancewicz Thomas.; Duponchel Ludovic.; Tauler Roma. Chemometric Tools for Image Analysis. In *Infrared and Raman Spectroscopic Imaging*, 2 ed.; Salzer, R.; Siesler, H. W., Eds.; Wiley: Hoboken, 2014.
94. Ferrari, C.; Foca, G.; Calvini, R.; Ulrici, A., Fast exploration and classification of large hyperspectral image datasets for early bruise detection on apples. *Chemom. Intell. Lab. Syst.* **2015**, 146, 108-119.
95. Martinez-Sandoval, J. R.; Nogales-Bueno, J.; Rodriguez-Pulido, F. J.; Hernandez-Hierro, J. M.; Segovia-Quintero, M. A.; Martinez-Rosas, M. E.; Heredia, F. J., Screening of anthocyanins in single red grapes using a non-destructive method based on the near infrared hyperspectral technology and chemometrics. *J. Sci. Food Agric.* **2015**, Ahead of Print.
96. Ofner, J.; Kamilli, K. A.; Eitenberger, E.; Friedbacher, G.; Lendl, B.; Held, A.; Lohninger, H., Chemometric analysis of multisensor hyperspectral images of precipitated atmospheric particulate matter. *Anal. Chem. (Washington, DC, U. S.)* **2015**, 87 (18), 9413-9420.
97. Sacre, P. Y.; De Bleye, C.; Chavez, P. F.; Netchacovitch, L.; Hubert, P.; Ziemons, E., Data processing of vibrational chemical imaging for pharmaceutical applications. *J. Pharm. Biomed. Anal.* **2014**, 101 (Copyright (C) 2015 American Chemical Society (ACS). All Rights Reserved.), 123-140.
98. Zhu, F.-l.; He, Y.; Shao, Y.-n., Application of near-infrared hyperspectral imaging to predicting water content in salmon flesh. *Guangpuxue Yu Guangpu Fenxi* **2015**, 35, 113-117.
99. Chalmers, J. M.; Edwards, H. G. M.; Hargreaves, M. D. Vibrational Spectroscopy Techniques: Basics and Instrumentation. In *Infrared and Raman Spectroscopy in Forensic Science*, 2 ed.; Hargreaves, M. D.; Edwards, H. G. M.; Chalmers, J. M., Eds.; John Wiley & Sons: 2011.
100. Vidal, M.; Amigo, J. M., Pre-processing of hyperspectral images. Essential steps before image analysis. *Chemometrics and Intelligent Laboratory Systems* **2012**, 117 (0), 138-148.
101. Bocklitz, T.; Walter, A.; Hartmann, K.; Rösch, P.; Popp, J., How to pre-process Raman spectra for reliable and stable models? *Analytica Chimica Acta* **2011**, 704 (1-2), 47-56.

102. Sacré, P. Y.; De Bleye, C.; Chavez, P. F.; Netchacovitch, L.; Hubert, P.; Ziemons, E., Data processing of vibrational chemical imaging for pharmaceutical applications. *Journal of Pharmaceutical and Biomedical Analysis* **2014**, 101 (0), 123-140.
103. Rinnan, Å.; Berg, F. v. d.; Engelsen, S. B., Review of the most common pre-processing techniques for near-infrared spectra. *TrAC Trends in Analytical Chemistry* **2009**, 28 (10), 1201-1222.
104. Gemperline, P. *Practical Guide to Chemometrics*, 2 ed.; Taylor & Francis: Boca Raton, Florida, 2006.
105. Murali Mohan Babu, Y.; Subramanyam, M. V.; Giri Prasad, M. N., PCA based image denoising. *Signal & Image Processing: An International Journal (SIPIJ)* **2012**, 3 (2).
106. CytoSpec Spectral Preprocessing. <http://www.cytospec.com/specpreproc.php> (accessed 19/08/2015).
107. Liu, Y.; Chen, Y.-R.; Wang, C. Y.; Chan, D. E.; Kim, M. S., Development of a Simple Algorithm for the Detection of Chilling Injury in Cucumbers from Visible/Near-Infrared Hyperspectral Imaging. *Applied Spectroscopy* **2005**, 59 (1), 78-85.
108. Schmidt, K. S.; Skidmore, A. K., Spectral discrimination of vegetation types in a coastal wetland. *Remote Sensing of Environment* **2003**, 85 (1), 92-108.
109. Martens, H.; Stark, E., Extended multiplicative signal correction and spectral interference subtraction: New preprocessing methods for near infrared spectroscopy. *Journal of Pharmaceutical and Biomedical Analysis* **1991**, 9 (8), 625-635.
110. Esbensen, K. H. *Multivariate Data Analysis - In Practice*, 5th ed.; CAMO: Norway, 2004.
111. Paul, J. G. Principal Component Analysis. In *Practical Guide To Chemometrics, Second Edition*; CRC Press: 2006; pp 69-104.
112. Exelis Visual Information Solutions Exelis. [www.exelisvis.com](http://www.exelisvis.com) (accessed 30 October 2015).
113. Harris, A. T., Spectral mapping tools from the earth sciences applied to spectral microscopy data. *Cytometry. Part A* **2006**, 69 (8), 872-9.
114. Kruse, F. A.; Lefkoff, A. B.; Boardman, J. W.; Heidebrecht, K. B.; Shapiro, A. T.; Barloon, P. J.; Goetz, A. F. H., The spectral image processing system (SIPS)—interactive visualization and analysis of imaging spectrometer data. *Remote Sensing of Environment* **1993**, 44 (2-3), 145-163.
115. Wang, J.-J.; Zhang, Y.; Bussink, C., Unsupervised multiple endmember spectral mixture analysis-based detection of opium poppy fields from an EO-1

- Hyperion image in Helmand, Afghanistan. *Science of The Total Environment* **2014**, 476–477, 1-6.
116. Petrovic, A.; Khan, S. D.; Thurmond, A. K., Integrated hyperspectral remote sensing, geochemical and isotopic studies for understanding hydrocarbon-induced rock alterations. *Marine and Petroleum Geology* **2012**, 35 (1), 292-308.
117. Brereton, R. G. *Chemometrics for Pattern Recognition*; Wiley: Hoboken, NJ, USA, 2009.
118. Bro, R., Multivariate calibration: What is in chemometrics for the analytical chemist? *Analytica Chimica Acta* **2003**, 500 (1–2), 185-194.
119. Gowen, A. A.; O'Donnell, C. P.; Taghizadeh, M.; Cullen, P. J.; Frias, J. M.; Downey, G., Hyperspectral imaging combined with principal component analysis for bruise damage detection on white mushrooms (*Agaricus bisporus*). *Journal of Chemometrics* **2008**, 22 (3-4), 259-267.
120. Koonsanit, K.; Jaruskulchai, C.; Eiumnoh, A., Band Selection for Dimension Reduction in Hyper Spectral Image Using Integrated Information Gain and Principal Components Analysis Technique. *International Journal of Machine Learning and Computing* **2012**, 2 (3).
121. Rodarmel, C.; Shan, J., Principal Component Analysis for Hyperspectral Image Classification. *Surveying and Land Information Systems* **2002**, 62 (2).
122. Kwok, K.; Taylor, L. S., Analysis of counterfeit Cialis® tablets using Raman microscopy and multivariate curve resolution. *Journal of Pharmaceutical and Biomedical Analysis* **2012**, 66 (0), 126-135.
123. Tauler, R.; Kowalski, B., Selectivity, local rank, three-way data analysis and ambiguity in multivariate curve resolution. *Journal of Chemometrics* **1995**, 9 (1), 31-58.
124. Tauler, R., Multivariate curve resolution applied to second order data. *Chemometrics and Intelligent Laboratory Systems* **1995**, 30 (1), 133-46.
125. de Juan, A.; Tauler, R., Multivariate Curve Resolution (MCR) from 2000: Progress in Concepts and Applications. *Critical Reviews in Analytical Chemistry* **2006**, 36 (3-4), 163-176.
126. Silva, C. S.; Pimentel, M. F.; Honorato, R. S.; Pasquini, C.; Prats-Montalban, J. M.; Ferrer, A., Near infrared hyperspectral imaging for forensic analysis of document forgery. *Analyst* **2014**, 139 (20), 5176-5184.
127. Tauler, R.; Barcelo, D., Multivariate curve resolution applied to liquid chromatography-diode array detection. *Trends in Analytical Chemistry* **1993**, 12 (8), 319-27.

128. Ahmadvand, M.; Sereshti, H.; Parastar, H., Second-order calibration for the determination of fatty acids in pomegranate seeds by vortex-assisted extraction-dispersive liquid-liquid micro-extraction and gas chromatography-mass spectrometry. *RSC Adv.* **2015**, 5, 11633-11643.
129. Alcaraz, M. R.; Bortolato, S. A.; Goicoechea, H. C.; Olivieri, A. C., A new modeling strategy for third-order fast high-performance liquid chromatographic data with fluorescence detection. Quantitation of fluoroquinolones in water samples. *Anal. Bioanal. Chem.* **2015**, 407, 1999-2011.
130. Ardila, J. A.; Funari, C. S.; Andrade, A. M.; Cavalheiro, A. J.; Carneiro, R. L., Cluster Analysis of Commercial Samples of Bauhinia spp. Using HPLC-UV/PDA and MCR-ALS/PCA Without Peak Alignment Procedure. *Phytochem. Anal.* **2015**, 26 (5).
131. Jalali-Heravi, M.; Moazeni-Pourasil, R. S.; Sereshti, H., Thorough analysis of Iranian spearmint essential oil: combination of chemometrics and gas chromatography-mass spectrometry. *Anal. Methods* **2014**, 6, 6753-6759.
132. Ortiz-Villanueva, E.; Jaumot, J.; Benavente, F.; Pina, B.; Sanz-Nebot, V.; Tauler, R., Combination of CE-MS and advanced chemometric methods for high-throughput metabolic profiling. *Electrophoresis* **2015**, 36 (18).
133. Pisano, P. L.; Silva, M. F.; Olivieri, A. C., Exploration of liquid chromatographic-diode array data for Argentinean wines by extended multivariate curve resolution. *Chemom. Intell. Lab. Syst.* **2014**, 132, 1-7.
134. Piqueras, S.; Krafft, C.; Beleites, C.; Egodage, K.; von Eggeling, F.; Guntinas-Lichius, O.; Popp, J.; Tauler, R.; de Juan, A., Combining multiset resolution and segmentation for hyperspectral image analysis of biological tissues. *Analytica Chimica Acta* **2015**, 881 (0), 24-36.
135. Felten, J.; Hall, H.; Jaumot, J.; Tauler, R.; de Juan, A.; Gorzsás, A., Vibrational spectroscopic image analysis of biological material using multivariate curve resolution-alternating least squares (MCR-ALS). *Nat. Protocols* **2015**, 10 (2), 217-240.
136. Budevská, B. O.; Sum, S. T.; Jones, T. J., Application of Multivariate Curve Resolution for Analysis of FT-IR Microspectroscopic Images of in Situ Plant Tissue. *Applied Spectroscopy* **2003**, 57 (2), 124-131.
137. Vajna, B.; Bodzay, B.; Toldy, A.; Farkas, I.; Igricz, T.; Marosi, G., Analysis of car shredder polymer waste with Raman mapping and chemometrics. *eXPRESS Polym. Lett.* **2012**, 6, 107-119.
138. Lopes, M. B.; Wolff, J.-C.; Biucas-Dias, J. M.; Figueiredo, M. A. T., Near-Infrared Hyperspectral Unmixing Based on a Minimum Volume Criterion for Fast and Accurate Chemometric Characterization of Counterfeit Tablets. *Anal. Chem. (Washington, DC, U. S.)* **2010**, 82 (4), 1462-1469.



139. Alexandrino, G. L.; Khorasani, M. R.; Amigo, J. M.; Rantanen, J.; Poppi, R. J., Monitoring of multiple solid-state transformations at tablet surfaces using multi-series near-infrared hyperspectral imaging and multivariate curve resolution. *European Journal of Pharmaceutics and Biopharmaceutics* **2015**, 93, 224-230.
140. Vajna, B.; Patyi, G.; Nagy, Z.; Bodis, A.; Farkas, A.; Marosi, G., Comparison of chemometric methods in the analysis of pharmaceuticals with hyperspectral Raman imaging. *J. Raman Spectrosc.* **2011**, 42, 1977-1986.
141. Zhang, X.; Tauler, R., Application of Multivariate Curve Resolution Alternating Least Squares (MCR-ALS) to remote sensing hyperspectral imaging. *Analytica Chimica Acta* **2013**, 762 (0), 25-38.
142. Silva, C. S.; Pimentel, M. F.; Honorato, R. S.; Pasquini, C.; Prats-Montalban, J. M.; Ferrer, A., Near infrared hyperspectral imaging for forensic analysis of document forgery. *Analyst (Cambridge, U. K.)* **2014**, 139, 5176-5184.
143. Braz, A.; Lopez-Lopez, M.; Garcia-Ruiz, C., Raman imaging for determining the sequence of blue pen ink crossings. *Forensic Sci. Int.* **2015**, 249, 92-100.
144. Kwok, K.; Taylor, L. S., Analysis of counterfeit Cialis tablets using Raman microscopy and multivariate curve resolution. *J. Pharm. Biomed. Anal.* **2012**, 66, 126-135.
145. Windig, W.; Antalek, B.; Lippert Joseph, L.; Batonneau, Y.; Bremard, C., Combined use of conventional and second-derivative data in the SIMPLISMA self-modeling mixture analysis approach. *Analytical Chemistry* **2002**, 74 (6), 1371-9.
146. Windig, W.; Guilment, J., Interactive self-modeling mixture analysis. *Analytical Chemistry* **1991**, 63 (14), 1425-32.
147. Windig, W., The use of second-derivative spectra for pure-variable based self-modeling mixture analysis techniques. *Chemometrics and Intelligent Laboratory Systems* **1994**, 23 (1), 71-86.
148. Windig, W.; Stephenson, D. A., Self-modeling mixture analysis of second-derivative near-infrared spectral data using the SIMPLISMA approach. *Analytical Chemistry* **1992**, 64 (22), 2735-42.
149. Windig, W., Spectral data files for self-modeling curve resolution with examples using the Simplisma approach. *Chemometrics and Intelligent Laboratory Systems* **1997**, 36 (1), 3-16.
150. ACD Labs *Reference Manual: SIMPLISMA Algorithm*.
151. Masoum, S.; Ghasemi-Estarki, H.; Seifi, H.; Ebrahimabadi, E. H.; Parastar, H., Analysis of the volatile chemical constituents in *Mindium laevigatum* by gas chromatography — Mass spectrometry and correlative chemometric resolution methods. *Microchemical Journal* **2013**, 106 (0), 276-281.

152. Asadollahi-Baboli, M., Chemometric resolution techniques combined with GC-MS to enhance determination of the volatile chemical constituents of bay leaves. *Analytical Methods* **2013**, 5 (22), 6368-6375.
153. Moreau, J.; Rinnert, E., Fast identification and quantification of BTEX coupling by Raman spectrometry and chemometrics. *Analyst* **2015**, 140 (10), 3535-3542.
154. Hasani, M.; Emami, F., Coupling of soft-modeling methods with multivariate pattern recognition technique for the identification of nitroaniline isomers. *Journal of Chemometrics* **2013**, 27 (10), 341-352.
155. Sui, R.; Rizkalla, A. S.; Charpentier, P. A., Kinetics Study on the Sol-Gel Reactions in Supercritical CO<sub>2</sub> by Using In situ ATR-FTIR Spectrometry. *Crystal Growth & Design* **2008**, 8 (8), 3024-3031.
156. Vajna, B.; Szepesvary, P.; Keglevich, G.; Marosi, G., Methods of vibrational chemical imaging and their evaluation with chemometric methods. *Magy. Kem. Foly., Kem. Kozl.* **2010**, 116, 77-85.
157. Bogomolov A.; Hachey M.; Williams A., Software for interactive curve resolution using SIMPLISMA. In 2005.
158. Bro, R.; Harshman, R. A.; Sidiropoulos, N. D.; Lundy, M. E., Modeling multi-way data with linearly dependent loadings. *Journal of Chemometrics* **2009**, 23 (7-8), 324-340.
159. Bro, R.; Kiers, H. A. L., A new efficient method for determining the number of components in PARAFAC models. *Journal of Chemometrics* **2003**, 17 (5), 274-286.
160. Bro, R., Review on Multiway Analysis in Chemistry -2000-2005. *Critical Reviews in Analytical Chemistry* **2006**, 36, 279-293.
161. Murphy Kathleen R.; Stedmon Colin A.; Graeber Daniel.; Bro, R., Fluorescence spectrometry and multi-way techniques. PARAFAC. *Analytical methods* **2013**, 5 (23), 6541-6882.
162. Rinnan, Å.; Booksh, K. S.; Bro, R., First order Rayleigh scatter as a separate component in the decomposition of fluorescence landscapes. *Analytica Chimica Acta* **2005**, 537 (1-2), 349-358.
163. Andersson, C. A.; Bro, R., The N-way Toolbox for MATLAB. *Chemometrics and Intelligent Laboratory Systems* **2000**, 52 (1), 1-4.
164. Engelen, S.; Frosch, S.; Jorgensen, B. M., A fully robust PARAFAC method for analyzing fluorescence data. *Journal of Chemometrics* **2009**, 23 (3), 124-131.
165. Smilde, A.; Bro, R.; Geladi, P. *Multi-way Analysis with Applications in the Chemical Sciences*; John Wiley & Sons, Ltd: England, 2004.

166. Australian Crime Commission (ACC). *Illicit Drug Data Report 2013-14*; Technical Report for ACC: 2015; (accessed
167. Morelato, M.; Beavis, A.; Tahtouh, M.; Ribaux, O.; Kirkbride, P.; Roux, C., The use of forensic case data in intelligence-led policing: The example of drug profiling. *Forensic Science International* **2013**, 226 (1–3), 1-9.
168. Spring, M.; Ricci, C.; Peggie, D. A.; Kazarian, S. G., ATR-FTIR imaging for the analysis of organic materials in paint cross sections: case studies on paint samples from the National Gallery, London. *Analytical and Bioanalytical Chemistry* **2008**, 392 (1-2), 37-45.
169. Palombo, F.; Danoux, C. B.; Weinberg, P. D.; Kazarian, S. G., Measurement of drug and macromolecule diffusion across atherosclerotic rabbit aorta ex vivo by attenuated total reflection-Fourier transform infrared imaging. *Journal of Biomedical Optics* **2009**, 14 (4), 044008/1-044008/9.
170. Joseph, E.; Ricci, C.; Kazarian, S. G.; Mazzeo, R.; Prati, S.; Ioele, M., Macro-ATR-FT-IR spectroscopic imaging analysis of paint cross-sections. *Vibrational Spectroscopy* **2010**, 53 (2), 274-278.
171. Reese, E. S.; Harrington, P. B., The analysis of methamphetamine hydrochloride by thermal desorption ion mobility spectrometry and SIMPLISMA. *J Forensic Sci* **1999**, 44, 68-76.
172. Buxton, T. L.; Harrington, P. d. B., Rapid multivariate curve resolution applied to identification of explosives by ion mobility spectrometry. *Analytica Chimica Acta* **2001**, 434 (2), 269-282.
173. Edelman, G. J.; van Leeuwen, T. G.; Aalders, M. C., Visualization of Latent Blood Stains Using Visible Reflectance Hyperspectral Imaging and Chemometrics. *J. Forensic Sci.* **2015**, 60, S188-S192.
174. Lavine, B. K.; Allen, M. D.; Nishikida, K.; Sandercock, M. Infrared imaging and multivariate curve resolution for the forensic examination of automotive paints. Presented at 2015; ANYL-224.
175. Cole, C.; Jones, L.; McVeigh, J.; Kicman, A.; Syed, Q.; Bellis, M., Adulterants in illicit drugs: a review of empirical evidence. *Drug Testing and Analysis* **2011**, 3 (2), 89-96.
176. Rutledge, H. T. Multivariate and multiway analysis of hyperspectral and fluorescence landscape data. University of Technology, Sydney, 2011.
177. Pavia D.L.; Lampman G.M.; G.S., K. *Introduction to Spectroscopy*, 3rd ed.; Thomson Learning Inc: USA, 2001.
178. Jordá, J. D.; Jordán, M. M.; Ibanco-Cañete, R.; Montero, M. A.; Reyes-Labarta, J. A.; Sánchez, A.; Cerdán, M., Mineralogical analysis of ceramic tiles by FTIR: A quantitative attempt. *Applied Clay Science* **2015**, 115, 1-8.

179. Chalmers, J. M. Mid-infrared Spectroscopy: Anomalies, Artifacts and Common Errors. In *Handbook of Vibrational Spectroscopy*; Chalmers, J. M.; Griffiths, P. R., Eds.; John Wiley: New York, 2002.
180. Lavine Barry K; Fasasi Ayuba; Mirjankar Nikhil; Nishikida Koichi; Campbell Jay, Simulation of attenuated total reflection infrared absorbance spectra: applications to automotive clear coat forensic analysis. *Applied Spectroscopy* **2014**, 68 (5), 608-15.
181. Boulet-Audet Maxime; Buffeteau Thierry; Boudreault Simon; Daugey Nicolas; Michel, P., Quantitative determination of band distortions in diamond attenuated total reflectance infrared spectra. *Journal of Physical Chemistry. B* **2010**, 114 (24), 8255-61.
182. Friedrich, F.; Weidler, P. G., Contact pressure effects on vibrational bands of kaolinite during infrared spectroscopic measurements in a diamond attenuated total reflection cell. *Appl. Spectrosc.* **2010**, 64 (5), 500-6.
183. Guy, M.; Freeman, S.; Alder, J. F.; Brandt, S. D., The Henry reaction: Spectroscopic studies of nitrile and hydroxylamine by-products formed during synthesis of psychoactive phenylalkylamines. *Cent. Eur. J. Chem.* **2008**, 6, 526-534.
184. Technical and Forensic Intelligence, SIR Australia 2013: Bomb statistics. In Australian Federal Police, Ed. 2014.
185. Akhavan, J. *Chemistry of Explosives (3rd Edition)*; Royal Society of Chemistry: 2011.
186. Barron, L.; Gilchrist, E., Ion chromatography-mass spectrometry: A review of recent technologies and applications in forensic and environmental explosives analysis. *Analytica Chimica Acta* **2014**, 806 (0), 27-54.
187. Royds, D.; Lewis, S. W.; Taylor, A. M., A case study in forensic chemistry: The Bali bombings. *Talanta* **2005**, 67 (2), 262-268.
188. Polsky, R.; Stork, C. L.; Wheeler, D. R.; Steen, W. A.; Harper, J. C.; Washburn, C. M.; Brozik, S. M., Multivariate analysis for the electrochemical discrimination and quantitation of nitroaromatic explosives. *Electroanalysis* **2009**, 21 (3-5), 550-556.
189. Yinon, J. Chapter 2 - Detection of Explosives by Mass Spectrometry. In *Counterterrorist Detection Techniques of Explosives*; Elsevier Science B.V.: Amsterdam, 2007; pp 41-59.
190. Eiceman, G. A.; Schmidt, H.; Cagan, A. A. Chapter 3 - Explosives Detection Using Differential Mobility Spectrometry A2 - Yinon, Jehuda. In *Counterterrorist Detection Techniques of Explosives*; Elsevier Science B.V.: Amsterdam, 2007; pp 61-90.

191. Ramalingam, S.; Periandy, S.; Govindarajan, M.; Mohan, S., FTIR and FTRaman spectra, assignments, ab initio HF and DFT analysis of 4-nitrotoluene. *Spectrochimica Acta Part A: Molecular and Biomolecular Spectroscopy* **2010**, 75 (4), 1308-1314.
192. Banas, A.; Banas, K.; Bahou, M.; Moser, H. O.; Wen, L.; Yang, P.; Li, Z. J.; Cholewa, M.; Lim, S. K.; Lim, C. H., Post-blast detection of traces of explosives by means of Fourier transform infrared spectroscopy. *Vib. Spectrosc.* **2009**, 51, 168-176.
193. Arno, J.; Frunzi, M.; Kittredge, M.; Sparano, B., Advancements in the safe identification of explosives using a Raman handheld instrument (ACE-ID). *Proc. SPIE* **2014**, 9101, 91010Q/1-91010Q/9.
194. Verma, K. K.; Dubey, S. K., Detection of aromatic nitro compounds by means of their pi-complexes with N,N-diethylaniline. *Talanta* **1981**, 28 (7A), 485-6.
195. Qureshi S.; Qureshi P.M.; Haque S., A novel and sensitive spot-test for m-dinitroaromatics and their derivatives with sodium sulphite and dimethylsulphoxide. *Talanta* **1985**, 32 (1), 51-53.
196. Larki A.; Rahimi Nasrabadi M.; Pourreza N., UV-vis spectrophotometric determination of trinitrotoluene (TNT) with trioctylmethylammonium chloroside as ion pair assisted and disperser agent after dispersive liquid-liquid microextraction. *Forensic Sci. Int.* **2015**, 251, 77-82.
197. Uzer A.; Ercag E.; Apak R., Spectrophotometric determination of cyclotrimethylenetrinitramine (RDX) in explosive mixtures and residues with the Berthelot reaction. *Analytica Chimica Acta* **2008**, 612, 53-64.
198. Harper, R. J.; Furton, K. G. Chapter 13 - Biological Detection of Explosives A2 - Yinon, Jehuda. In *Counterterrorist Detection Techniques of Explosives*; Elsevier Science B.V.: Amsterdam, 2007; pp 395-431.
199. Jimenez, A. M.; Navas, M. J. Chapter 1 - Detection of Explosives by Chemiluminescence A2 - Yinon, Jehuda. In *Counterterrorist Detection Techniques of Explosives*; Elsevier Science B.V.: Amsterdam, 2007; pp 1-39.
200. Germain, M. E.; Knapp, M. J., Optical explosives detection: from color changes to fluorescence turn-on. *Chemical Society Reviews* **2009**, 38 (9), 2543-2555.
201. Hughes, A. D.; Glenn, I. C.; Patrick, A. D.; Ellington, A.; Anslyn, E. V., A pattern recognition based fluorescence quenching assay for the detection and identification of nitrated explosive analytes. *Chem.--Eur. J.* **2008**, 14 (6), 1822-1827.
202. Content, S.; Trogler, W. C.; Sailor, M. J., Detection of Nitrobenzene, DNT, and TNT Vapors by Quenching of Porous Silicon Photoluminescence. *Chemistry – A European Journal* **2000**, 6 (12), 2205-2213.

203. Kovalev, I. S.; Taniya, O. S.; Slovesnova, N. V.; Kim, G. A.; Santra, S.; Zyryanov, G. V.; Kopchuk, D. S.; Majee, A.; Charushin, V. N.; Chupakhin, O. N., Fluorescent Detection of 2,4-DNT and 2,4,6-TNT in Aqueous Media by Using Simple Water-Soluble Pyrene Derivatives. *Chem. - Asian J.* **2016**, Ahead of Print.
204. Wang, A.; Cui, Y.; Tao, F.; Gu, C.; Wang, S.; Li, T., Fluorescent film sensor for nitroaromatics prepared via grafting a conjugated polymer on a glass slide surface. *Russ. J. Phys. Chem. A* **2016**, 90, 399-405.
205. Ueland, M.; Blanes, L.; Taudte, R. V.; Stuart, B. H.; Cole, N.; Willis, P.; Roux, C.; Doble, P., Capillary-driven microfluidic paper-based analytical devices for lab on a chip screening of explosive residues in soil. *J. Chromatogr. A* **2016**, Ahead of Print.
206. Bandela, A. K.; Bandaru, S.; Rao, C. P., A Fluorescent 1,3-Diaminonaphthalimide Conjugate of Calix[4]arene for Sensitive and Selective Detection of Trinitrophenol: Spectroscopy, Microscopy, and Computational Studies, and Its Applicability using Cellulose Strips. *Chem. - Eur. J.* **2015**, 21, 13364-13374.
207. Ma, J.; Bock, W. J., Fiber-optic sensors for explosives detection. *Open Opt. J.* **2013**, 7, 141-158, 18 pp.
208. Lai, B.; Chen, Z.; Fang, S.; Zhou, Y., A Combined Treatment Approach Using Fe<sub>0</sub>/Air and Fenton's Reagent for the Treatment of Delay Explosive Wastewater. *Ind. Eng. Chem. Res.* **2015**, 54, 7094-7101.
209. Hua, B.; Dolan, F.; McGhee, C.; Clevenger, T. E.; Deng, B., Water-source characterization and classification with fluorescence EEM spectroscopy: PARAFAC analysis. *International Journal of Environmental Analytical Chemistry* **2007**, 87 (2), 135-147.
210. Hall, G. J.; Kenny, J. E., Estuarine water classification using EEM spectroscopy and PARAFAC-SIMCA. *Analytica Chimica Acta* **2007**, 581 (1), 118-124.
211. Campbell, S. D.; Tremblay, D. P.; Daver, F.; Cousins, D., Wavelength comparison study for bioaerosol detection. *Proceedings of SPIE - The International Society for Optical Engineering* **2005**, 5778 (Pt. 1, Sensors, and Command, Control, Communications, and Intelligence (C3I) Technologies for Homeland Defense IV), 130-138.
212. Damiani, P. C., Determination of atenolol in human urine by emission-excitation fluorescence matrices and unfolded partial least-squares with residual bilinearization. *Talanta* **2011**, 85, 1526-1534.
213. Mujumdar, N.; Goicoechea, H.; Munoz de la Pena, A.; Campiglia, A. Forensic identification and differentiation of visually indistinguishable fiber pairs using excitation-emission fluorescence microscopy paired with multi-way chemometric analysis. Presented at 2015; SERMACS-SWRM-431.

214. Ram, S.; Ehrenkaufner, R. E., A general procedure for mild and rapid reduction of aliphatic and aromatic nitro compounds using ammonium formate as a catalytic hydrogen transfer agent. *Tetrahedron Letters* **1984**, 25 (32), 3415-18.
215. Gowda D.C.; Mahesh B.; Gowda S., Zinc-catalyzed ammonium formate reductions: Rapid and selective reduction of aliphatic and aromatic nitro compounds. *Indian Journal of Chemistry* **2001**, 40B, 75-77.
216. Kumarraja, M.; Pitchumani, K., Simple and efficient reduction of nitroarenes by hydrazine in faujasite zeolites. *Appl. Catal., A* **2004**, 265 (2), 135-139.
217. Petrini, M.; Ballini, R.; Rosini, G., Reduction of aliphatic and aromatic nitro compounds with sodium borohydride in tetrahydrofuran using 10% palladium-on-carbon as catalyst. *Synthesis* **1987**, (8), 713-14.
218. Zeynizadeh, B.; Setamdideh, D., NaBH<sub>4</sub>/Charcoal: A New Synthetic Method for Mild and Convenient Reduction of Nitroarenes. *Synthetic Communications: An International Journal for Rapid Communication of Synthetic Organic Chemistry* **2006**, 36 (18), 2699 - 2704.
219. Bandstra, J. Z.; Miehr, R.; Johnson, R. L.; Tratnyek, P. G., Reduction of 2,4,6-trinitrotoluene by iron metal: kinetic controls on product distributions in batch experiments. *Environ. Sci. Technol.* **2005**, 39 (1), 230-238.
220. Jafarpour, B.; Imhoff, P. T.; Chiu, P. C., Quantification and modelling of 2,4-dinitrotoluene reduction with high-purity and cast iron. *Journal of Contaminant Hydrology* **2005**, 76 (1-2), 87-107.
221. Oh, S.-Y.; Cha, D. K.; Kim, B. J.; Chiu, P. C., Reductive transformation of hexahydro-1,3,5-trinitro-1,3,5-triazine, octahydro-1,3,5,7-tetranitro-1,3,5,7-tetrazocine, and methylenedinitramine with elemental iron. *Environmental Toxicology and Chemistry* **2005**, 24 (11), 2812-2819.
222. Oh, S.-Y.; Cha, D. K.; Chiu, P. C., Graphite-mediated reduction of 2,4-dinitrotoluene with elemental iron. *Environmental Science & Technology* **2002**, 36, 2178-2184.
223. Kung, M. C.; Kung, H. H.; Bethke, K. A.; Yan, J. Y.; Park, P. W., Catalytic NO<sub>x</sub> reduction with hydrocarbons over alumina-supported catalysts. *Spec. Publ. - R. Soc. Chem.* **1999**, 235, 246-253.
224. Abidova, M. F.; Pitsaris, V. K.; Sultanov, A. S.; Freidlin, L. K., Reduction of nitrobenzene and nitrocyclohexane in the presence of tin catalysts. *Uzb. Khim. Zh.* **1963**, 7, 60-5.
225. Mahdavi, H.; Tamami, B., Reduction of nitro-aryl compounds with zinc in the presence of poly[N-(2-aminoethyl)acrylamido]trimethylammonium chloride as a phase-transfer catalyst. *Synth. Commun.* **2005**, 35 (8), 1121-1127.

226. Lou, X.-B.; He, L.; Qian, Y.; Liu, Y.-M.; Cao, Y.; Fan, K.-N., Highly Chemo- and Regioselective Transfer Reduction of Aromatic Nitro Compounds using Ammonium Formate Catalyzed by Supported Gold Nanoparticles. *Adv. Synth. Catal.* **2011**, 353, 281-286.
227. Saha, A.; Ranu, B., Highly Chemoselective Reduction of Aromatic Nitro Compounds by Copper Nanoparticles/Ammonium Formate. *J. Org. Chem.* **2008**, 73, 6867-6870.
228. Ram S.; Ehrenkaufner R.E., A general procedure for mild and rapid reduction of aliphatic and aromatic nitro compounds using ammonium formate as a catalytic hydrogen transfer agent. *Tetrahedron Letters* **1984**, 25 (32), 3415-3418.
229. Tapuhi Y.; Grushka E. Detection and determination of nitro and nitroso compounds. In *Amino, Nitroso and Nitro compounds and their derivatives: Volume 2*; Patai S., Ed.; John Wiley & sons: 1982.
230. Friedman, M., Applications of the Ninhydrin Reaction for Analysis of Amino Acids, Peptides, and Proteins to Agricultural and Biomedical Sciences. *Journal of Agricultural and Food Chemistry* **2004**, 52 (3), 385-406.
231. Guo, K.; Chen, Y., Simple and rapid detection of aromatic amines using a thin layer chromatography plate. *Anal. Methods* **2010**, 2, 1156-1159.
232. Kato, N.; Ogamo, A., A TLC visualization reagent for dimethylamphetamine and other abused tertiary amines. *Sci. Justice* **2001**, 41, 239-244.
233. Friedman, M., Applications of the ninhydrin reaction for analysis of amino acids, peptides, and proteins to agricultural and biomedical sciences. *Journal of agricultural and food chemistry* **2004**, 52 (3), 385-406.
234. Roth, M., Fluorescence reaction for amino acids. *Anal. Chem.* **1971**, 43 (7), 880-2.
235. Kulla, E.; Zuman, P., Reactions of orthophthalaldehyde with ammonia and 2-aminoethanol. *Organic & Biomolecular Chemistry* **2008**, 6 (20), 3771-3780.
236. Gyimesi-Forrás, K.; Leitner, A.; Akasaka, K.; Lindner, W., Comparative study on the use of ortho-phthalaldehyde, naphthalene-2,3-dicarboxaldehyde and anthracene-2,3-dicarboxaldehyde reagents for alpha -amino acids followed by the enantiomer separation of the formed isoindolin-1-one derivatives using quinine-type chiral stationary phases. *J. Chromatogr., A* **2005**, 1083 (1-2), 80-88.
237. Hanczkó, R.; Jámbor, A.; Perl, A.; Molnár-Perl, I., Advances in the o-phthalaldehyde derivatizations: Comeback to the o-phthalaldehyde-ethanethiol reagent. *Journal of Chromatography A* **2007**, 1163 (1-2), 25-42.
238. Csapo, J.; Pohn, G.; Varga-Visi, E.; Csapo-Kiss, Z.; Terlaky-Balla, E., Mercaptoethanesulfonic acid as the reductive thiol-containing reagent



- employed for the derivatization of amino acids with o-phthalaldehyde analysis. *Chromatographia* **2004**, 60 (Suppl. 1), S231-S234.
239. Kuo, C.-T.; Wang, P.-Y.; Wu, C.-H., Fluorometric determination of ammonium ion by ion chromatography using postcolumn derivatization with o-phthalaldehyde. *J. Chromatogr., A* **2005**, 1085 (1), 91-97.
240. Zuman Petr., Reactions of orthophthalaldehyde with nucleophiles. *Chemical Reviews* **2004**, 104 (7), 3217-3237.
241. Meisch H.; Wannemacher., Fluorometric determination of 5-aminolevulinic acid after derivatisation with o-phthalaldehyde and separation by reverse-phase high-performance liquid chromatography. *Anal. Chem. (Washington, DC, U. S.)* **1986**, 58, 1372-1375.
242. Benson, J. R.; Hare, P. E., O-phthalaldehyde: fluorogenic detection of primary amines in the picomole range. Comparison with fluorescamine and ninhydrin. *Proceedings of the National Academy of Sciences of the United States of America* **1975**, 72 (2), 619-622.
243. Carlson, R. G.; Srinivasachar, K.; Givens, R. S.; Matuszewski, B. K., New derivatizing agents for amino acids and peptides. 1. Facile synthesis of N-substituted 1-cyanobenz[f]isoindoles and their spectroscopic properties. *J. Org. Chem.* **1986**, 51 (21), 3978-3983.
244. Manica, D. P.; Lapos, J. A.; Daniel Jones, A.; Ewing, A. G., Analysis of the stability of amino acids derivatized with naphthalene-2,3-dicarboxaldehyde using high-performance liquid chromatography and mass spectrometry. *Anal. Biochem.* **2003**, 322 (1), 68-78.
245. Pawlowska, M.; Zukowski, J.; Armstrong, D. W., Sensitive enantiomeric separation of aliphatic and aromatic amines using aromatic anhydrides as non-chiral derivatizing agents. *J. Chromatogr., A* **1994**, 666 (1-2), 485-91.
246. Karukstis, K. K.; Krekel, D. A.; Weinberger, D. A.; Bittker, R. A.; Naito, N. R.; Bloch, S. H., Resolution of the excited states of the fluorescence probe TNS using a trilinear analysis technique. *The Journal of Physical Chemistry* **1995**, 99 (1), 449-453.
247. Ross, R. T.; Lee, C.-H.; Davis, C. M.; Ezzeddine, B. M.; Fayyad, E. A.; Leurgans, S. E., Resolution of the fluorescence spectra of plant pigment-complexes using trilinear models. *Biochimica et Biophysica Acta (BBA) - Bioenergetics* **1991**, 1056 (3), 317-320.
248. Nie, J.; Wu, H.; Wang, X.; Zhang, Y.; Zhu, S.; Yu, R., Determination of testosterone propionate in cosmetics using excitation-emission matrix fluorescence based on oxidation derivatization with the aid of second-order calibration methods. *Analytica Chimica Acta* **2008**, 628 (1), 24-32.

- 
249. Silva, L. C.; Trevisan, M. G.; Poppi, R. J.; Sena, M. M., Direct determination of propranolol in urine by spectrofluorimetry with the aid of second order advantage. *Anal. Chim. Acta* **2007**, 595, 282-288.
250. Parsons, B. A.; Marney, L. C.; Hoggard, J. C.; Wright, B. W.; Synovec, R. E. Forensic analysis of diesel using comprehensive 2D gas chromatography with time-of-flight mass spectrometry detection. Presented at 2013; ANYL-163.
251. Hoggard, J. C.; Wahl, J. H.; Synovec, R. E.; Mong, G. M.; Fraga, C. G., Impurity Profiling of a Chemical Weapon Precursor for Possible Forensic Signatures by Comprehensive Two-Dimensional Gas Chromatography/Mass Spectrometry and Chemometrics. *Anal. Chem. (Washington, DC, U. S.)* **2010**, 82, 689-698.
252. Borusiewicz, R.; Zadora, G.; Zieba-Palus, J., Chemical analysis of post explosion samples obtained as a result of model field experiments. *Talanta* **2013**, 116, 630-636.
253. Chen R.F.; Scorr C.; Trepman E., Fluorescence properties of o-phthalaldehyde. *Biochimica et Biophysica Acta* **1979**, 576, 440-445.